MINISTÉRIO DA EDUCAÇÃO
UNIVERSIDADE FEDERAL DO RIO GRANDE DO SUL
ESCOLA DE ENGENHARIA
PROGRAMA DE PÓS-GRADUAÇÃO EM ENGENHARIA DE MINAS,
METALÚRGICA E DE MATERIAIS
PPGE3M

RICHARD DE MEDEIROS CASTRO

INVESTIGAÇÃO DO COMPORTAMENTO TRIBOLÓGICO DO REVESTIMENTO WC-CoCr/HVOF APLICADO A COMPONENTES HIDRÁULICOS SOB PRINCÍPIOS DA *GREEN TRIBOLOGY*

Porto Alegre
2021

RICHARD DE MEDEIROS CASTRO

INVESTIGAÇÃO DO COMPORTAMENTO TRIBOLÓGICO DO REVESTIMENTO WC-CoCr/HVOF APLICADO A COMPONENTES HIDRÁULICOS SOB PRINCÍPIOS DA *GREEN TRIBOLOGY*

Tese realizada no Departamento de Metalurgia da Escola de Engenharia da Universidade Federal do Rio Grande do Sul (UFRGS), no âmbito do Programa de Pós-Graduação em Engenharia de Minas, Metalúrgica e de Materiais (PPGE3M), como parte dos requisitos para obtenção do título de Doutor em Engenharia – Área de Concentração: Processos de Fabricação.

Orientador: Prof. Dr. Eng. Alexandre da Silva Rocha (PPGE3M – UFRGS)

Porto Alegre
2021

CIP - Catalogação na Publicação

Castro, Richard de Medeiros
INVESTIGAÇÃO DO COMPORTAMENTO TRIBOLÓGICO DO REVESTIMENTO WC-CoCr/HVOF APLICADO A COMPONENTES HIDRÁULICOS SOB PRINCÍPIOS DA *GREEN TRIBOLOGY* /Richard de Medeiros Castro. 12/2021.
157 f.
Orientador: Dr. Alexandre da Silva Rocha (PPGE3M – UFRGS).

Tese (Doutorado) - Universidade Federal do Rio Grande do Sul, Escola de Engenharia, Programa de Pós-Graduação em Engenharia de Minas, Metalúrgica e de Materiais, Porto Alegre, BR-RS, 2021.

1. Atrito e Desgaste. 2. WC-CoCr. 3. HVOF. 4. Refusão à laser. 5. Eficiência energética. 6. Componentes hidráulicos. 7. Óleos biodegradáveis. 8. Green Tribology. I. da Silva Rocha, Dr. Alexandre, orient. II. Título.

Elaborada pelo Sistema de Geração Automática de Ficha Catalográfica da UFRGS com os dados fornecidos pelo(a) autor(a).

RICHARD DE MEDEIROS CASTRO

INVESTIGAÇÃO DO COMPORTAMENTO TRIBOLÓGICO DO REVESTIMENTO WC-CoCr/HVOF APLICADO A COMPONENTES HIDRÁULICOS SOB PRINCÍPIOS DA *GREEN TRIBOLOGY*

Esta Tese foi analisada e julgada adequada para a obtenção do Título de Doutor em Engenharia – Área de Concentração: Processos de Fabricação, e aprovada em sua forma final pelo Orientador e pela Banca Examinadora designada pelo Programa de Pós-Graduação em Engenharia de Minas, Metalúrgica e de Materiais (PPGE3M), da Escola de Engenharia da Universidade Federal do Rio Grande do Sul (UFRGS).

Prof. Dr. Alexandre da Silva Rocha (PPGE3M – UFRGS)
Orientador

Prof. Dr. Afonso Reguly
Coordenador do PPGE3M – UFRGS

Aprovado com Louvor em: 06/12/2021

BANCA EXAMINADORA:

Prof. Dr. Elvys Isaías Mercado Curi – PPGEM/UniSATC

Prof. Dr. Milton Pereira – POSMEC/UFSC

Prof. Dr. Rodrigo Lima Stoeterau – PPGEM/USP

Porto Alegre
2021

“Depois da família, tenho duas coisas muito importante na minha vida: o trabalho e a competência (conhecimento, habilidade e atitude) que devo ter para executar este trabalho com excelência.” Victor Prates.

AGRADECIMENTOS

Ao meu orientador, Prof. Dr. Eng. Alexandre da Silva Rocha, pelo estímulo, atenção e colaboração na evolução desta pesquisa.

Ao meu coorientador não oficial, Prof. Dr. Eng. Elvys Isaías Mercado Curi, que além de colaborar no desenvolvimento desta pesquisa, sobretudo no processamento de dados de ensaios e coautoria dos artigos, foi também um grande incentivador.

Aos professores do PPGE3M/UFRGS, em especial ao Prof. Dr. Eng. Jaime Alvarez Spim Junior (in memoriam), Profª. Dra. Eng. Célia de Fraga Malfatti, Profª. Dra. Eng. Rejane Maria Candiota Tubino, pelos conhecimentos transmitidos e incentivo a pesquisa.

Ao Reitor do centro universitário - UNISATC, Sr. Carlos Antônio Ferreira, por ter me dado a oportunidade de realizar este estudo dentro e fora da instituição.

Ao coordenador do curso de engenharia mecânica do centro universitário - UNISATC, prof. Dr. Eng. Luiz Carlos de Cesaro Cavaler, pelo incentivo a pesquisa, motivação e oportunidade para desenvolver os estudos.

A todos os técnicos do LABMAT/UFSC, em especial ao Daniel Auri Schaefer e Sílvia Ramôa, pela execução dos ensaios de caracterização dos óleos hidráulicos.

A toda equipe do Laboratório de Mecânica de Precisão – LMP/UFSC que disponibilizaram a estrutura para a refusão a laser dos revestimentos depositados por aspersão térmica, em especial ao prof. Dr. Eng. Milton Pereira e aos bolsistas, MSc. Eng. Rafael Gomes Nunes Silva e ao MSc. Eng. Adriano de Souza Pinto Pereira.

A indústria metalúrgica Rijeza por ter disponibilizado os equipamentos e ligas para a preparação das amostras revestidas por HVOF, minha gratidão especial ao Sr. Darlan Geremia e o Eng. Gabriel Cogo.

A empresa Laboroil LTDA que foi responsável pelas análises de composição química e física dos óleos hidráulicos.

Aos meus colegas de trabalho do centro universitário - UNISATC, pelo incentivo ou, de alguma forma contribuíram com a pesquisa, Franco Wronski Comeli, Pascoal Meller Neto, Luciano Dagostin Biléssimo, Luan de Campos Correa, Anderson Diogo Spacek, Cleber Lourenço Izidoro, Alexandre Milanez, Fábio Peruch.

A toda minha família, em especial a minha esposa, Ladislei Marques Felipe Castro e as minhas filhas, Larissa Felipe Castro e Tuany Felipe Castro que foram pacientes e compreensivas comigo durante toda a elaboração deste trabalho, sobretudo no período que estive mais ausente. Também a minha mãe que, com suas orações, mostrou estar sempre presente ao longo desses anos.

Às instituições de ensino que frequentei ao longo da minha existência: Colégio Dehon, Tubarão/SC, Colégio Rogacionista Pio XII, Criciúma/SC, Escola Técnica SATC, Criciúma/SC, Universidade do Extremo Sul de Santa Catarina - UNESC, Criciúma/SC, Instituto Federal de Santa Catarina – IFSC, Florianópolis/SC, Universidade Federal do Rio Grande do Sul, Porto Alegre/RS.

RESUMO

A busca por eficientes técnicas para tratamentos de superfícies e o uso de lubrificantes ecológicos têm sido objetos de pesquisa no mundo inteiro, devido à necessidade de redução do consumo de energia e os danos ambientais gerados pela indústria. As energias de atrito e desgaste, assim como a lubrificação biodegradável, ainda são temas a serem explorados. A hipótese dessa tese é que os revestimentos de aspersão térmica HVOF, seguido de tratamento à laser, sejam técnicas eficientes para melhorar o desempenho de superfícies de componentes hidráulicos. O objetivo principal deste estudo foi avaliar o potencial da liga WC-CoCr, como opção aos revestimentos de cromo duro e testar o desempenho das superfícies revestidas, em condições a seco e lubrificadas, após o processo de refusão a laser. Caracterizou-se os revestimentos, quanto a microdureza, microestrutura, resistência a flexão e desempenho tribológico. Posteriormente, os óleos hidráulicos biodegradáveis HEES e HEPR foram selecionados e comparados com o óleo mineral HLP, em diferentes regimes de lubrificação. Em seguida, novas amostras revestidas foram tratadas à laser com densidades de energia de 33,3 e 150 J/mm^2, e novamente submetidas a testes tribológicos, estimando-se as eficiências energéticas das superfícies. Os resultados demonstram boas características do revestimento de WC-CoCr para melhoria das superfícies. Mesmo com maior dureza, uma menor densidade de trincas foi observada para a liga WC-CoCr, comparada ao cromo duro. Usando o conceito de Abbott-Firestone, a rugosidade Rmr diminui de 90,57 para 80,29 % na superfície revestida, resultado que foi atribuído à combinação entre dureza, resistência ao desgaste e baixo coeficiente de atrito (COF). O óleo biodegradável HEPR promoveu uma maior estabilidade do COF, para as diferentes pressões de contato. Os resultados de desgaste e atrito confirmaram as diferenças dos coeficientes de pressão-viscosidade e da concentração inferior de aditivos anti-desgaste para o óleo HEES. A amostras tratadas à laser com 33,3 J/mm^2, mostraram que a distribuição adequada das fases W_2C e Co_3W_3C, a concentração de CrC e a densificação na camada do revestimento, reduziram o atrito, a dissipação de calor e o desgaste na superfície, proporcionando a esta, maior eficiência energética. A falta de homogeneização, com acúmulos de debris no disco, promoveram o fenômeno de adesão na amostra não refundida. A baixa adesão e os mecanismos de desgaste das superfícies, indicaram que o óleo HEPR não conseguiu prevenir totalmente o desgaste, porém reduziu 50 % do COF. Este estudo mostra que é possível melhorar a eficiência energética e ambiental dos sistemas hidráulicos, além de incentivar o desenvolvimento da *Green Tribology*.

Palavras-chave: Atrito e desgaste; WC-CoCr; HVOF; Refusão a laser; Eficiência energética; Componentes hidráulicos; Óleos biodegradáveis; Green Tribology.

ABSTRACT

The search for efficient techniques for surface treatments and the use of eco-friendly lubricants has been the subject of worldwide research, because of the need to reduce energy consumption and environmental harm caused by industry. Frictional and wear energies, along with biodegradable lubrication, remain to be explored. The hypothesis of this PhD thesis is that HVOF thermal spray coatings, followed by laser treatment, are effective techniques to improve the performance of surfaces of hydraulic components. The main objective of this study was to evaluate the potential of WC-CoCr alloy as an alternative to hard chromium coatings, and to test the performance of sprayed surfaces, under dry and lubricated conditions, following the laser remelting process. The coatings were characterized for concerning the microstructure microhardness, bending strength and tribological performance. Subsequently, HEES and HEPR biodegradable oils were selected and compared to HLP mineral oil under different lubrication regimes. Following this comparison, new sprayed samples were laser-treated at energy densities of 33.3 and 150 J/mm^2, and again subjected to tribological tests, estimating surfaces' energy efficiency. The results demonstrate good features of the WC-CoCr coating to improve the surfaces of the hydraulic components. Even with greater hardness, a lower crack density was observed for WC-CoCr compared to hard chromium. Using the Abbott-Firestone concept, the Rmr roughness decreases from 90.57 to 80.29 % on the pulverized surface, result attributed to combining hardness, wear resistance and low coefficient of friction (COF). The biodegradable HEPR oil promoted the stability of the COF at different contact pressures. The wear and friction results confirmed the differences between the pressure-viscosity coefficients and the lowest anti-wear concentration for HEES oil. Laser-treated samples with 33.3 J/mm^2 showed that the proper distribution of phases W_2C and Co_3W_3C, the concentration of CrC and the densification of the coating layer contributed to the reduction of friction, heat dissipation and wear on the surface, resulting in greater energy efficiency. The lack of homogenization, with accumulation of debris on the disc, promoted the phenomenon of adhesion in the non-remelted sample. The low adhesion and surface wear mechanisms indicated that the HEPR oil could not completely prevent wear but reduced the COF by 50 %. This study shows that it is possible to improve the energy and environmental efficiency of hydraulic systems, in addition to promoting the development of Green Tribology.

Keywords: Friction and Wear; WC-CoCr; HVOF; Laser remelting; Energy efficiency; Hydraulic components; Biodegradable oils, Green Tribology.

SUMÁRIO

LISTA DE FIGURAS

LISTA DE TABELAS

LISTA DE ABREVIATURA E SIGLAS

AISI	*American Iron and Steel Institute*
ASTM	*American Society for Testing and Materials*
ASTN	*Aerospace Sealing Technology News*
COF	*Friction Coefficient*
CVD	*Chemical Vapor Deposition*
CW	*Continuous Wave*
DIN	*Deutsches Institut für Normung*
EDS	*Energy Dispersive Spectroscopy*
EHC	*Electrodeposited Hard Chromium*
FEM	*Finite Element Simulation*
HAZ	*Heat Affected Zone*
HEES	*Hydraulic Environmental Ester Oil Synthetic*
HEPR	*Hydraulic Oil Environmental Polyalphaolefine and Related Products*
HETG	*Hydraulic Oil Environmental Triglyceride*
HLP	*Hydraulic Mineral Oil*
HV	*Vickers Hardness*
HVOF	*High Velocity Oxygen Fuel*
ICP	*Inductively Coupled Plasma Spectrometry*
ISO	*International Organization for Standardization*
LdTM	*Laboratório de Transformações Mecânicas*
LM1	*Revestimento refundido a 33,3 J/mm^2*
LM2	*Revestimento refundido a 150 J/mm^2*
PVD	*Physical Vapor Deposition*
RMS	*Root Mean Square*
SAE	*Society of Automotive Engineers*
SEM	*Scanning Electron Microscopy*
WEDM	*Wire Electrical Discharge Machining*
WLR	*Revestimento não refundido*
WSD	*Wear Scar Diameter*
XRD	*X-Ray Diffraction*
ZDDP	*Zinc Dialkyldithiophosphate*
ZTA	*Zona Termicamente Afetada*

LISTA DE SÍMBOLOS

ARTICLE #1

$\dot{m}_a$	$[kg/s]$	*Feed rate of abrasive*
F_n	$[N]$	*Normal load*
G_a	$[\mu m]$	*Abrasive granulometry*
d_p	$[mm]$	*Diâmetro da haste*
r_{disc}	$[mm]$	*Track Radius*
Δs	$[m]$	*Sliding distance*
Ø	$[mm]$	*Diameter*
Ra	$[\mu m]$	*Roughness average*
Rmáx	$[\mu m]$	*Maximum theoretical roughness*
Rmr	[%]	*Relative material ratio*
Rz	$[\mu m]$	*Mean roughness depth*
α	[º]	*Bending angle*
μ	[---]	*Friction coefficient*
ρ	$[kg/\mu m^3]$	*Density*
Vr	$[mm^3]$	*Mean volume removed*
dw	$[mm]$	*Diameter of rubber wheel*
n	$[rpm]$	*Rotating speed*
v	$[m/s]$	*Linear speed*

ARTICLE #2

η_0	$[Ns/m^2]$	*Dynamic viscosity at atmospheric pressure*
U_e	$[m/s]$	*Speed of rotation of the shaft*
$P_{máx}$	$[N/m^2]$	*Maximum contact pressure*
σ_{RMS}	$[\mu m]$	*Root-mean-square roughness of the surfaces*
h	$[m]$	*Removed height of pin*
ω	$[rad/s]$	*Speed of rotation*
S	$[m]$	*Linear distance traveled*
T_A	$[K]$	*Absolute temperature*
α	$[mm^2/N]$	*Coefficient of pressure-viscosity*
η_P	$[Ns/m^2]$	*Dynamic viscosity at pressure* P_{mean}
a	$[m]$	*Radius of the contact area*
R'	$[m]$	*Equivalent radius of curvature*

E'	$[N/m^2]$	*Equivalent Young's modulus*
E_1	$[N/m^2]$	*Young's modulus - pin*
E_2	$[N/m^2]$	*Young's modulus - disk*
v_1	$[non-dimensional]$	*Poisson's coefficient - pin*
v_2	$[non-dimensional]$	*Poisson's coefficient - disk*
R_X	$[m]$	*Radius of curvature in the X*
R_Y	$[m]$	*Radius of curvature in the Y*
H	$[HV]$	*Hardness Vickers*
S_q	$[\mu m]$	*Roughness RMS*
S_{q1}	$[\mu m]$	*Roughness RMS - pin*
S_{q2}	$[\mu m]$	*Roughness RMS - disk*
k	$[non-dimensional]$	*Ellipticity parameter*
h_{min}	[µm]	*Minimum film thickness*
Hs	$[non-dimensional]$	Hersey number
λ	$[non-dimensional]$	*film parameter*
$WSD\ (d)$	$[mm]$	*Wear scar diameter*
r	$[m]$	*Pin (ball) radius*
K	$[mm^3/Nm]$	*Wear coefficient*
Q	$[m^3]$	*Removed volume*
Q_i	$[mm^3]$	*Cumulative removed volume*
F_n	$[N]$	*Normal load*

ARTICLE #3

T_0	$[°C]$	*Initial surface temperature*
h_d	$[W/(m^2.°C]$	*Thermal convection of the disc*
A_d	$[mm^2]$	*Profile area measurement*
A_n	$[m^2]$	*Nominal contact area*
E'	$[\mathrm{N/m^2}]$	*Equivalent Young's modulus*
E_1	$[N/m^2]$	*Young's modulus - pin*
E_2	$[N/m^2]$	*Young's modulus - disc*
E_{Tf}	$[J]$	*Total energy of friction*
E_c	$[J]$	*Thermal energy dissipated*
E_p	$[J/mm^2]$	*Energy density*
E_s	$[J]$	*Wear energy generated by abrasive particles*
E_w	$[J]$	*Wear energy*
F_f	$[N]$	*Frictional force*
F_n	$[N]$	*Applied load*

Q_t	$[J]$	*Thermal energy dissipated*
R'	$[m]$	*Equivalent radius of curvature*
T_0	[ºC]	*Initial temperature*
T_s	$[°C]$	*Final surface temperature*
U_E	$[J]$	*Stored elastic energy*
U_P	$[J]$	*Mechanical potential energy*
U_T	$[J]$	*Energy wear debris*
U_s	$[J]$	*Loss of energy to the surface*
V_p	$[mm^3]$	*Volume removed - pin*
W_a	$[J/m^2]$	*Energy of deformation and adhesion per unit area*
W_f	$[J]$	*Energy stored in the rubbing materials*
k_p	$[W/(m.°C]$	*Thermal conductivity of the pin*
l_p	$[m]$	*Length of the heat paths*
q_{disc}	$[W/m^2]$	*Heat dissipated on disc*
q_{pin}	$[W/m^2]$	*Heat dissipated on pin*
q_t	$[W/m^2]$	*Total heat dissipation due to friction per unit area*
r_0	$[m]$	*External radius of the disc*
r_p	$[m]$	*Pin (ball) radius*
v_1	$[non-dimensional]$	*Poisson's coefficient of pin material*
v_2	$[non-dimensional]$	*Poisson's coefficient of disc material*
z_{max}	$[\mu m]$	*Thickness affected by the heat source*
η_s	[%]	*Surface efficiency*
Δs	$[m]$	*Sliding distance*
Δt	$[s]$	*Duration of sliding tests*
h	$[mm]$	*Worn scar height*
Ra	$[\mu m]$	*Roughness average*
Rmr	[%]	*Relative material ratio*
Rz	$[\mu m]$	*Mean roughness depth*
WSD (d)	$[m]$	*Wear scar diameter*
ρ	$[kg/m^3]$	*Density*
Cp	$[J/(kg.K)]$	*Specific heat*
H	$[N/m^2]$	*Surface hardness*
P	$[W]$	*Laser beam power*
R	$[mm]$	*Radius of wear track*
Zr	$[mm]$	*Stand-off distance*
a	$[m]$	*Circular contact radius of the pin on the disc*
d	$[nm]$	*Length of the real contacts*
di	$[mm]$	*Laser incident diameter*

k	$[W/(m.K)]$	*Thermal conductivity*
ti	$[s]$	*Laser irradiation time on the surface*
v	$[mm/s]$	*Scanning speed*
α	$[m^2/s]$	*Thermal diffusivity*
μ	$[non-dimensional]$	*Friction coefficient*

ORGANIZAÇÃO DA TESE

Essa tese será apresentada na forma de artigos científicos, publicados em periódicos internacionais e será organizada em três (03) partes, cada uma sendo constituída pelos seguintes itens, conforme mostrados a seguir:

PARTE I

Introdução, objetivo geral e específicos, justificativa para a realização da pesquisa e integração de artigos científicos.

PARTE II

Artigos Científicos - Cada artigo científico representa um capítulo, que será dividido em, no mínimo: Resumo, Introdução, Procedimento Experimental, Resultados e Discussão, Conclusões, Agradecimentos e Referências. Nessa parte os artigos serão apresentados na íntegra, conforme foram publicados nos periódicos.

PARTE III

Conclusões, sugestões para trabalhos futuros, referências bibliográficas complementares e apêndices.

PARTE I

1. INTRODUÇÃO

O atrito e o desgaste no âmbito da sustentabilidade energética, afetam praticamente todas as áreas de engenharia. Atualmente, existe um grande esforço por parte da comunidade científica e da indústria, em promover a redução do atrito em máquinas e equipamentos, pois sabe-se que mais de 30 % na energia no mundo é utilizado por esse setor (JOST, 1966; HOLMBERG e ERDEMIR, 2017; IGARTUA et al, 2020). Além disso, ações que venham contribuir com a eficiência energética da indústria, impactaria de forma positiva no meio ambiente e promoveria benefícios a toda sociedade. Outros estudos mostram que cerca de 30 % dos recursos de energia do mundo são consumidos por atrito e aproximadamente 80 % dos componentes mecânicos falham devido ao desgaste (LUO & ZHOU, 2020 apud DAŠIĆ et al, 2003; JOST, 2005). Portanto, o desenvolvimento de novas tecnologias para minimizar os efeitos de atrito e desgaste, ou ainda sistemas de lubrificação mais sustentáveis, tornaram-se um alvo importante para economizar energia, minimizar os impactos ambientais e as emissões de CO_2 na atmosfera (LUO e ZHOU, 2020; IGARTUA et al, 2020).

Pesquisas no campo da tribologia e engenharia da superfície tem mostrado que o uso de revestimentos depositados por aspersão térmica em HVOF, *Physical Vapor Deposition* (PVD), deposição ou tratamentos por laser, ou ainda tratamentos de superfícies por nitretação, cementação tem-se apresentado como excelentes alternativas aos revestimentos de cromo duro eletrodepositado. Esses processos alternativos são úteis para diversas aplicações em deslizamento relativo e minimizam os impactos ambientais que é gerado partir da técnica de eletrodeposição. O interesse destas pesquisas, além de propor alternativas ao cromo duro eletrodepositado (EHC), é obter uma superfície com baixo coeficiente de atrito, reduzir do desgaste, além de proporcionar em alguns casos, o aumento da eficiência energética entre os contatos tribológicos (CASTRO et al, 2014; KHADEM et al, 2017; AL-SAYED ALI *et al.*, 2017; RACHIDI *et al.*, 2017; WANG et al, 2019; IGARTUA et al, 2020).

No campo da tribologia moderna, uma das áreas que está relacionado diretamente a este trabalho é a '*Green Tribology*', a qual trata dos aspectos relacionados as emissões de CO_2. Esse novo conceito tribológico, pretende a redução drástica dessas emissões geradas pelas indústrias, motivando a aplicação de tecnologias de superfície inovadoras, materiais e sistemas de lubrificação mais eficientes. Essa área também trata de sistemas com lubrificação biodegradável, energia sustentável, minimização do desgaste, modificação das superfícies, monitoramento em tempo real das condições tribológicas e revestimentos que proporcionam menor impacto ambiental (CIULLI, 2019; KUMAR e BHARJ, 2020).

Nesse contexto, essa tese teve por objetivo promover o desenvolvimento de revestimentos eficientes e lubrificantes mais sustentáveis para componentes hidráulicos, e dessa forma proporcionar um menor impacto ambiental. Também, combiná-las com uso de óleos biodegradáveis usados na transmissão de potência hidráulica e promover uma lubrificação sustentável. Nesse contexto, o desenvolvimento desse trabalho está alinhado com alguns requisitos destacados pelo movimento da Green Tribology. Estes resultados contribuirão ao acréscimo da vida útil dos componentes hidráulicos, através da melhoria nas propriedades mecânicas e tribológicas das superfícies em contato. A combinação de tribologia e cuidados do meio ambiente é uma visão da indústria do futuro, assim a procura de materiais de melhor desempenho e de menor impacto ambiental deve ser incentivado (MYSHKINA e GORYACHEVAB, 2016; ARORA et al., 2019).

Durante o movimento relativo entre duas superfícies, o uso de lubrificantes se torna indispensável para prolongar o tempo de vida dos componentes. Nos sistemas hidráulicos, o óleo mineral é amplamente consumido pela indústria pelo baixo custo. Entretanto, a utilização do óleo mineral será extremamente prejudicial ao ecossistema em caso de derramamento, tendo em vista que apenas um litro de óleo mineral demora mais de 250 anos para se degradar e causa danos praticamente irreversíveis a 1 milhão de litros de água (CONAMA, 2005). Neste cenário, uma das soluções para modificar este quadro de degradação é a substituição dos óleos minerais por biodegradáveis, seja tanto para sistemas de lubrificação quanto para transmissão de potência hidráulica. MENDONZA, 2013; TULÍK *et al*., 2017; JOHN DEERE, 2016, citam a necessidade de pesquisa e aplicação dos óleos biodegradáveis em máquinas que operam na agricultura, indústria petrolíferas (*offshore*), florestais, transportadores de lixo urbano, centrais hidrelétricas, entre outros.

Na maioria dos casos, as características tribológicas que os componentes hidráulicos devem atender, não são bem compreendidas, o que afeta a performance e no consumo de energia das máquinas, elevando os custos de manutenção e causa falhas nesses sistemas. Aliado a esse interesse mundial de cuidado com o meio ambiente, diversas ligas são disponibilizadas comercialmente em forma de pós, para a fabricação de revestimentos por HVOF, como metais, ligas metálicas, polímeros e cerâmicos, ou a combinação destes. As principais ligas que se destacam para revestimentos de componentes hidráulicos, são as ligas de carboneto de tungstênio, cromo, cobalto e níquel (WC-CoCr e WC-Ni). Estas podem ser úteis em aplicações que demandam da combinação de deslizamento do tipo *reciprocating* lubrificado com óleo biodegradável, juntamente com o sistema de vedação [KALIN et al, 2008; MAJDIC e PEZDIRNIK, 2010; STRMČNIK et al, 2019; CASTRO et al, 2020].

A motivação para esta pesquisa se dá pelo fato de que regulamentos de proteção ambiental estão se tornando cada vez mais rigorosos no mundo. As alternativas que se oferecem são o uso de lubrificantes não poluentes e o desenvolvimento de novas rotas tecnológicas de processos de deposição de revestimentos, em substituição a tradicional eletrodeposição de cromo (SAPAWE *et al*., 2014). Além disso, desenvolver novos revestimentos e superfícies que oferecem um menor impacto ambiental e que promovem uma maior sustentabilidade dos processos industriais, é o propósito dessa pesquisa. Do mesmo modo, realizar este estudo, é dar um passo positivo ao cumprimento de leis e obrigações ambientais que estarão por vir. Durante as últimas décadas, os esforços de investigação têm sido menores, mas há uma preocupação e interesse contínuo no mundo para uso destes fluidos (KOSKINEN e RIIPINEN, 2008).

O ineditismo desta pesquisa se deve ao fato de que não há trabalhos divulgados na literatura que apresentem resultados sobre a caracterização do processo de deslizamento, sob a ação do uso de óleos biodegradáveis, combinado com revestimentos fabricados por HVOF com a liga WC-CoCr aplicando-se refusão ou tratamento térmico a laser nas superfícies. Além disso, a maioria das pesquisas investigadas que estudam o uso da técnica de HVOF, avaliam seu desempenho em deslizamento a seco, sem considerar o comportamento termodinâmico das superfícies revestidas (GENG *et al*., 2016; LIU *et al*., 2017). Portanto, é importante dar atenção ao comportamento tribológico desse processo de deslizamento, principalmente sobre os aspectos de atrito, desgaste e consumo de energia, visando algumas características de fabricação de componentes hidráulicos, justifica e valida a pesquisa no aspecto de originalidade e ineditismo.

Com base nas pesquisas realizadas na literatura e da metodologia teórica e experimental proposta, espera-se contribuir de forma científica e tecnológica para a compreensão dos fenômenos tribológicos, com ênfases nos elementos constituintes das superfícies usadas em componentes hidráulicos. O levantamento de dados e os resultados dos ensaios e da correlação com os dados teóricos, permitiu obter conclusões importantes para propor um melhor sistema à indústria fabricante de componentes hidráulicos. Projetos tribológicos sustentáveis devem ter um novo conceito, ou seja, combinar conhecimento tecnológico da engenharia de superfícies, com as novas concepções de lubrificação ambientalmente correta. Nessa combinação, aplicações de equipamentos utilizados na indústria do petróleo, máquinas e implementos de uso agrícolas, pequenas centrais hidrelétricas (PCH’s), embarcações e algumas aplicações da indústria da mineração podem ser beneficiadas e, consequentemente, toda a sociedade.

1.1 Objetivo geral

Esta tese teve por objetivo contribuir para o desenvolvimento de superfícies mais eficientes para componentes hidráulicos, especificamente na caracterização do revestimento fabricado a partir da liga WC-CoCr/HVOF, combinadas ao deslizamento lubrificado com óleos hidráulicos biodegradáveis sintéticos do tipo HEES e HEPR, dando ênfase nas questões de sustentabilidade energética e ambiental. Também, avaliar a potencialidade do processo de refusão a laser nas superfícies revestidas por HVOF, especialmente nos aspectos tribológicos, considerando o comportamento termodinâmico das superfícies durante os ensaios de desgaste por deslizamento.

1.2 Objetivos específicos

A fim de atingir os requisitos do objetivo geral, têm-se os seguintes objetivos específicos deste trabalho, tais como:

- Caracterização a microestrutura e avaliar a resistência mecânica por dobramento e microdureza do revestimento fabricado com a liga WC-10Co4Cr depositado por HVOF, em comparação aos revestidos por eletrodeposição de cromo duro;
- Avaliação do COF e dos mecanismos de desgaste por deslizamento a seco, rugosidade e medição da topografia das superfícies fabricadas com WC-CoCr e cromo duro;
- Avaliação do desempenho dos óleos hidráulicos em função da viscosidade, temperatura e pressão de contato, em diferentes regimes de lubrificação, utilizando a curva de Stribeck e a quantificação pelo número de Hersey;
- Obtenção dos coeficientes de atrito e desgaste das amostras revestidas sob deslizamento lubrificado com os óleos HEES e HEPR, identificação dos mecanismos de desgaste e sua correlação com a contaminação dos óleos, após os ensaios de curta e longa duração em um tribômetro do tipo pino sobre disco;
- Melhoria das propriedades microestruturais, mecânicas e tribológicas do revestimento fabricados por HVOF, usando o processo de refusão a laser;
- Desenvolvimento de uma modelagem de cálculo para estimar a eficiência energética das superfícies através do comportamento termodinâmico;
- Estudo e aplicação da refusão a laser nos revestimentos fabricados por HVOF;
- Identificação dos mecanismos de desgaste após o deslizamento a seco e lubrificado, usando óleo biodegradável HEPR, quantificar os coeficientes de atrito e a rugosidade das superfícies refundidas e sem refusão;
- Transferência do conhecimento adquirido à indústria e a sociedade, por meio de palestras e divulgação científica.

1.3 Justificativa e Contribuições para a Pesquisa

Como uma tecnologia de transmissão, um sistema hidráulico pode continuamente transmitir uma ampla faixa potência, em que essa grandeza pode ser controlada facilmente e com grande precisão. Atualmente, os sistemas hidráulicos têm sido aplicados em diversos setores industriais. Essas aplicações são geralmente feitas em condições de trabalho hostil e de especificidade quanto ao uso de óleos, como para industriais da mineração, marinha (*offshore*), aviação, equipamentos agrícolas e metalurgia (OHE *et al*., 2009; MENDONZA, 2013; MAJDAN, *et al.*, 2013; KOWALSKI e ZLOTO, 2014). Geralmente nestes ambientes, todo sistema hidráulico é exposto agentes contaminantes e condições severas de trabalhos como, água do mar, alta temperatura e locais com muito particulado sólido, como é o caso de equipamentos hidráulicos usados na extração de minerais (BURMA, 2014; NG, *et al*., 2017). Na Figura 1.1 são apresentadas algumas das diversas aplicações dos sistemas hidráulicos (CATERPILLAR, 2016; BOSCH REXROTH, 2017; JOHN DEERE, 2016; TRELLEBORG, 2011), justificando esta pesquisa, no âmbito dos revestimentos metálicos pela técnica de HVOF, e que podem ainda, em alguns casos, ser combinado com uso de óleos biodegradáveis.

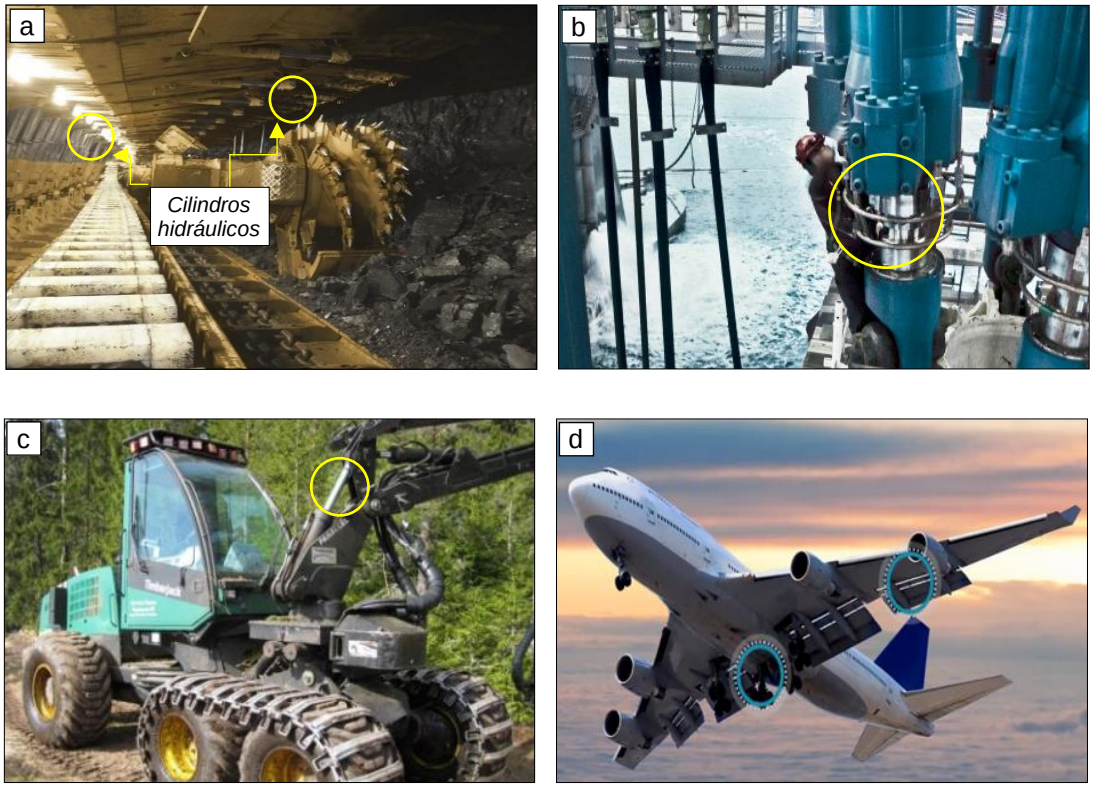

Figure 1.1 - Aplicações dos cilindros hidráulicos para alguns setores industriais: a) extração de minério, b) *offshore*, c) agricultura e d) aviação (CATERPILLAR, 2016; BOSCH REXROTH, 2017; JOHN DEERE, 2016; TRELLEBORG, 2011).

Consequentemente a essas características ambientais adversas, alguns componentes hidráulicos são tradicionalmente revestidos usualmente com cromo duro eletrodepositado. O objetivo é obter uma superfície com melhorias nas propriedades mecânicas e tribológicas, tais como, maior dureza superficial, resistência à corrosão e resistência ao desgaste, com intuito de prolongar a vida útil dos componentes. Em alguns casos, proporcionar a redução do atrito, para que a maior parcela energia de suprimento, possa ser convertida em trabalho útil. Todavia, a técnica de eletrodeposição de cromo apresenta uma ampliação gradual da área de apoio/sustentação aos elementos de vedação e guias, interferindo diretamente na lubrificação da haste, ocasionando danos aos elementos de vedação, causando vazamentos (CASTRO, *et al.*, 2014). Outro apelo contrário à utilização do processo de revestimento com cromo, é a presença, em elevados níveis, de cromo hexavalente Cr+6, apresentando alto poder cancerígeno e de contaminação ambiental (SILVA Jr. *et al*., 2017).

No caso de aplicações, como por exemplo, equipamentos de *offshore*, máquinas de uso na agricultura, de Pequenas Centrais Hidrelétricas (PCH's) e até mesmo embarcações, o problema está relacionado quanto à restrição do uso do óleo mineral, que fica iminente ao risco de derramamento, podendo afetar significativamente os recursos hídricos. Até mesmo, porque há uma tendência gradativa do aumento de pressão de suprimento em sistemas hidráulicos, permitindo maiores potências, com componentes mais reduzidos, aumentando os riscos de vazamentos, motivando a busca por alternativas ao óleo mineral (HAMID, 2008). Por isso, MENDONZA (2013), estimula o desenvolvimento de projetos hidráulicos, com a utilização de óleos biodegradáveis, já que há um interesse mundial na produção de combustíveis e lubrificantes derivados de óleos vegetais e ésteres naturais e sintéticos. Contudo, superfícies usadas em componentes hidráulicos, tais como, bombas, válvulas e os cilindros hidráulicos, não se encontram ainda adequadas para este lubrificante, necessitando-se de pesquisas para atender essa futura demanda.

Técnicas alternativas à eletrodeposição de cromo, além de tratamentos superficiais a laser, indicam melhorias no desempenho nos componentes (VAITHILINGAM *et al.*, 2016; CUI *et al.*, 2017; HAILANG *et al*., 2018). Nesse contexto ambiental e tecnológico, diferentes estudos também promovem a utilizações de óleos biodegradáveis para aplicações em sistemas hidráulicos (KALIN *et al*. 2008; ENEKES e MURRENHOFF, 2010; MAJDIČ *et al*., 2013; STRMČNIK *et al*., 2019; OLSZAK *et al*,, 2020). Contudo, não existem pesquisas abrangentes direcionadas a sistemas hidráulicos, que tratam o tema, combinando os dois interesses, ou seja, técnicas de deposição e revestimentos mais eficientes e de menor impacto ambiental, e o uso de óleos biodegradáveis. Por isso, esse trabalho tem um papel fundamental, por promover o movimento da "*Green Tribology*" no Brasil.

2. INTEGRAÇÃO DOS ARTIGOS

A presente tese é uma continuação da pesquisa iniciada a partir dos resultados, conclusões e perspectivas da dissertação de mestrado desenvolvida nas áreas de engenharia de superfícies e tribologia (CASTRO, 2012). Na ocasião, foi desenvolvido estudos com uso de revestimentos metálicos, com o propósito de melhorar as superfícies utilizadas na fabricação de cilindros hidráulicos e ao mesmo tempo, combinar um método de fabricação de revestimentos de menor impacto ambiental. Para tanto, a continuidade e os avanços desta pesquisa se darão de acordo com os objetivos e metas estabelecidas anteriormente. Desse modo, os principais avanços e metas tecnológicas do trabalho foram:

I. A caracterização das propriedades microestruturais, mecânicas e tribológicas dos revestimentos metálicos alternativos ao cromo duro eletrodepositado, usando a liga WC-CoCr, depositada por aspersão térmica HVOF, com intuito de melhorar as propriedades das superfícies de componentes hidráulicos, além de estar em concordância com as futuras questões energéticas e ambientais no Brasil;

II. Os revestimentos caracterizados de WC-CoCr, foram avaliados, a partir de testes de deslizamento lubrificado com óleos hidráulicos biodegradáveis HEES e HEPR. O comportamento dos regimes de lubrificação foi identificado pela curva de Stribeck, usando modelos matemáticos e requisitos de ensaios tribológicos para avaliação das condições de contato e dos coeficientes de desgaste das superfícies. A comparação dos biodegradáveis foi feita com o óleo mineral HLP, comumente aplicado em sistemas hidráulicos.

III. Promover a melhoria da performance tribológica e energética dos revestimentos por WC-CoCr/HVOF com o uso do processo de tratamento e refusão à laser. Nesse estudo, o comportamento termodinâmico das superfícies foi considerado, com intuito de obter um melhor comparativo da eficiência energética para as diferentes superfícies. Esse estudo mostrou que a fabricação de superfícies depositadas por HVOF pode ser ainda melhorada utilizando parâmetros otimizados do processamento dos materiais com laser.

IV. A transferência do conhecimento adquirido ao setor produtivo de componentes hidráulicos, por meio de palestras, cursos de formação continuada/extensão, publicações em periódicos e apresentações em congressos nacionais e internacionais.

V. Discussão acerca da técnica e dos revestimentos por HVOF, combinados ao processo lubrificado com óleos hidráulicos biodegradáveis, como alternativa aos óleo minerais. Estes passos serão os objetos de estudo para a continuidade das publicações, em que toda esta proposta de integração destes artigos científicos, alcançará o objetivo proposto para esta finalização da tese de doutorado.

2.1 A Comparison of Microstructural, Mechanical and Tribological Properties of WC-10Co4Cr - HVOF Coating and Hard Chrome to Use in Hydraulic Cylinders

Article published in American Journal of Materials Science, Volume 8 (1), 2018, Pages: 15-26, DOI: 10.5923/j.materials.20180801.03.

O uso de revestimentos metálicos depositados pela técnica de aspersão térmica ultrassônica - HVOF, atualmente é muito difundida, porque apresenta uma série de vantagens em relação a tradicional eletrodeposição de cromo, utilizada a mais de 100 anos. As principais vantagens do HVOF são pertinentes as propriedades mecânicas e tribológicas de algumas ligas, como por exemplo, alta dureza, alta resistência a impacto e ao desgaste, além de proporcionar baixo coeficiente de atrito para algumas ligas. Também, o processo de HVOF é uma alternativa de deposição ambientalmente segura, sem grandes riscos à saúde e segurança dos trabalhadores que ficam em exposição a esta operação. Contudo, é de conhecimento público que equipamentos de aspersão ultrassônica, apresentam um elevado ruído (≅ 135 dB), que é originado pelo processo de combustão e a alta vazão do ar comprimido. Este fluido é responsável para impulsionar os pós sobre as superfícies, para que a adesão do revestimento ao substrato ocorra com maior eficiência. Dessa forma, deposições de maior porte que demandam de um maior tempo, são realizadas por robôs que ficam enclausurados em cabines acústicas.

Um vantagem eminente ao processo de HVOF, é a enorme quantidade de ligas que são disponibilizadas comercialmente, com intuito de formar os revestimentos e aumentar a vida útil dos componentes mecânicos. Ao comparar o processo eletrolítico de cromo com a técnica de aspersão, esta técnica apresenta uma elevada taxa de deposição, ou seja, utiliza menor quantidade de energia, avaliando-se na mesma quantidade de área depositada. Ao final, o setor de serviços e a indústria são beneficiados pela redução de custo de suas etapas, disponibilidade de máquinas e consequentemente, uma maior sustentabilidade dos seus processos produtivos. Uma análise comparativa de custo/benefício para substituição do EHC com HVOF, feita por Sartwell and Legg, considerando aspectos ambientais para vários cenários, mostram que haveria um aumento de custo anual líquido entre 2.000 e 26.000 dólares. No entanto, a revisão de alguns componentes mecânicos que usam revestimentos depositados com HVOF, é 20 % inferior da carga de trabalho, referente ao processo de EHC, justificando o uso desta técnica de aspersão térmica.

Diversas são os setores que utilizam revestimentos depositados via HVOF, entre as principais estão, aeronáutico, indústria da mineração e agricultura. Essas aplicações e setores foram impulsionados pelos riscos ambientais que o cromo em sua forma Cr^{+6}, traz a sociedade, sem falar do alto interesse econômico. Nesse contexto, o primeiro artigo apresenta um estudo comparativo entre o revestimento WC-CoCr depositado por HVOF em relação ao cromo duro, validando o revestimento em determinados parâmetros de uso. Com este estudo, buscou-se apresentar a comunidade científica e a indústria, a melhoria propriedades tribológicas, e consequentemente, o ganho econômico e ambiental que técnica de HVOF pode trazer as superfícies dos cilindros hidráulicos, entre outros componentes, Dessa forma, aumentaria o desempenho dos elementos envolvidos, principalmente aos sistemas de vedação, além de reduzir o descarte de materiais ao meio ambiente. Os resultados são discutidos a partir da caracterização inicial das propriedades microestruturais, mecânicas e tribológicas do revestimento. Nessa pesquisa, o foco foi dado na qualidade de deposição do revestimento de carboneto de tungstênio, sob os aspectos comparativos ao cromo duro, e por isso, os testes tribológicos foram desenvolvidos ainda na condição a seco.

2.2 Analysis of the Tribological Performances of Biodegradable Hydraulic Oils HEES and HEPR in the Sliding of Cu-Zn/WC-CoCr Alloys Using the Stribeck Curve

Article published in Journal of the Brazilian Society of Mechanical Sciences and Engineering, Volume 42 (2), 2020, Pages: 1-20, DOI: 10.1007/s40430-019-2080-5

Os resultados iniciais obtidos com a comparação dos revestimentos de cromo duro e da liga WC-CoCr, permitiram identificar o desempenho da técnica de aspersão térmica HVOF, frente à caracterização das propriedades mecânicas e tribológicas dos revestimentos. Nesta pesquisa do item 2.1, o atrito e desgaste dos revestimentos foram avaliados sob testes a seco em tribômetros de roda de borracha e areia e pino sobre disco, com intuito de avaliá-los na condição mais crítica. Contudo, em diversas aplicações, como por exemplo, em máquinas agrícolas, hidrelétricas, *offshore*, entre outras, os componentes dos sistemas hidráulicos, não só operam com óleos minerais, mais em alguns casos, ocorre o uso de os óleos biodegradáveis com intuo de reduzir os riscos ambientais.

Há muitos anos, os óleos fabricados à base do petróleo estabeleceram-se como o lubrificante universal para a maioria das aplicações industriais. Entretanto, estima-se que 50 % de todos os lubrificantes do mundo, acabam sendo derramados no ambiente, que ocorre por eliminação inadequada, vazamentos, acidentes, entre outros meios. Portanto, há alguns

anos, o mundo inteiro começou a desenvolver tecnologia para que os óleos hidráulicos biodegradáveis e os biolubrificantes industriais e automotivos, pudessem ser uma alternativa eficiente e econômica, ao tradicional óleo mineral.

Os biolubrificantes são classificados como naturais (base vegetal ou animal) e os sintéticos (base de ésteres). Por questões de maior aplicação industrial, nesta pesquisa avaliou-se os óleos HEES e HEPR, que são de características sintéticas, fabricado a base de ésteres e polialfaolefinas, classificados como rapidamente biodegradáveis, sendo especificados pela norma ISO 15380. No entanto, além de atender as questões ambientais, estes devem conter propriedades que minimizem o atrito e o desgaste, mesmo que estejam submetidos a elevadas pressões. O óleo HEES, possui como características principais, uma alta capacidade de extrema pressão, elevada afinidade para superfícies metálicas e boa propriedade antidesgaste. No entanto, o HEPR, possui características semelhantes aos óleos minerais, com menor grau de biodegrabilidade comparado ao HEES, boa estabilidade térmica e oxidativa, além de aprimorada propriedades anti-fricção.

Neste segundo artigo teve-se como objetivo avaliar o desempenho dos revestimentos produzidos a partir da liga WC-CoCr, combinado ao deslizamento lubrificado com óleos biodegradáveis do tipo HEES e HEPR. Estes óleos foram selecionados por atender a maioria das aplicações industriais, quanto a pressão máxima, rapidamente biodegradável e maior compatibilidade com materiais de vedação (GAULE, G., & MÜLLER-ZERMINI, 2016; MAJDAN et al. 2013; MILLER, 2012). Nesse estudo, um tribômetro é utilizado nos ensaios de deslizamento, e os resultados tribológicos serão obtidos a partir das propriedades físico-químicas do lubrificantes. A caracterização dos lubrificantes e superfícies foram obtidas, a partir dos regimes de lubrificação (curvas de Stribeck) e sua quantificação foi feita utilizando modelo matemático proposto por Hersey, além de correlacionar o desgaste das superfícies pela concentração de contaminantes presentes nos lubrificantes a cada ensaio.

2.3 Laser Remelting of WC-CoCr Surface Coated by HVOF: Effect on the Tribological Properties and Energy Efficiency

Article published in Surface and Coating Technology, Volume 427, 2021, Pages: 1-19,
DOI: 10.1016/j.surfcoat.2021.127841

O desempenho do óleo biodegradável do tipo HEPR avaliado durante o deslizamento das superfícies de Cu-Zn/WC-CoCr, comparado com óleo mineral HLP e o biodegradável HEES, motiva a continuidade da pesquisa. Entretanto, as microporosidades e a

homogeneidade dos revestimentos por HVOF, mostraram ser uma influência nos regimes de lubrificação e na espessura do filme, além de instabilidade no coeficiente de atrito, em alguns casos. Esse fato mostra que o desempenho tribológico dos revestimentos depositados com a técnica de HVOF podem ser ainda melhorados, utilizando processos complementares de tratamentos de superfícies, como é o caso do laser industrial.

Atualmente, o laser apresenta-se como uma poderosa fonte de energia para o processamento de materiais. Sem dúvida, o laser tem desempenhado um papel cada vez mais importante em vários setores de manufatura industrial, destacando-se, a manufatura aditiva, texturização de superfícies, tratamentos térmicos de alta intensidade, além de processamento de ligas de alto desempenho. Também, o uso do laser para processamento de materiais está classificado em alguns itens da "Green Tribology", que trata temas, tais como, *environmental implications of coatings, minimization of wear, surface texturing e minimization of heat and energy dissipation.*

Nesse terceiro artigo, a influência do tratamento a laser nas propriedades tribológicas e na eficiência energética das superfícies, foram avaliadas. A avaliação das eficiências energéticas de cada tipo de superfície, foram obtidas a partir dos ensaios de deslizamento a seco e lubrificado com óleo biodegradável HEPR. Ainda, com intuito de obter os valores da eficiência energética nos ensaios de deslizamento a seco, foi considerado o comportamento termodinâmico de cada superfície, usando as propriedades termofísicas do par tribológico.

A seleção das melhores densidades energia do laser, foram obtidas a partir diferentes combinações de potências e velocidade de varredura (apêndice A.3.2), obtendo-se duas destas com o melhor desempenho. Com a densidade de energia de 33,3 J/mm^2, identificou-se uma melhora na homogeneização do revestimento, comparada as superfícies sem refusão. No entanto, com 150 J/mm^2, foi observada uma boa diluição do revestimento ao substrato, porém com significativas alterações da microestrutura, o que impactou nos mecanismos de desgaste, resultando na baixa eficiência energética dessa superfície.

Finalizando, essa pesquisa apresenta importantes resultados com o uso da técnica de refusão e tratamento com o laser de alta energia, sobre revestimentos depositados por HVOF, podendo-se obter importante ganho energético para as superfícies aplicadas em componentes de sistemas hidráulicos. Esses resultados podem ser aplicados em outras superfícies que operam com deslizamento a seco ou lubrificado. Também, os resultados dessa pesquisa mostram que o laser usado como processamento de materiais pode ser uma alternativa para a inovação dos processos de manufatura, que atualmente alguns fabricantes buscam em seus processos produtivos.

PARTE II

3. A COMPARISON OF MICROSTRUCTURAL, MECHANICAL AND TRIBOLOGICAL PROPERTIES OF WC-10Co4Cr - HVOF COATING AND HARD CHROME TO USE IN HYDRAULIC CYLINDERS

Richard de Medeiros Castro[1], Alexandre da Silva Rocha[2], Elvys Isaías Mercado Curi[1], Fábio Peruch[1]

[1]Department of Mechanical Engineering, SATC College, Criciúma-SC, Brazil
[2]Department of Metallurgical Engineering, UFRGS - Federal University of Rio Grande do Sul, Porto Alegre-RS, Brazil

Abstract

In order to obtain a wear and oxidation resistant surface, hydraulic cylinders are commonly coated with electrodeposited hard chromium. However, due to the wear, this type of coating exhibits a gradual increase of the bearing area for the sealing elements, interfering in the lubrication of the hydraulic rod, causing damage to the sealing elements and, consequently, oil leakage. Currently, the High Velocity Oxygen Fuel (HVOF) process appears as an alternative coating technique to Hard Chrome Plating, using composites (metal-ceramic), which provide low wear rates and a low friction. This work aims to compare the mechanical and tribological properties of hard chrome plated and WC-CoCr HVOF coated AISI 1045 steel for the use as hydraulic rods. The selected coatings thickness was in the order of 100-170 μm aiming to meet best wear test conditions, to facilitate the analysis of the microstructure, and to obtain better results regarding the hardness of each coating. Roughness measurements, hardness, bending and wear tests, including the measurements of friction coefficients were carried out for the coatings. Additionally, a microstructural analysis was performed by optical, and Scanning Electron Microscopy (SEM) supported by Energy Dispersive Spectroscopy (EDS). The results indicated superior properties of the WC-CoCr HVOF coated steel in comparison to the chrome hard plated one, especially regarding roughness, friction, and wear.

Keywords Wear, Friction, Thermal Spraying, WC-CoCr, Hydraulic Rods.

3.1 Introduction

As a power transmission element, the hydraulic cylinder can continuously transmit a wide range of power, which can be controlled easily and with accuracy. Its application usually occurs under difficult working conditions, in mining, offshore, aviation, agricultural equipment, and metallurgy. Hydraulic rods are normally exposed to extreme and hos-tile environments such as seawater or high temperature, and environments with a high number of solid particles, as is the case of mineral extraction, which lead to rapid wear of the cylinders (Pawlowski, 2008). Consequently, the rods of the hydraulic cylinders are coated with a layer of protective material, usually hard chrome. The purpose of this coating is to improve surface characteristics and mechanical properties such as surface hardness, corrosion resistance, wear resistance, and even reduce friction. However, the electrode-posited hard-chrome layer, as the wear progresses, causes a gradual increase of the supporting area to the sealing elements and guides. This interferes directly in the lubrication of the rods, causing damage to the sealing elements and promoting fluid leakages. This is because the roughness peaks are broken during sliding and, thus, the height of the valleys decrease dramatically, not holding the lubrication oil anymore. Another problem in the use of Hard Chrome Plating is the presence of Cr6+ hexavalent chromium in high levels, leading to high carcinogenic and environmental contamination (Flitney, 2007; Sartwell, *et al*. 2006).

Nowadays, several processes are under consideration as alternatives to replace Hard Chrome Plating. The main ones are Chemical and Physical Vapor Deposition (CVD and PVD) and Laser Cladding, but the main disadvantages of these processes are the difficulties in the retreatment of the parts. Recent publications have shown that the High Velocity Oxygen Fuel (HVOF) technique can be used both for the manufacture of new coatings and for the recovery of rods that have already been used (Mojena *et al.,* 2017; Pathak e Saha, 2017). An advantage of the HVOF process is that is produces a coating with high density, low oxide content and good adhesion (Pawlowski, 2008; Degennaro, 1999).

Driven by the need to improve the wear of the components, some sealing industries are looking for new technologies to establish themselves in the market. They also allocate all set of actions carried out by environmental strategists on alternatives to hard chromium. A survey published by the Aerospace Sealing Technology News (ASTN) in 1999 presented results to the US Air Force over alternatives to Hard Chromium Plating in fluid power system

components. In this study the WC-CoCr HVOF coatings have been evaluated, demonstrating excellent results (Ghabchi *et al*, 2010; Wesmann e Espallargas, 2016).

The characteristics most often used to describe the topography of a surface are the roughness parameters Ra, Rz and Rmáx (μm), defined in DIN/ISO 4287. However, for hydraulic cylinders, it is necessary to know the parameter Rmr (%), which determines the support area for the seal. In several cases, different surfaces can have similar Ra values but, for other roughness parameters, totally different values can be found. According to Steep and Wüstenhagen (2006), 80 % for Rmr should be an optimal value for hydraulic cylinders (Leach, 2001; Steep e Wüstenhagen, 2006).

With the objective of identifying the performance of the WC-CoCr coating and establishing a comparison with the traditional hard chromium coating, the metallurgical, mechanical and tribological properties of an AISI 1045 steel used in hydraulic cylinder rods were evaluated. The tests were selected according to the conditions under which the coatings would be subjected. The coating thickness selected was of the order of 100-170 μm in order to meet the best wear test conditions, to facilitate the analysis of the micro-structure and to obtain better results in relation to the hardness of each coating. Roughness, hardness, bending, and wear measurements were performed, including the coefficient of friction measurements for both coatings. Additionally, the microstructural analysis was performed by optical microscopy and scanning electron microscopy (SEM) supported by energy dispersive spectroscopy (EDS). The bending tests were done according to ASTM E290, common in weld coatings, in order to identify the crack density for each bend angle (ASTM E 290-92, 2008). The tribological evaluation was performed by the abrasive wear method, a mechanism that normally occurs during sliding of the hydraulic rods, so was selected the rubber and sand wheel method (ASTM G65-00, 2001). However, to identify and provide results on the coefficient of friction for both coatings, the pin on disk method was chosen (ASTM G99-00, 2000).

3.2 Experimental procedure

3.2.1 *Characteristics of the material of substrate*

Specimens of AISI 1045 steel in the as delivered state (as hot-rolled), used to obtain the chemical composition of the material of substrate, were manufactured with 25 mm of diameter and 30 mm of height. The chemical composition presented in Table 3.1 was obtained using mass atomic spectrometry. After preparation, the samples were coated with

two different types of coating: Hard Chrome, which is an electroplating process, and WC-CoCr - HVOF which is a thermal spraying process.

Table 3.1 - Chemical composition of the AISI 1045 used as substrate.

Chemical Element	**AISI 1045 standard (% wt.)**	**Analyzed (% wt.)**
C	0.42 - 0.50	0.45
Cr	-	0.11
Ni	-	0.09
P	0.04 Max.	0.013
Fe	Balance	98.2
Si	0.15 - 0.30	0.16
Mn	0.50 - 1.00	0.70
S	0.05 Max.	-
Others	-	0.28

3.2.2 *Electroplating process - hard chrome*

Before hard chromium deposition, specimens were sandblasted to obtain an Ra roughness of 0.28 μm and then cleaned for improved adhesion. Basically, the process of cleaning the surface of the base material was carried out by chemical means, using a solvent, by cold degreasing and an aqueous solution to remove oxide layers. The roughness of the substrate in AISI 1045 in hard chromium deposition is lower than those used by HVOF. This average roughness value is necessary so that after the hard chromium deposition does not appear the scratches of the machining.

The chrome plating procedure occurred as follows: the specimens were immersed in a reservoir containing the Cr_2O_3 compound, dissolved in water. H_2SO_4 acid was added to this solution to act as a catalyst. The specimens (cathode) were connected at the negative pole and the positive pole (anode) was a sheet metal made of inert metal (93Pb7Sn). The final chrome layer thickness was of approximately 101 ± 3 μm with a deposition time of 2 hours. After of hard chrome deposition a fine machining process, with sandpaper and polishing was done to remove the more peaks, leaving with the surface finish used on hydraulic rods.

3.2.3 *Thermal spray process - HVOF/ WC-CoCr*

Before thermal spraying deposition, surfaces were grit-blasted with aluminium oxide (Al_2O_3) and cleaned with isopropyl alcohol in order to remove the impurities and obtain adequate roughness for the adhesion of the coatings, remaining with a roughness Ra of 6.4

μm. This roughness Ra difference, 0.28 to 6.4 um, is justified by the need for mechanical anchoring of the coating to the substrate by HVOF, requiring greater surface irregularity to fix the thermal spray coating.

The spraying equipment was an HP-HVOF and commercial powder of WC-CoCr with a density between 4.8 to 5.0 g/cm^3 was used for deposition. Fig. 3.1 shows the morphology of the as-received powder under a scanning electron microscope (SEM) with particle sizes in the range of 45 to +15 μm. The chemical composition of the powder was confirmed by electron dispersive spectrometer (EDS) analysis. In the present study, WOKA 3653 powder was commercially provided by the company Oerlikon Metco and the chemical composition of this product is compared by measuring EDS (Table 3.2).

The parameters for HVOF spraying are presented in Table 3.3. The distance between the torch and the specimens was set at 305 mm with a gun size of 152.4 mm and the powder feed rate was set at 15 × 10^{-4} kg/s. At the end of the coating deposition process, the specimens were submitted to the grinding and polishing process, resulting in an average roughness Ra of 0.12 μm, used for hydraulic cylinder rods.

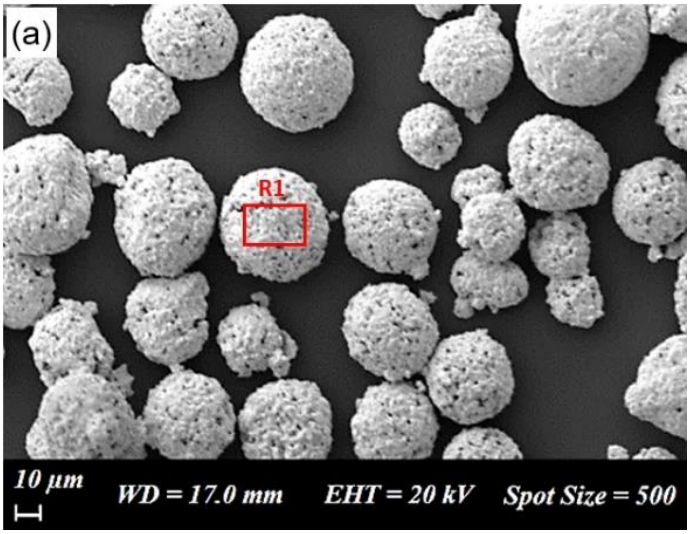

Figure 3.1 - SEM micrographs of WC-CoCr powder

Table 3.2 - Comparison of the Chemical Composition of WC-10Co4Cr

Material	**Content of elements in weight - %**				
	W	**Co**	**Cr**	**C (total)**	**Fe (max.)**
WC-CoCr (Oerlikon)	Balance	8.5 - 11.5	3.4 - 4.6	4.8 – 5.6	0.2
WC-CoCr (measure)	Balance	10.3	4.3	4.7	0.2

Table 3.3 - Thermal spray deposition parameters to WC-CoCr

Elements	**Parameters**	
	Pressure [Pa]	**Flow [m^3/s]**
Nitrogen	$15.0 \pm 1.0 \times 10^5$	$8652.2 \pm 8.3 \times 10^{-8}$
Oxygen	$9.7 \pm 0.3 \times 10^5$	$2016.7 \pm 2.1 \times 10^{-8}$
Kerosene	$9.1 \pm 0.3 \times 10^5$	$644.4 \pm 0.8 \times 10^{-8}$
Combustion	$7.0 \pm 0.3 \times 10^5$	----------

The HVOF coatings had a final thickness of about 167 ± 7 μm with a deposition time of 5 minutes in total. The coating thickness was controlled by a defined number of passes by the substrate and according to the parameters of Table 3.3.

3.2.4 *Microstructural characterization and hardness test*

For the microstructural characterization of the coatings and hardness tests (hardness profiles), specimens were cut in the cross section, then sanding and polishing. Vickers $HV_{0.01}$ microhardness profiles with automatic loading and unloading rate and dwell time of 15 seconds were obtained by using an HMV-02 TADW-SHIMADZU microhardness tester, and tests were based on ASTM E 384-89. For each microhardness profile, four indentations were created in the substrate and twelve in the coating. This was repeated for three different regions of each specimen. An average microhardness profile was calculated from the 3 obtained profiles. Optical microscopy analysis was carried out in an OLYMPUS microscope model BX 51M with non-etched samples.

3.2.5 *Guided bending test*

Guided bending tests were carried out according to the procedures of ASTM E-290, using a Shimadzu® universal test machine, model AG-X plus 100 kN. A sketch of the test apparatus is shown in Fig. 3.2.

The specimens were bent at bending angles of 24, 90, and 180º around a mandrel with a diameter of 15mm, and an approximate feed speed of 10mm/min was used. At each test, the load was released, and the bended sample retracts so that the final permanent angle of the tested specimens is smaller than the angles tested. In this test condition, the coating receives efforts of tension and compression. The specimens evaluated were strips with 50 mm of width and 100 mm of length, all with a thickness of 3 mm. The bending resistance and adhesion of WC-CoCr and hard chrome coatings were evaluated by analyzing the formed cracks on the specimens after the bend.

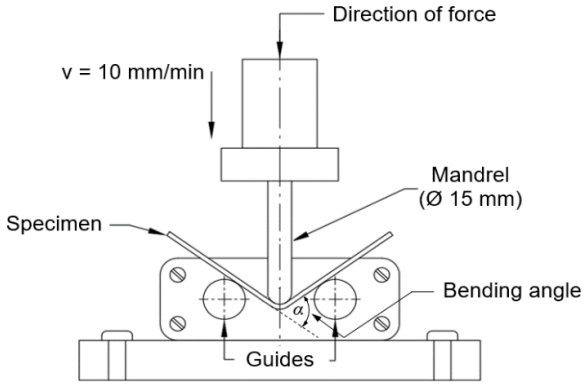

Figure 3.2 - Principle of the bend test.

After the bending test was performed for each angle, measurements and identification of cracks were carried out using a digital microscope with a magnification of 500 x. For each test specimen, the lengths of 20 cracks were measured to obtain a mean and a standard deviation at each angle, as shown in Fig. 3.6.

3.2.6 *Wear and friction tests*

In order to characterize the wear and friction properties of the coatings, two different methods were employed: rubber and sand wheel wear test and pin-on-disc wear test. For the rubber and sand wheel wear test, the procedure A of the ASTM G65 (Test duration – 30 min) standard was used. This test was used because it would simulate the worst abrasive wear condition a hydraulic rod would have. The test conditions are summarized in Table 3.4.

Table 3.4 - Parameters of wear tests: ASTM G65

Nº	**Parameters**	**Symbol**	**Value**	**Unit**
1	Diameter of rubber wheel	dw	228.6	mm
2	Rotating speed	n	200	rpm
3	Abrasive granulometry - SiO_2	G_a	212 a 300	µm
4	Normal load	F_n	130	N
5	Feed rate of abrasive	$\dot{m}_a$	5.33×10^{-3}	kg/s

This is a relatively severe test which will rank materials abrasion resistance. The wear response (loss of volume) was obtained according to Equation 1. The weight loss was measured using an electronic balance with 0.1 mg in accuracy. The wear tests were performed using the parameters of Table 3.4.

$$Volume\ loss = \frac{weight\ loss\ (g)}{density\ (g/cm^3)} \times 1000\ [mm^3] \quad (1)$$

The friction measurement was performed using the procedures of ASTM G99 through the pin on disk test. The friction tests were performed using the same parameters of Table 3.5 for hard chromium and WC-CoCr coatings. For the friction test, a tungsten carbide sphere was used as the pin, with an average hardness of 1376 $HV_{0.01/15}$, and a disc with 50 mm diameter. The experimental results of this wear test were determined by means of a profilometer model XP-2 from AMBIUS Technology, evaluating the average removed volume after five measurements by specimens. Additionally, the friction coefficients were monitored in the tests.

Table 3.5 - Parameters of wear tests: ASTM G99

Nº	**Parameters**	**Symbol**	**Value**	**Unit**
1	Normal load	F_n	30	N
2	Linear speed	v	0.47	m/s
3	Sliding distance	Δs	1000	m
4	Track Radius	r_{disc}	15	α
5	Pin diameter	d_p	6	mm

To characterize the WC-CoCr coatings and to identify the wear micro mechanisms after rubber and wheel testing, Scaning Electron Microscopy equipped with Energy Dispersive X-ray (SEM-EDS) was used. The scanning electron microscope was an EVO MA 10 - ZEISS equipped with u QUANTAX. The surface roughness evaluation was performed before and after the rubber and sand wheel wear tests, using an SJ-210 roughness meter of Mitutoyo, with the Ra, Rz and Rmáx recorded in μm and Rmr recorded in percentage, obtaining contact area of support the seal.

3.3 Results and discussion

3.3.1 *Microstructure and hardness of the coatings*

The microstructures of the WC-CoCr coatings are shown in Fig. 3.3. A lamellar structure, typical of HVOF coatings was observed, containing a discrete oxide film in the lamella boundaries and a low number of pores (Vencl et al, 2011).

The level of porosity indicated in Fig. 3.3 (b) was evaluated by image analysis (software Image-Tool). The tungsten carbide-based coatings had a mean porosity of 1.0 % with a standard deviation of 0.26 %, which is in accordance with the criteria specified by the powder manufactures for this kind of coating (Oerlikon Metco) that establishes a mean

porosity of less than 1.0 %. In Fig. 3.4 (b), microcracks can be observed in the hard chrome coating.

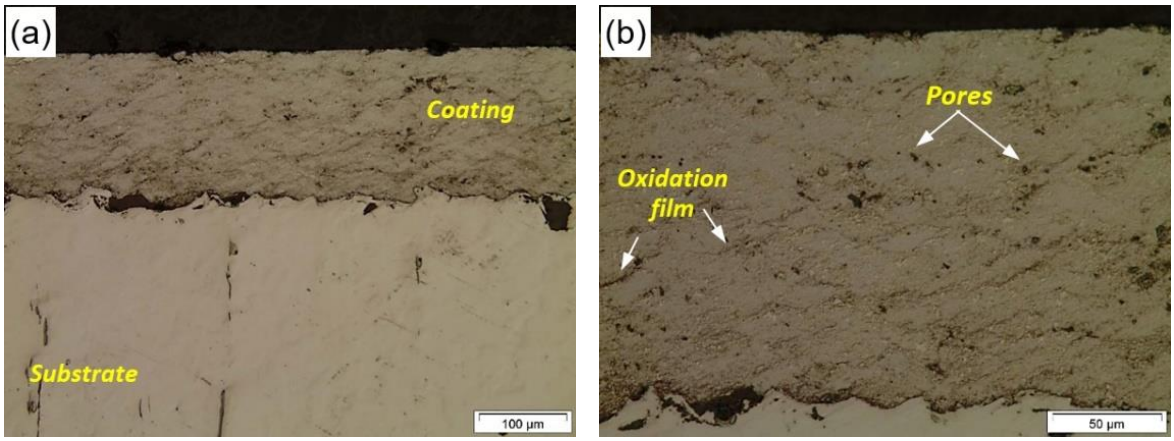

Figure 3.3 - Micrographs of the WC-CoCr: (a) 200x and (b) 500x. Not etched.

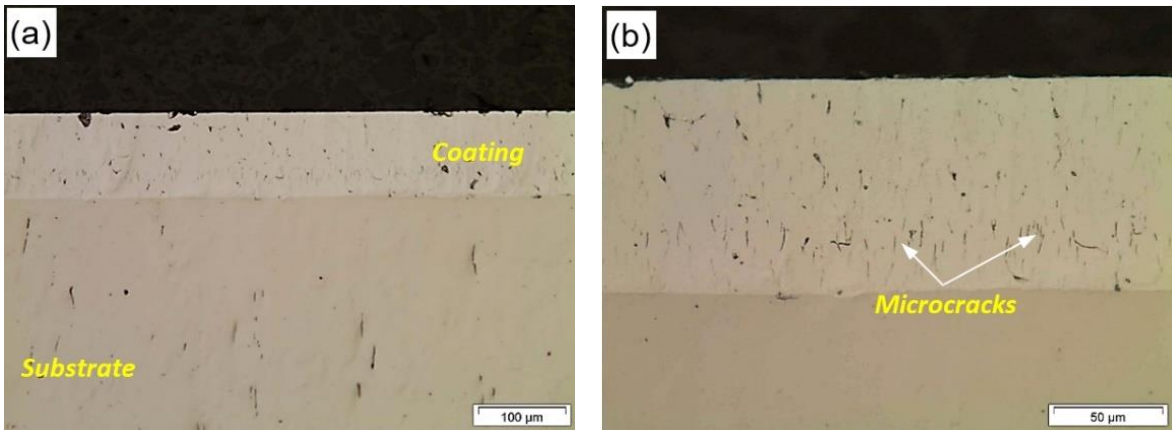

Figure 3.4 - Micrographs of the Hard Chrome: (a) 200x and (b) 500x. Not etched.

According to the literature, electrodeposited hard chromium coatings exhibit this micro-cracked morphology because of residual stress relief (Agüero et al, 2011). These aligned cracks facilitate the entry of oxygen to the substrate, easily causing oxidation which leads to a very rapid deterioration of the hydraulic component (Bailey, 2011). However, the cracks can be positive when controlled the quantity, as it would aid in the lubrication of the rods.

The WC-CoCr coating had an average thickness of 167 µm, with a standard deviation of 7 µm. On the other hand, the hard chrome coating had an average thickness of 101 µm with a standard deviation of 3 µm. The lower standard deviation in the thickness indicates that there is a greater regularity in the hard chromium electrodeposition process compared to the HVOF process. In Fig. 3.5 Vickers microhardness profiles for the two different coatings are presented.

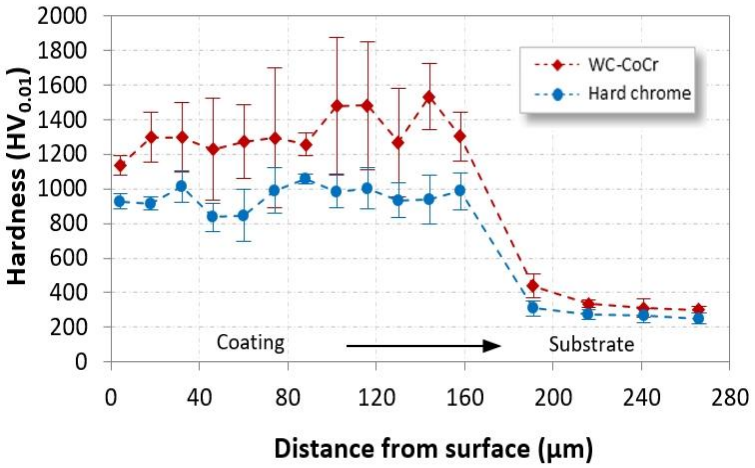

Figure 3.5 - Microhardness profiles of the coatings.

A larger hardness dispersion for the WC-CoCr is seen due to its heterogeneous microstructure (see Fig. 3.3) in comparison to hard chrome coating. Some studies show that the coatings sprayed with WC-based materials are described as metal-ceramic composites, and the microhardness values found are influenced by each microconstituent (Chatha et al, 2012). The average value for the coating deposited by HVOF was in the order of 1256 $HV_{0.01,}$ while the value for the electrodeposited chromium was of 952 $HV_{0.01}$.

3.3.2 *Bend Test - Analysis of Cracks and Delamination*

The three-point bending test performed according to ASTM E-290 is a usual test to evaluate the adhesion of the coating to the substrate, i.e., to check if cracks and/or peeling of the coating will occur. In this work, the specimens made of AISI 1045 steel are bended and the coatings on the surface are subjected to tensile and compression stress according to the specimen's side (upper or lower). After the bending tests were performed in 24, 90 and 180 degrees, the cracks and delamination of the coatings were analyzed quantitatively and visually, according to Fig. 3.6.

After the bending test, almost all the coatings remained adhered to the substrate with no spallation or peeling phenomena. However, all coatings presented cracks. In the case of the hard chrome coating, the microcracks were in higher quantities than for WC-CoCr, and they very heterogeneous in size. Previous research has pointed out that higher bending angle values increase the damage level with an increase in cracking density (Iacoviello et al, 2005). Also, with hard chrome coating, spalling was observed at a 90° bend angle, influenced by the partial breakage of the substrate (see Fig. 8). However, for HVOF coating, the distance

between the cracks is greater due to the lower adhesion force between the coating and the substrate. The adhesion process of the tungsten carbide to the substrate results from the impact shrinkage process, being related to a mechanical process of anchoring whereas in hard chrome it occurs an electrolytic adhesion.

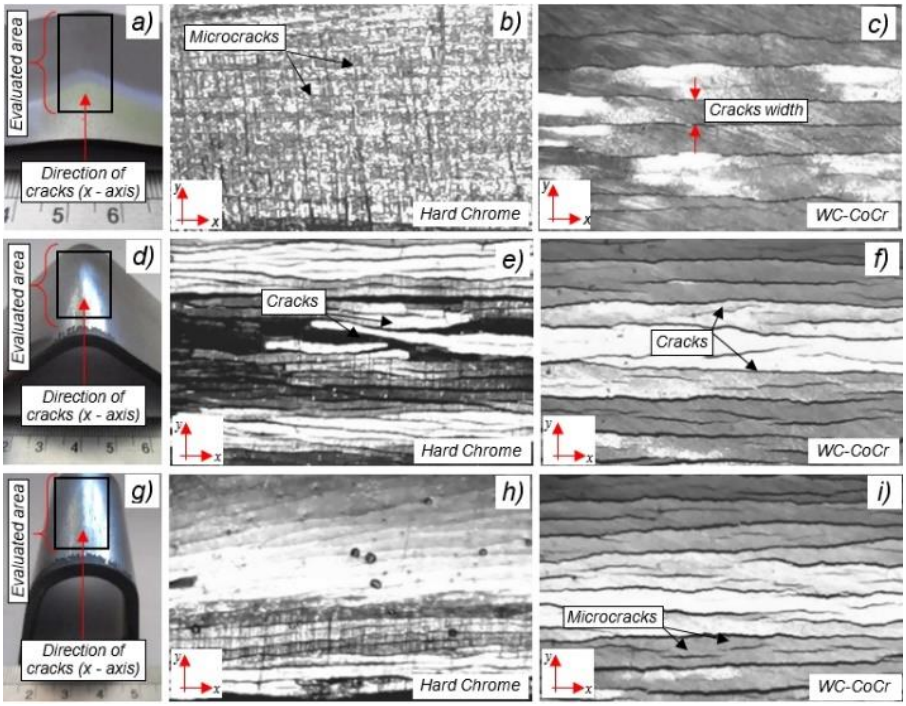

Figure 3.6 - Results of the bend test: (a, b, c) 24º, (d, e, f) 90º and (g, h, i) 180º.

The results of the bending tests are summarized in Table 3.6. In Fig. 3.7, the density of the radial cracks is presented as a function of the bending angle, proving that there is a linear relationship between bend angle and radial cracks size. For smaller bend angles, the distances between the cracks are larger, than with a larger angle. Cracks occur in proportion to the bend angle. In general, the failure mechanisms were similar for both coatings, but with longer cracks in the case of hard chrome and a faster increase in crack size with decreasing bending angle (higher inclination of the curve in Fig. 3.7). It should be noted that these tests are intended to characterize coatings under extreme conditions that would hardly be required for hydraulic cylinder applications. Fig. 3.8 (a) and (b) show the failures in the edge of the specimens.

Fig. 3.8 shows the behavior of the coatings in regions considered to be critical, i.e., at the edge of the specimen, where the coating is not supported on the side. Failure mechanisms, such as cracking, delamination and spalling have occurred in this area. A crack initiation was also observed on the substrates at 90 and 180° bending angles, both for hard

chromium and WC-CoCr. For a 24° angle with the WC-CoCr coating, no critical failure mechanisms were found, only microcracks that had been observed before, in Fig. 3.6.

Table 3.6 - Influence of bending angle on the frequency of cracks.

Coatings	Angle - α [°]	Crack Average Size [mm]	Crack density [cracks / mm]
Hard Chrome	24	0.402 ± 0.021	2.49 ± 0.12
	90	0.269 ± 0.041	3.71 ± 0.59
	180	0.238 ± 0.030	4.21 ± 0.55
WC-CoCr	24	0.823 ± 0.102	1.22 ± 0.16
	90	0.584 ± 0.086	1.71 ± 0.25
	180	0.483 ± 0.057	2.07 ± 0.24

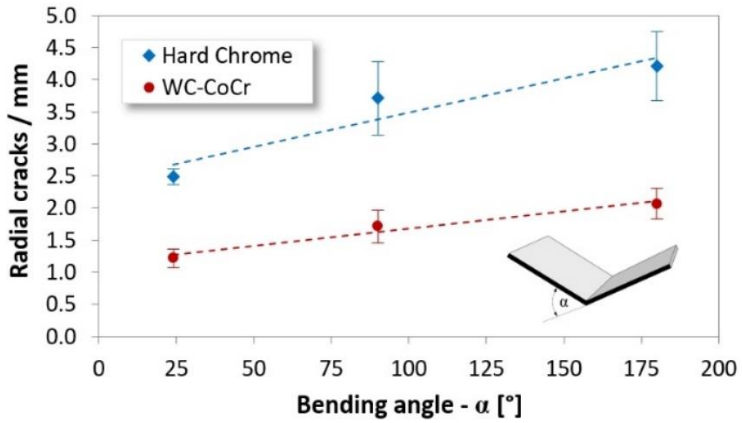

Figure 3.7 - Influence of bending angle on the frequency of radial cracks.

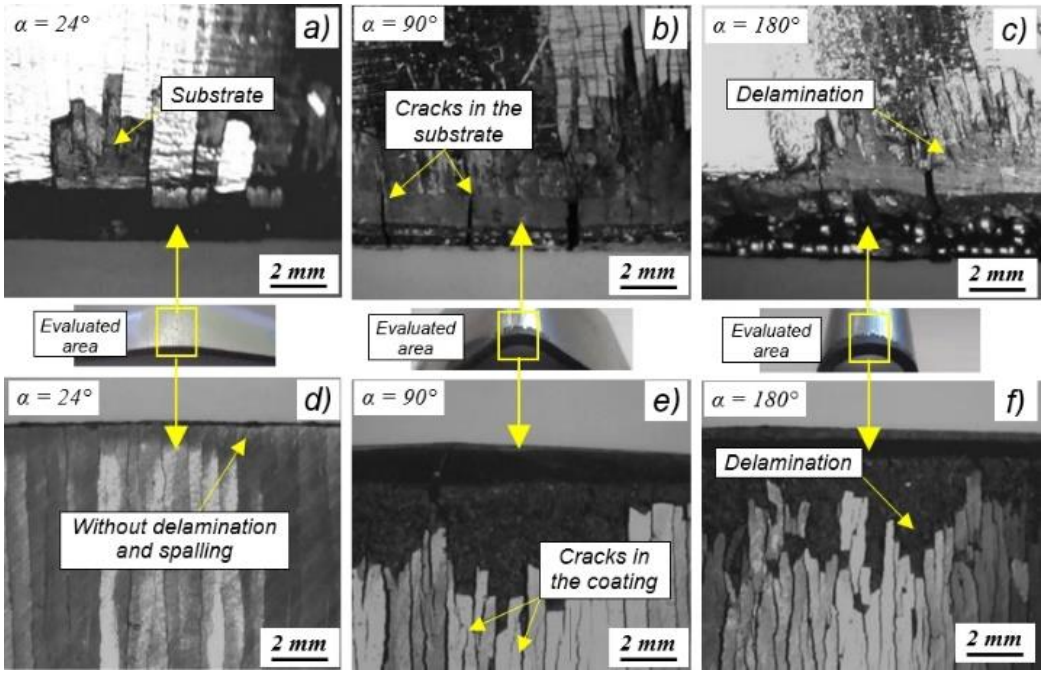

Figure 3.8 - Macrographic images of specimens for identification of failures on the edge for each bend angle: (a, b, c) Hard Chrome and (d, e, f) WC-CoCr.

3.3.3 *Friction and wear performance*

Evolution of the friction coefficient and wear rate for the coatings were evaluated by carrying out tests according to ASTM G99 and ASTM G65. During the polishing of the specimens, the initial roughness was controlled to avoid exceeding the Ra value of 0.8 µm so that the roughness does not influence the surface cracks and the wear rate. Table 3.7 presents the initial roughness values for the established parameters of these surfaces.

Table 3.7 - Measurement of initial roughness of specimens.

Coatings	**Average – before test**			
	Ra [µm]	**Rz [µm]**	**Rmáx [µm]**	**Rmr [%]**
Hard Chrome	0.26	1.79	2.49	61.68
WC-CoCr	0.12	1.08	1.68	90.57

First, the results of the pin on disc are presented for three specimens of each coating. During the tests, the evolution of the friction coefficients for the two coatings was evaluated (Fig. 3.9).

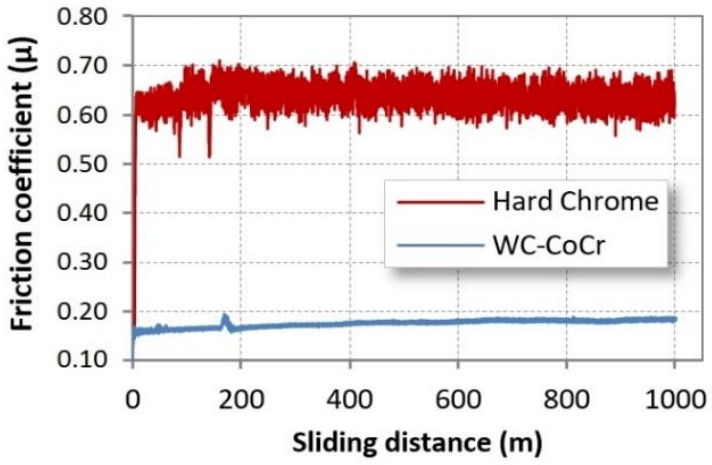

Figure 3.9 - Results of pin-on-disc test for the coatings: evolution of the friction coefficient.

The hard chrome coating showed an unstable friction coefficient from the beginning of the test. This instability is explained by plastic deformation contribution in the wear mechanism for this coating, observed in Fig. 3.10. Cancundo (2009) further justifies that, in the beginning of friction tests, a zone of instability occurs, i.e., the friction mechanisms are basically originated by the adhesion phenomenon. The frictional force of the relative movement between the pin and the disk should be enough to overcome the inertial force and

then the opposition to the motion generated by the initial peaks of roughness. These mechanisms were more evident in the hard chromium coating, identified up to the first 100 m of sliding, according to Fig. 3.9 (a). Blau (2005) states that this temporary fluctuation is a phenomenon called running-in, historically presented by Abbott Firestone in 1933. The author explains that this initial instability of the coefficient of friction in time not only has relation to aspects of asperities but also occurs in the materials adjacent to the surfaces, such as elastic and plastic irreversible deformation. During that deformation process, changes in crystallographic orientation and the state of work hardening (especially in metals) can occur (Blau, 2005). Debris can accumulate, and interfacial transfer can occur. Therefore, not only do the shape, texture, and roughness of the surface features change but their substructure and micro-mechanical properties do as well, and this can best justify the region of initial instability. However, in the WC-CoCr coating, these phenomena were practically not observed. Almost throughout the whole test time, material removal from the coating surface in the form of chips was observed. In the WC-CoCr coating, there was a stabile behavior of the coefficient of friction, characteristic of a lubricated sliding, which was justified by the detachment of fine reddish-brown particles. According to Fang (2009), the low friction of WC-CoCr is due to the formation of oxides particles (WO_3) that have lubricating properties, resulting in lower friction coefficients (Fang, 2009; Wesmann e Espallargas, 2014). Fig. 3.10 shows the wear tracks formed from the friction tests.

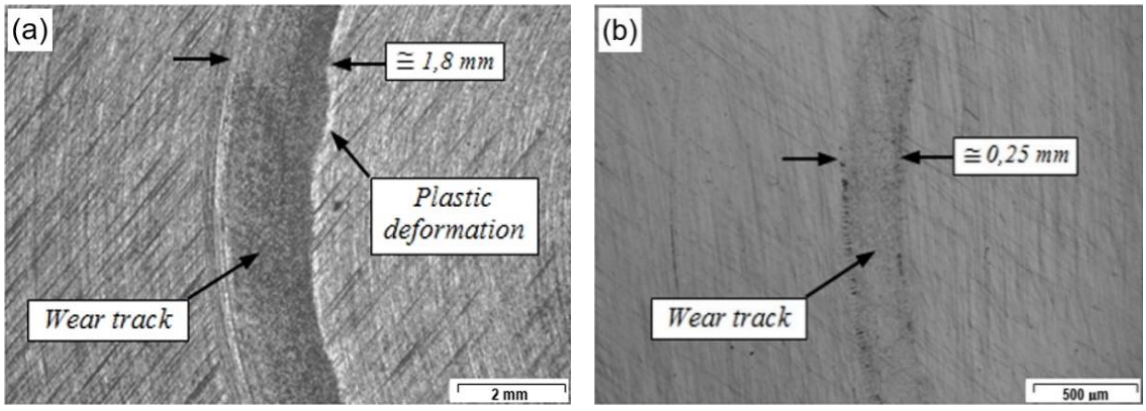

Figure 3.10 - Wear tracks for coatings: (a) Hard chrome and (b) WC-CoCr

The first observation is that for the same pin diameter used in tests, the tracks showed different widths. This fact is associated with the high hardness of the spray coating in comparison to the chrome coating, which inhibited plastic deformation and surface material pull-out. In the WC-CoCr coating, only a mild wear path was observed. However, for hard

chrome, the wear mechanisms such as plastic deformation and micro-cutting are confirmed by Fig. 3.10 (a) and 3.10 (b), respectively.

Also, Fig. 3.11 shows the significant difference of wear depth relative to the surface. For the carbide-based coating, the value was of 0.28 μm and, for hard chrome, this value exceeded 10 μm. According to Table 8, it is observed that the WC-CoCr test samples showed greater regularity in their values in relation to the volume of removed material. Considering the methodology used to quantify the volume withdrawn from the material, the hard chromium presented an approximate amount of removed material 212 times higher than that of the WC-CoCr coating, for a selected line width and its mean radius.

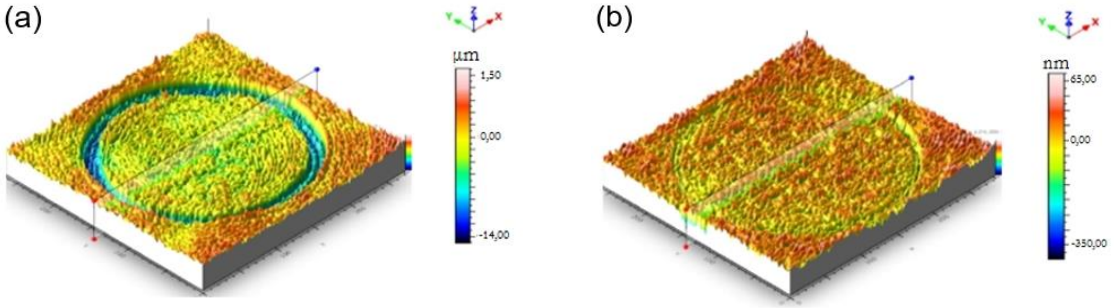

Figure 3.11 - 3D topography of surface (True Map software): (a) Hard chrome and (b) WC-CoCr.

With the top images of the surfaces, created with 2D/3D profilometry, it was possible to estimate the wear volume by the average profile of each coating, as presented in Table 3.8.

Table 3.8 - Removed material volume of coatings quantified by profilometry.

Coatings	**Mean volume removed, Vr [mm^3]**
WC-CoCr	0.0045 ± 0.0011
Hard Chrome	0.977 ± 0.333

For hard chrome, the mean width of the track was approximately 1.8 mm, while for WC-CoCr it was 0.25 mm. According to Bailey (2011), the high wear on electrodeposited hard chrome coating is justified by the density of microcracks presented by the hard chromium coating [Bailey, 2011). This method of measurement did not consider plastic deformation occurring during sliding in the hard chromium coating. However, this result was important to show only one qualitative on the WC-CoCr coating, confirmed also later by Fig. 3.16.

After the friction tests, the coatings were subjected to the abrasive wear test using dry sand and rubber wheel. To understand the wear behaviour, the worn coatings were examined using SEM. Fig. 3.12 and 3.13 shows the worn surface of each coating wiped by rounded silica sand (SiO_2) of 250-300 μm after 30 minutes, shown in two levels of magnification.

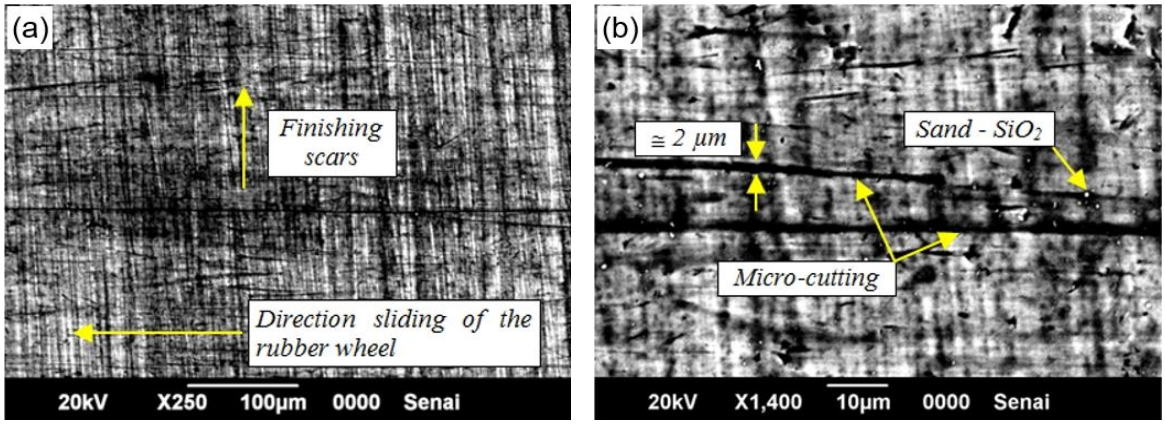

Figure 3.12 - Surface of hard chrome coated surfaces after wear test. No etched.

In Fig. 3.12 (b), scratches with a width of approximately 2 μm in the sliding direction are seen. This characterizes the action of a micro-cutting mechanism in the surface of the hard chrome. It is also important to note the concentration of sand particles (SiO_2) embedded in the tested surface. Fig. 3.13 shows the surface of the WC-CoCr before the abrasion test and after the abrasion test for the worn and not worn regions.

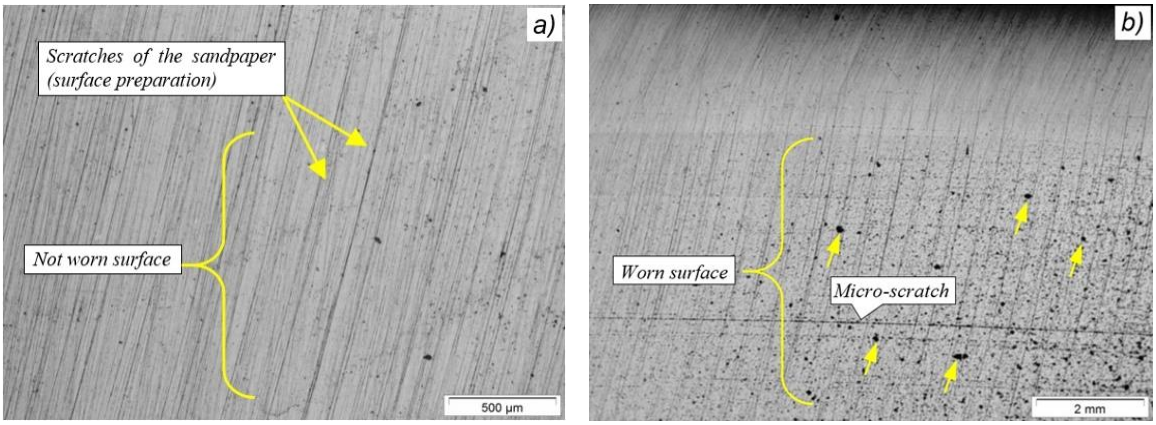

Figure 3.13 - Microstructural analysis of the WC-CoCr surface at different magnifications: a) not worn surface and b) worn surface.

After the abrasion test, the WC-CoCr micrograph reveals carbide removal (marked by arrows in Fig. 13 b). However, with a reduction of ploughing mechanisms, compared to the hard chromium coating. The evidence, even when punctual, of the WC matrix pull-out

is visible, and occurs due to the low hardness of the binder (Co). Removal of cobalt leads to a lack of bonding material, eventually resulting in carbides being plucked from the surface (Sudaprasert et al, 2003; Stewart et al, 1999; Wang et al, 2013). Carbide removal is evidenced by the increase of the roughness Ra (Table 9) and by the images produced with SEM-EDS analysis. Additionally, Fig. 3.13 (b) showed some micro-scratches from the test process but with extremely small track width dimensions (approximately 0.033 μm) compared to hard chrome. Figures 3.14 and 3.15 show the SEM-EDS analysis. Fig. 3.14 (a) shows the coating's topography; Fig. 3.14 (b) shows the splitting of the WC matrix; Fig. 3.14 (c) shows microcracks; and in Fig. 3.14 (d) shows a remaining grain of sand resulting from the sandblasting process.

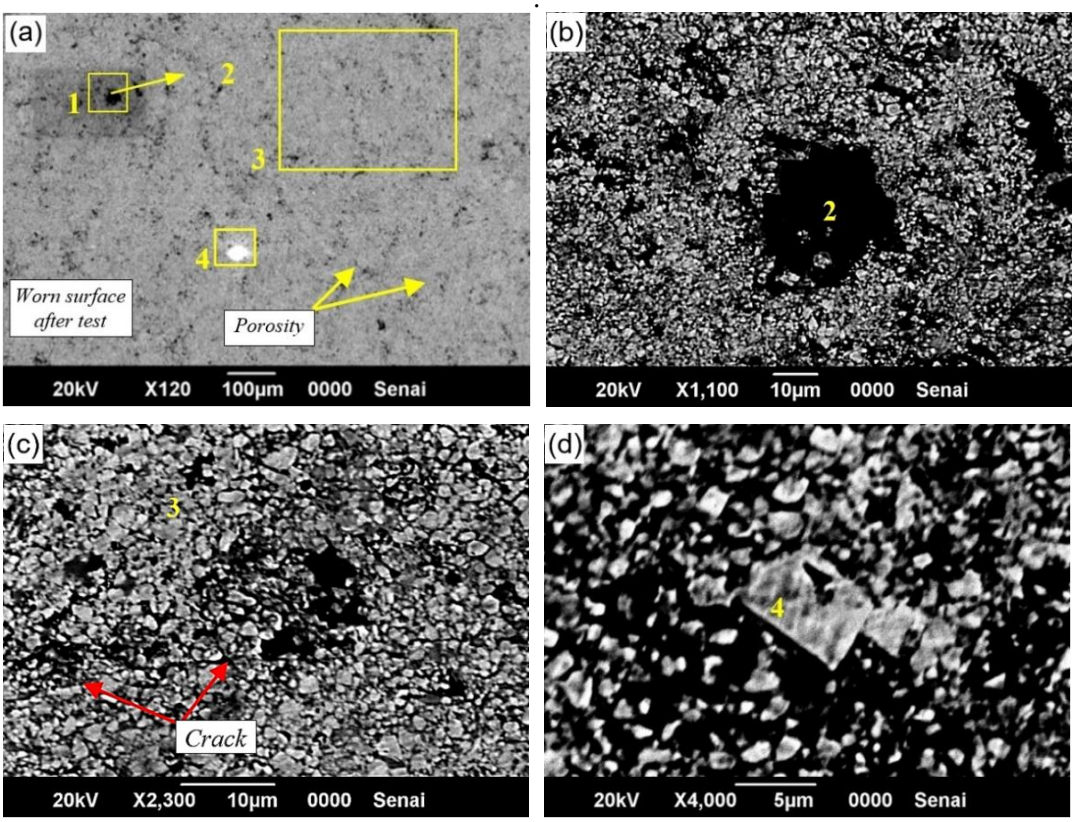

Figure 3.14 - SEM micrographs after abrasive wear test in WC-CoCr specimens. a) worn surface after test, b) splitting of the WC matrix, c) crack and d) grain of sand

The first observations obtained by SEM of the specimens sprayed with WC-CoCr (Fig. 3.14 a) showed a high-density coating characteristic of the HVOF process, although porosity is present, as a characteristic of the HVOF process. Fig. 3.14 (b) shows a structure with a pull-out characteristic of the WC matrix (hard phase), which was then confirmed by EDS analysis at this point (point 2). Cracks were detected in the longitudinal direction of the sprayed layer (Fig. 3.14 (c)). Usually, this defect is related to incorrect procedures in the

preparation of the surface for the wear test, as high speed and force used in the sanding and polishing of the specimens. Fig. 3.14 (d) shows an SiO_2 particle, which was the abrasive material used in the wear tests. The same image shows, even after the cleaning performed to obtain the images, that a small particle of silica of approximately 10 to 15 μm remained embedded in the surface of the coating. Fig. 3.15 shows the composition of the elements identified by SEM at the points indicated in Fig. 3.14.

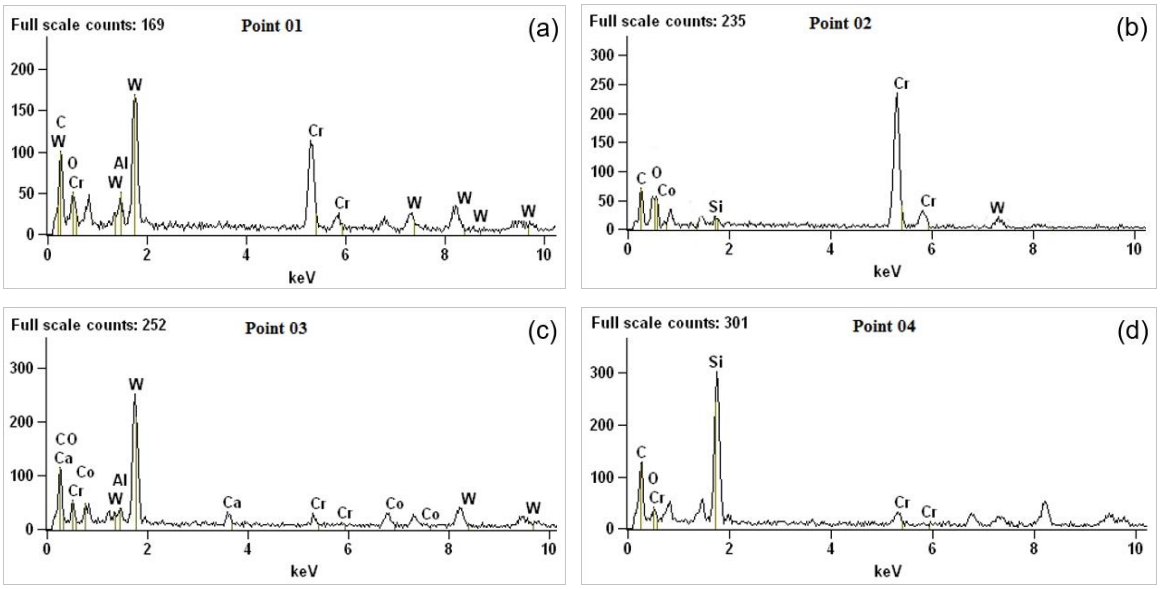

Figure 3.15 - EDS patterns of the four points analyzed for WC-CoCr coatings: (a) point 1, (b) point 2, (c) point 3 and (d) point 4.

In order to identify the defects produced in the WC-CoCr tests, images were captured at the points 1, 2, 3 and 4 of the microstructures. For the point 1 in Fig. 3.15 (a), the EDS spectra identified particles containing carbide and chromium, which are main elements of the sprayed coating, confirming it was a pore. At point 2, a large concentration of chromium was found and a smaller amount of cobalt. It is estimated that, with the sliding of the SiO_2 grain particles, pull-out of hard WC particles occurred, with only residues of the CoCr binder matrix remaining. At point 3, a coating region containing the WC-CoCr alloy was also identified in higher concentration. Point 4 revealed the presence of the silicon element present in the abrasive material (SiO_2), which means that, at some points, the abrasive material remained in the coating.

The tracks characteristic of the abrasive test made by rubber wheel and sand, as well as the wear volumes of the tested coatings, are shown and quantified in Fig. 3.16. The hard chrome specimen (Fig. 3.16 a) shows a more visually pronounced wear than the WC-CoCr specimen. In Fig. 3.16 (b) the HVOF coating presented a higher performance than that of

the hard chrome, with volume removed of 2.2E-10 m^3 and 14.8E-10 m^3, respectively. The wear rate occurs due to the higher difference in hardness between the abrasive material (SiO_2, $HV_{0.01} \approx 1100$) and hard chromium ($HV_{0.01} \approx 952$). According to the literature, this would lead to higher plastic deformation increasing the removed material rate (Magnani, 2014). For the WC-CoCr coating, a higher hardness (1256 $HV_{0.01}$) was identified than that of the abrasive material, resulting in a low volume of removed material.

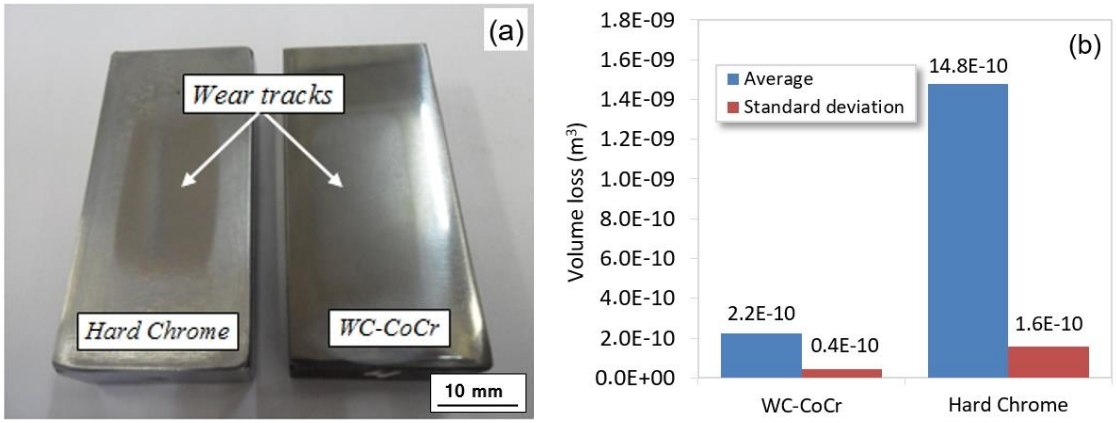

Figure 3.16 - Results of wear test - ASTM G65-00: (a) Track characteristics of the test and (b) mean of the removed volume according to equation 1.

To evaluate the surface finishing of the coatings after testing, roughness was measured. The comparative values of the measurements are shown in Table 3.9. Based on the presented results, it is possible to state that the WC-CoCr coating presented better performance in relation to the main parameters, Ra and Rmr, because was found the best indexes applied to the sealing surfaces in application of hydraulic cylinders (Flitney, 2007).

Table 3.9 - Measurement of roughness before and after the wear test.

Parameters	**Average – before test**		**Average – after test**	
	Hard Chrome	**WC-CoCr**	**Hard Chrome**	**WC-CoCr**
Ra [µm]	0.26	0.12	0.11	0.17
Rz [µm]	1.79	1.08	0.83	1.25
Rmáx [µm]	2.49	1.68	1.07	1.42
Rmr [%]	61.68	90.57	93.01	80.29

It was observed that an increase in roughness values (Ra) occurred for WC-CoCr coatings. This increase occurs due to the pull-out of carbides (appearance of pores) seen in the SEM images, Fig. 3.14 (a) and (b). Koutsomichalis et al., (2017) describe the phenomenon of pull-out of carbides in wear tests. However, for the hard chrome coating, the Rmr values would be not promising for hydraulic sealing applications due to its polishing,

observed by the Ra drop and the Rmr increase in relation to the values recommended by literature (Leach, 2001; Steep and Wüstenhagen, 2006), which should be around 80 % while the observed values after the wear tests are of 93 %. The polishing effect would cause the deformation of the sealing member due to the difficulty of lubrication by the low levels of valleys on the surface. However, for the Ra parameter, the chrome coating still appears within the limit range for sealing surfaces.

It is important to point out that these results alone do not define an ideal condition for surfaces applied to hydraulic seals. Other factors in actual working conditions for the hydraulic rods will also be important in determining a new coating, and it is important to obtain data from dynamic tests of rods and hydraulic sealing behavior measuring the leakage rates.

3.4 Conclusions

- The microstructure of the WC-CoCr coating showed a discrete oxide film between the layers with low porosity (<1.0%). Moreover, the sprayed coating presented high hardness, of the order of 1250 $HV_{0.01/15}$, but with a higher standard deviation when compared to hard chromium coating, which presented microcracks in the analyzed layer. This shows that the electrodeposited process contributes and anticipates the abrasive wear and the oxidation of the base material. However, microcracks, when in controlled amounts, can become positive, in the lubricated contact, which is the case of hydraulic rods.
- In bending tests, cracking and peeling of the coating depends on the bending angle. Low crack density was observed in the WC-CoCr coating compared to hard chromium. Additionally, no scattering was found at the 24º bend angle. In the tests, there was radial cracking and delamination of the coatings at the specimen edges. The number of cracks was smaller for thicker coatings.
- In the pin on disc tests, the WC-CoCr coating presented a lower friction coefficient, resulting in a wear track of significantly smaller width than for hard chrome. Furthermore, the WC-CoCr coating presented a lower friction coefficient, resulting in a significantly smaller wear track than for hard chrome. In these tests, the hard chromium presented greater deformation and greater removed volume than the WC-CoCr coating. Also, the low values of the coefficients of friction of the WC-CoCr coating are due to the formation of oxides WO3, previously described.

- The abrasion wear resistance of the WC-CoCr coating is much higher than that of the hard chromium coating due to surface hardness. In the tests of hard chrome, the abrasive mechanisms of micro cuts and micro-scratches were present. However, in the WC-CoCr coating, only the spalling of carbide micro particles, which was caused by the removal of the cobalt matrix, was observed.
- Roughness measurement of the parameter Rmr for the WC-CoCr coating results, for seal support area, in a value of 80 %, showing that the coating produced by HVOF benefits the hydraulic sealing systems of the rod. This result is mainly related to the topographic characteristics of the WC CoCr coating produced by HVOF.

3.5 Acknowledgements

The authors thank Rijeza Metalúrgica LTDA for the cooperation in this project supplying the coatings and equipment for thermal spraying, the colleagues of the Surface Engineering Group (GES) of the LdTM-UFRGS, and the Faculty SATC for the availability of the laboratories. The authors would also like to thank Brazilian CNPq (National Council for Scientific and Technological Development) for the support in the process 311348/2015-7.

3.6 References

[1] PAWLOWSKI, L. **The Science and Engineering of Thermal Spray Coatings**. 2nd. ed. England: John Willey & Sons; 2008.

[2] FLITNEY, B. **Alternatives to Chrome for Hydraulic Actuators**. Sealing Technology. 10: 8-12, 2007.

[3] SARTWELL, B. D.; LEGG, K. O.; ZIMMERMAN, Z.; REYNOLDS, M.; GRIBRO, J.; MASON, R. **Validation of HVOF Thermal Spray Coatings as a Replacement for Hard Chrome Plating on Hydraulic/Pneumatic Actuators**. U.S. Department of Defense, Environmental Security Technology Certification Program (ESTCP), Washington, USA; 2006.

[4] MOJENA, M. A. R.; OROZCO, M. S.; FALS, H. C.; ZAMORA, R. S.; LIMA, C. R. C. **A Comparative Study on Slurry Erosion Behavior of HVOF Sprayed Coatings**. Revista DYNA, 84: 239-246, 2017.

[5] PATHAK, S.; SAHA, G. C. **Development of Sustainable Cold Spray Coatings and 3D Additive Manufacturing Components for Repair/Manufacturing Applications: A Critical Review**. Coatings, 7 (122): 1-27, 2017.

[6] DEGENNARO, T. **Evaluation of Chrome Rod Alternative Coatings**. ASTN - Aerospace Sealing Technologic News, 11: 3-4, 1999.

[7] GHABCHI, A.; VARIS, T.; TURUNEN, E.; SUHONEN, T.; LIU, X.; HANNULA, S. P. **Behavior of HVOF WC-10Co4Cr Coatings with Different Carbide Size in Fine and Coarse Particle Abrasion**. Journal Thermal Spray Technology, 19: 368–377, 2010.

[8] WESMANN, J. A. R.; ESPALLARGAS, N. **Effect of Atmosphere, Temperature and Carbide Size on the Sliding Friction of Self-mated HVOF WC–CoCr Contacts**. Tribology International, 101: 301-313, 2016.

[9] LEACH, R. **The Measurement of Surface Texture Using Stylus Instrument. Measurement Good Practice Guide**. 2001: 37. United Kingdom.

[10] STEEP, F.; WÜSTENHAGEN, G. **Counter Surface Hydraulic Seals for Heavy Duty Applications**. Sealing Technology, 8-9, 2006.

[11] ASTM E 384-89. **Standard Test Method for Microindentation Hardness of Materials**. West Conshohocken: ASTM International, 2017.

[12] ASTM E 190-92. **Standard Test Method for Guided Bend Test for Ductility of Welds**. West Conshohocken: ASTM International, 2014.

[13] ASTM G65-00. **Standard Test Method for Measuring Abrasion Using the Dry Sand/Rubber Wheel Apparatus**. West Conshohocken: ASTM International, 2016.

[14] ASTM G99-04. **Standard Test Method for Wear Testing Whit a Pin on Disc Apparatus**. West Conshohocken: ASTM International, 2017.

[15] VENCL, A., AROSTEGUI, S., FAVARO, G., ZIVIC, F., MRDAK, M., MITROVIC, S., POPOVIC, V. **Evaluation of Adhesion/Cohesion Bond Strength of the Thick Plasma Spray Coatings by Scratch Testing on Coatings Cross-sections**. Tribology International, 44: 1281–1288, 2011.

[16] AGÜERO, A.; CAMÓN, F.; GARCÍA, J.; HOYO, J. C.; MUELAS, R., SANTABALLA, A.; ULARGUI, S.; VALLÉS, P. **HVOF-Deposited WC-CoCr as**

Replacement for Hard Cr in Landing Gear Actuators. Journal of Thermal Spray Technology, 20: 1292-1309, 2011.

[17] BAILEY, M. **Case Study - Hard Chrome Plating Problems - Crazing and Pin Holes**, 2011. http://www.finishing.com/157/56.shtml (Accessed 12 July 2014)..

[18] CHATHA, S. S, SIDHU, H. S, SIDHU, B. S. **Characterization and Corrosion-Erosion Behaviour of Carbide based Thermal Spray Coatings**. Journal of Minerals & Materials Characterization & Engineering, 11 (6): 569-586, 2012.

[19] IACOVIELLO F.; DI COCCO, V.; Natali, V. **Cracking Mechanisms in a Hot-Dip Zinc Coated Steel**. In: 11th International Conference on Fracture (ICF11); 2005. March 20-25; Turin, Italy.

[20] CANGUNDO, E. M. **Avaliação Experimental da Condição Tribológica no Processo de Corte por Arranque de Apara**. Dissertação de Mestrado, IST – Instituto Superior de Lisboa, 2009.

[21] BLAU, P. J. **On the Nature of Running-in**. Tribology International, 38: 1007-1012, 2005.

[22] FANG, W. C. **Processing Optimization, Surface Properties and Wear Behavior of HVOF Spraying WC–CrC–Ni Coating**. Journal of Materials Processing Technology, 209: 3561-3567, 2009.

[23] WESMANN, J. A. R.; ESPALLARGAS, N. **Investigation of Oxide Formation on Sliding Interfaces of WC-CoCr in Relation to Friction and Wear.** ASM International, Proceedings from the International Thermal Spray Conference, 6: 674-679, 2014.

[24] SUDAPRASERT, T.; SHIPWAY, P. H.; MCCARTNEY, D. G. **Sliding Wear Behaviour of HVOF Sprayed WC–Co Coatings Deposited with Both Gas-Fuelled and Liquid-Fuelled Systems**, Wear, 255, p 943–949, 2003.

[25] STEWART, D. A.; SHIPWAY, P. H.; MCCARTNEY, D. G. **Abrasive Wear Behaviour of Conventional and Nanocomposite HVOF-Sprayed WC–Co Coatings**, Wear, 225: 789-798, 1999.

[26] WANG, Q.; ZHANG, S.; CHENG, Y.; XIANG. J.; ZHAO, X.; YANG, G. **Wear and corrosion performance of WC-10Co4Cr coatings deposited by different HVOF and HVAF spraying processes.** Surface and Coatings, 218: 127-136, 2013.

[27] MAGNANI, M. **Estudo da Resistência ao Desgaste e à Corrosão de Revestimentos Metálicos-Cerâmicos Aplicados na Liga AA7050 Mediante Aspersão Térmica Oxi-combustível de Alta Velocidade (HVOF).** Tese de Doutorado, UNESP - Universidade Estadual Paulista, Araraquara, SP, Janeiro, 2014.

[28] KOUTSOMICHALIS, A.; VARDAVOULIAS, M.; VAXEVANIDIS, N. **HVOF sprayed WC-CoCr Coatings on Aluminum: Tensile and Tribological Properties**. IOP Conf. Series: Materials Science and Engineering, 174: 1-10, 2017.

4. ANALYSIS OF THE TRIBOLOGICAL PERFORMANCES OF BIODEGRADABLE HYDRAULIC OILS HEES AND HEPR IN THE SLIDING OF Cu-Zn/WC-CoCr ALLOYS USING THE STRIBECK CURVE

Richard de Medeiros Castro[1], Elvys Isaías Mercado Curi[1], Luiz Fernando Feltrin Inácio[1], Alexandre da Silva Rocha[2]

[1]Department of Mechanical Engineering, SATC College, Criciúma-SC, Brazil
[2]Department of Metallurgical Engineering, UFRGS - Federal University of Rio Grande do Sul, Porto Alegre-RS, Brazil

Abstract

In surface engineering, new coatings, and deposition techniques for decreasing wear have been proposed. However, the tribological behaviors of these coatings under lubricated sliding with biodegradable oils are unknown. The objective of this study is to evaluate the tribological behaviors of two hydraulic biodegradable oils, namely, hydraulic environmental ester oil synthetic (HEES) and hydraulic oil environmental polyalphaolefin (HEPR), with hydraulic mineral oil (HLP), using a pin-on-disk tribometer. In the sliding tests, a Cu-35Zn sphere against a flat surface is coated with WC-10Co4Cr alloy using a HVOF - thermal spray. The Stribeck curve was used to evaluate the performances of the lubricants. The coefficient of friction, the contact pressure, and the film thickness were determined. In addition, the coefficient of wear of the sphere was evaluated, and the oil with the lowest value was identified, which was HEPR in this case. In long-term tests, HEPR was affected by the stick-slip phenomenon, which increased the coefficients of friction and wear. Furthermore, the mechanism of adhesion of the sphere on the disk was more evident with the use of HEES compared to HLP. The highest concentrations of Zn and P and the pressure-viscosity coefficient value, which was detected in the mineral oil, caused friction reduction and lower damage to the surfaces. Therefore, it is important to evaluate the tribological conditions of synthetic bio-lubricants for applications in hydraulic systems.

Keywords: Biodegradable oil. Lubrication regimes. Stribeck curve. Coefficient of friction and wear. Cu-35Zn. WC-10Co4Cr.

4.1 Introduction

Tribology contributes to the development of new materials and manufacturing processes, thereby enabling the industry to be more efficient as it extends the lifetimes of elements of machines [1]. Although various improvements are realized, not all areas of engineering benefit equally, as in the case of components that are used in the fluid power systems. In addition, problems that are related to the disposal of materials must be supported by environmental laws that specify how to properly discard worn components of machines. The combination of tribology and environmental care is a vision for the industry of the future [2,3]. Thus, the use of materials and processes with higher performance and lower impact on the environment should be financially encouraged [3]. Anand et al. [4] describe this combination as "green tribology," which deals with interacting surfaces and considers energy/environmental sustainability. Green tribology primarily deals with friction and wear, which are principal factors from an energy conservation perspective. Green tribology also involves environmental aspects of lubrication, new materials and alloys, and surface modification techniques [3].

The use of eco-friendly/biodegradable oil as a substitute for mineral oil and the use of alternative surface coating techniques reduces the impact on the environment, which is required by the industry. The combination of biodegradable oils with surfaces that are coated with materials of lower environmental impact is important for the sustainability and growth of the modern industry. Sustainable and efficient hydraulic machine designs consider replacing mineral oils with vegetable oils and synthetic biodegradables. This replacement is due to the high probability of seal rupture and, consequently, oil leakage, which would result in major environmental pollution to water or soils. It is estimated that 50% of all lubricants in the world end up being spilled into the environment through improper disposal, leaks, and accidents. Researchers have discussed the need for new projects for biodegradable oil applications in machines that are using in agriculture, the oil industry (offshore), and hydroelectric plants, among other activities [5-8].

In recent decades, research on hydraulic oils has been strongly influenced by the need for the development of hydraulic components and systems, and the requirements and their new applications [8]. However, mineral hydraulic oils are subjected to even tighter controls every day due to their environmental and toxicological impacts [9]. Therefore, there is an incentive to use biodegradable fluids, and in some projects, biodegradability has become one

of the most important parameters for both fluid choice and lubricant formulation [10]. Three types of base fluids find applications in the formulation of biodegradable, environment-friendly lubricants: mineral oils, vegetable oils, and synthetic lubricants. For applications in hydraulic systems, rapidly biodegradable fluids are classified according to ISO 6743/4 and ISO 15380 as natural esters (HETG type), synthetic esters (HEES type), polyglycols (HEPG type), and polyalphaolefin or hydrocarbon (HEPR type) [11, 12].

Several studies on the use of biodegradable oils that involve bio-based lubricants are presented in the literature, in which results regarding the physicochemical properties and tribological performances were obtained. For the investigating tribological characteristics, various test methods and equipment have been used. However, the main objective remained the same, namely, to study the performance of a bio-based lubricant in terms of friction and wear behavior [13]. Majdam et al. [12] evaluated the wear and tear of a hydraulic pump for HEES and HEPR biodegradable hydraulic oils compared to mineral oil. The results demonstrated a lower loss of efficiency in mineral oil testing. However, in terms of eco-friendliness, HEPR had only a 1.03% efficiency loss, while for HEES, it was 7.3 %. Another study that was carried by Kučera el al. [14] compared a sliding pair with a B60 bearing and a journal with a contact surface that was made of 16MnCr5 steel. The lubricated tests were conducted using biodegradable oil HEES and mineral oil. In this study, the results demonstrated a satisfactory tribological performance for eco-friendly HEES. However, the mineral oil presented lower temperature at the end of the test. Tkáč et al. [15] examines the use of a biodegradable fluid in the hydraulic system of an agricultural tractor and demonstrates that this fluid had no negative impact on the sealing components of the system.

The function of lubricants is to prevent contact or to reduce friction between sliding surfaces [16]. However, the combination of the properties of biodegradable lubricants that are applied to coated surfaces must be investigated. These contact conditions require research on new materials and surfaces, to assess the synergy or incompatibility that may occur between eco-friendly lubricants and coated surfaces. Therefore, to evaluate the performances of lubricants on these new surfaces, it is necessary to perform sliding tests under various lubrication regimes. Typically, the Stribeck curve and the Hersey number are used for this evaluation [17].

The Stribeck curve is an experimental model that is used to determine the lubrication regimes of a metallic pair under lubricated sliding for evaluating the results of friction and wear [17,18]. The lubrication regimes may be classified into four types: boundary, mixed,

elastohydrodynamic, and hydrodynamic. This approach is linked with the viscosity properties of the lubricant (η_0), the speed of rotation of the shaft (U_e), the contact load (P_{mean}), the root-mean-square roughness of the surfaces (σ_{RMS}), and the coefficient of friction [19-21]. Typically, the ratio ($\eta_0.U_e/P_{mean}.\sigma_{RMS}$) is used in the abscissa axis of the diagram, which is proportional to the thickness of the lubricating film (h), which is calculated based on fluidic lubrication concepts.

Satisfactory engineering design in the field of fluid power yields improvements in the tribological system of the hydraulic components. These improvements increase the performance and decrease the power consumption of the machines, which reduces the maintenance cost and the frequency of failure in the sealing systems of these components. This concern with design and with the reduction in the energy consumption of the machines directly affects the environment, as it reduces the CO_2 emissions into the atmosphere [22].

Due to worldwide concern regarding the disposal of worn-out materials in the environment, several techniques for the deposition of metallic coatings can contribute to the improvement in the surface properties of these mechanical components, which, in some applications, must operate with biodegradable oils. Among the main techniques of deposition, the following are prominent: laser cladding, chemical and physical vapor deposition (CVD/PVD), and high-velocity oxygen fuel (HVOF) thermal spray [23–25]. For over 50 years, hard chrome plating has been used; however, this coating has poor tribological properties. In addition, the high levels of hexavalent chromium Cr^{+6} that are present have high carcinogenic power and result in environmental contamination [26]. The thermally sprayed WC–10Co4Cr alloy HVOF realizes satisfactory tribological performance and has lower environmental impact [27–29].

In this study, the authors present several results that demonstrate excellent mechanical and tribological characteristics for future applications in hydraulic system components. In this study, the tribological behaviors of the materials that are used in the manufacture of hydraulic pumps and cylinders were analyzed, which were subjected to lubricated sliding tests. The tests were conducted in a pin-on-disk tribometer, and biodegradable industrial synthetic oils (HEES and HEPR) and traditional mineral oil (HLP) were used as lubricants. An AISI 1045 steel disk that was coated with WC–CoCr alloy and manufactured via thermal spraying-HVOF, and a brass sphere (Cu35Zn) were used to simulate the contacts of the sliding materials. For the evaluation of the lubrication regimes and of the tribological aspects, namely, of the coefficients of friction and wear, mathematical

models from the scientific literature and the ASTM G99 standard, which was adapted for lubricated conditions, were used. In addition, measurements of the physical properties and chemical compositions of the lubricants were conducted, along with an analysis of the surfaces of the disk tracks via scanning electron microscopy and energy-dispersive spectrometry (SEM/EDS), to evaluate the friction and wear behaviors and the mechanisms of damage to the surfaces after sliding.

4.2 Experimental procedure

The analysis of the lubricating oils is conducted with identical tests and with rheological and tribological models that relate the variables of lubrication and the coefficients of friction and wear.

4.2.1 *Pin-on-disk tribometer*

A pin-on-disk tribometer, which was adapted from standard ASTM G99-17, was used to simulate the contact sliding of materials that are used in hydraulic components [27,30]. The pin-on-disk method utilizes a horizontal rotating disk and a pin that is loaded with a calibrated weight. In this study, a 6-mm spherical tip geometry was used as a pin, which supports the applied load (F_n) stationary against a rotating disk, as shown in Fig. 1. This tribometer enables the measurement of the force and the coefficient of friction, which are measured by a load cell. The speed of rotation (ω) and the linear distance that is traveled (S) during the test are monitored by an inductive proximity sensor. The sphere and disk slide inside a reservoir that is designated at “cup,” which contains lubricating oil.

The temperature and the humidity were maintained during the tests at 30±3 °C and 40±1.0 %, respectively. The experimental parameters are presented in Table 1. For all tests, the tangential speed of the disk was adjusted to 0.4 m/s. Prior to each test, all specimens (disk and sphere) were cleaned in an ultrasonic bath, washed with isopropyl alcohol, and dried. Two disposable syringes were used for the insertion and removal of the lubricant in the cup that was used as a reservoir. At each applied load or total completed time, the used lubricant was removed, and a new lubricant was inserted with a volume of 10 ml.

Two sets of tests were conducted. In the first set of tests (Test 1), the behaviors of the lubrication regimes, the friction coefficient evolution and the minimum film thickness

were evaluated using a disk radius of 18 mm for each normal load, as presented in Table 4.1. Additionally, in these tests, the contamination of the lubricants by solid particles was evaluated based on physicochemical properties, which were measured via inductively coupled plasma spectrometry (ICP). In the second set of tests (Test 2), tests with durations of 1, 2, 3, 4, and 5 h were conducted, thereby resulting in linear distances of 1500 to 7500 m. These tests were conducted using a normal 30 N load on a 20 mm radius disk. These long-term tests were to evaluate the mechanisms of damage on pin and disk surfaces and the trends of pin-on-disk wear and friction behaviors, in combination with the use of biodegradable hydraulic lubricants.

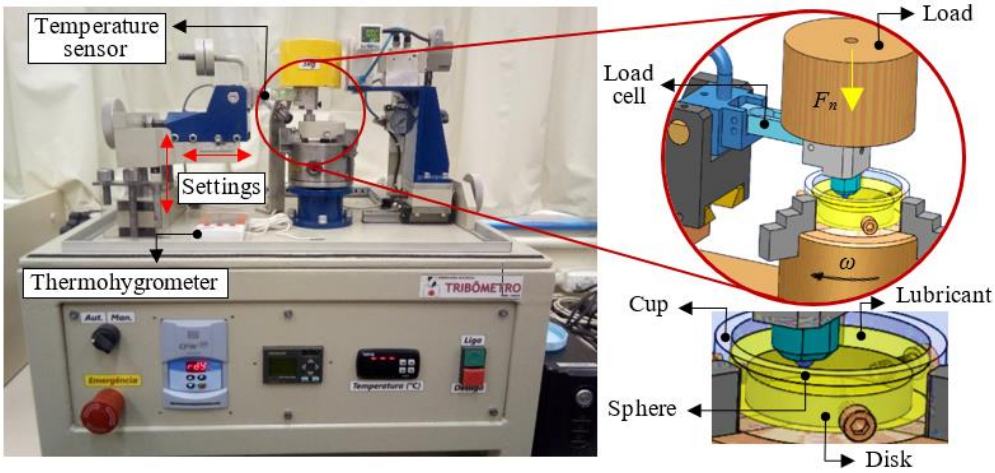

Figure 4.1 - Pin-on-disk tribometer: details of the lubricated sliding test.

Table 4.1 - Experimental conditions of the tests.

No	Quantities	Values – Test 1	Values – Test 2	Unit
1	Track radius - disc	18	20	mm
2	Disc diameter	60	60	mm
3	Normal load - F_n	0.3, 1, 4, 10, 30, 50, 60	30	N
4	Linear distance traveled	125	1500, 3000, 4500, 6000, 7500	m

4.2.2 *HVOF coating and sliding materials*

The disks that were used as test specimens were manufactured from AISI 1045 steel and coated with WC-10Co4Cr alloy using HVOF. As the body, a spherical pin of Cu-35Zn (brass) was used to simulate the materials that are used in the manufacture of hydraulic components. The chemical compositions of these materials are listed in Table 4.2.

Table 4.2 - Chemical composition (% in mass) of the disc and sphere coating surface.

Materials	W	Co	Cu	Cr	Zn	C (total)	Si	Ca	Fe (max)	O
Disc	Balance	10.72	---	4.53	---	4.72	---	---	0.032	0.21
Pin	---	---	Balance	---	37.2	---	0.538	0.032	---	---

The tungsten carbide coating was fabricated using a spray gun-HVOF. The main parameters, which are adjusted for deposition by thermal spraying, are presented in Table 4.3.

Table 4.3 - Parameters for thermal spraying – HVOF.

No.	Parameter	Value	Unit
1	Nitrogen flow	5.19E-3	m^3/s
2	Oxygen flow	1.21E-3	m^3/s
3	Kerosene flow	3.87E-4	m^3/s
4	Torch displacement speed	0.25	m/s
5	Powder feed rate	15E-4	kg/s
6	Distance from gun to specimen	0.305	m
7	Combustion pressure	7.1E5	Pa

4.2.3 *Lubricants*

Industrial biodegradable hydraulic lubricants with ISO viscosity grade 46 were selected: hydraulic environmental ester oil synthetic (HEES) that was produced from synthetic hydrocarbons, and hydraulic oil environmental polyalphaolefin (HEPR) and related products. In addition, mineral oil hydraulic fluid (HLP) was used in the tests to obtain data for comparison. Table 4.4 presents the specifications and physical-rheological properties, in which the viscosity for each lubricant was evaluated using a rheometer.

Table 4.4 - Characteristics of the lubricants.

No	Properties of lubricants	HEES	HLP	HEPR
1	Viscosity index	190	100	135
2	Kinematic viscosity at 40 ºC, mm^2/s	47.1	45.8	44.3
3	Kinematic viscosity at 100 ºC, mm^2/s	6.1	5.6	8.1
4	Density at 15 ºC, kg/m^3	923	876	881
5	Pressure-viscosity coefficient, mm^2/N	1.38×10^{-8}	1.82×10^{-8}	1.58×10^{-8}
6	Ecological damage level	Low	High	Low

The viscosity behavior as a function of the temperature was determined using the Reynolds mathematical model [31], which is expressed in Eq. 1, where η_0 is the dynamic viscosity at atmospheric pressure, T_A is the absolute temperature, and "b" and "a" are constants that are obtained empirically from measurements by the rheometer.

$$\eta_0 = be^{-aT_A} \ [Ns/m^2] \tag{1}$$

The coefficient of pressure-viscosity (α) is also specified in Table 4.4. This coefficient affects the formation of the lubrication film and the energy dissipation [32]. The authors show that the pressure–viscosity coefficient of a fluid is directly proportional to the average friction in a sliding contact in the elastohydrodynamic region. This ratio of pressure to viscosity is conventionally expressed by the Barus equation, which is presented as Eq. 2, where η_P is the dynamic viscosity at pressure P, η_0 is the dynamic viscosity at atmospheric pressure, and α is the pressure-viscosity coefficient.

$$\eta_P = \eta_0 e^{\alpha P} \ [Ns/m^2] \tag{2}$$

The HEES and HEPR ecological lubricant oils were selected according to the characteristics of the application in fluid power systems. HEPR-type lubricants are also classified as ecological fluids and have superior rheological properties over a wide range of temperatures compared to mineral-based oils of the same viscosity grade [33,34]. Although these ecological products cost approximately seven times more than mineral oils, they are typically used in hydraulic systems that operate at high pressure and at a high temperature. The main advantages of biodegradable fluids are their stability under temperature variation, their satisfactory lubrication properties, and their compatibility with the main types of seals [35].

4.2.4 *Contact conditions and test procedure*

The objective of the tests was to simulate the conditions of lubricated sliding contacts of surfaces that are used in components of hydraulic systems. The roughness of the disk and sphere surfaces was within the specifications that were used by the manufacturers of hydraulic cylinders and pumps [36].

In this case, the normal loads were applied according to Table 4.1, and the loads produced average contact pressures between the ball and the disc from about 173 to 1011

MPa. In addition, these seven normal load values, which are denoted as F_n and listed in Table 1, were used to calculate the Hersey number, which is related to the coefficient of friction. Hence, it is possible to identify the lubrication regimes. The mean contact pressure P_{mean} between the sphere and the disk are calculated via Eq. 3 [21]:

$$P_{mean} = \frac{F_n}{\pi a^2} \ [N/m^2] \tag{3}$$

where a is the radius of the contact area resulting from the contact pressure and F_n is the normal force applied during the test. The radius a is determined from the Hertz pressure via Eq. 4.

$$a = \left(\frac{3F_n R'}{E'}\right)^{\frac{1}{3}} \ [m] \tag{4}$$

where R' and E' are the radius of curvature and the equivalent Young's modulus, respectively. These two quantities can be defined by Eq. 5 and Eq. 6, where $R_{1X} = R_{1Y} = 3 \times 10^{-3}\ m$ (radius of the sphere) and $R_{2X} = R_{2Y} = \infty$ (radius of the disk).

$$\frac{1}{R'} = \frac{1}{R_X} + \frac{1}{R_Y} = \frac{1}{R_{1X}} + \frac{1}{R_{2X}} + \frac{1}{R_{1Y}} + \frac{1}{R_{2Y}} \ [m] \tag{5}$$

$$E' = \frac{E_1 E_2}{E_2(1-{v_1}^2)+E_1(1-{v_2}^2)} \ [N/m^2] \tag{6}$$

where $E_{1,2}$ is the Young's modulus and $v_{1,2}$ is the Poisson's coefficient for the sphere and the disk, respectively, and R_X and R_Y are the radius of curvature in the X and Y directions of the contact regions, as illustrated in Fig. 4.2c.

The characteristics of the materials that are used as test specimens are presented in Figs. 4.2a and 4.2b and in Table 4.5.

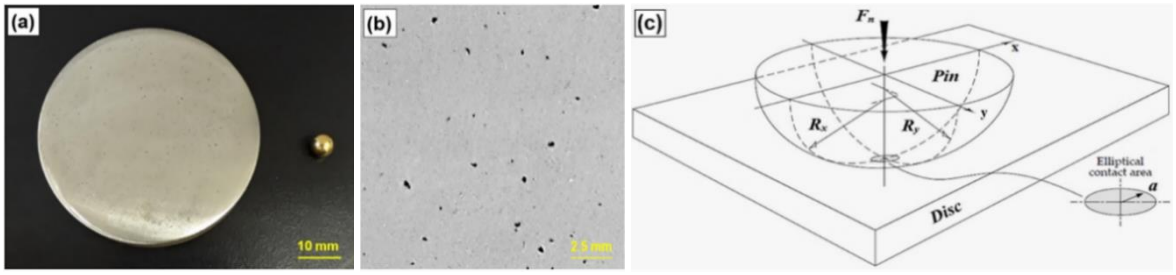

Figure 4.2 - Samples and point of contact: a) disk and pin (sphere), b) magnified view of the disk surface porosity and c) a schematic diagram of the contact region [37].

Table 4.5 - Characteristics of specimens - disc and pin.

No.	Properties of materials	Symbol	Disc parameters for each lubricant			Pin (sphere) for all fluids
			HEES	HLP	HEPR	
1	Young's modulus, GPa	E	580	580	580	110
2	Poisson's ratio	v	0.23	0.23	0.23	0.35
3	Microhardness, $HV_{0.02}$	H	1341 ± 55	1327 ± 61	1294 ± 73	172 ± 8
4	Roughness RMS - Rq, µm	S_q	0.135 ± 0.012	0.121 ± 0.010	0.105 ± 0.010	0.015 ± 0.004

To determine the thickness of the lubricant film for each loading condition and the lubricants, the elastohydrodynamic regime equation was used [38]. The minimum film thickness ($h_{mín}$) for a circular contact is calculated via Eq. 7:

$$h_{mín} = 3.63 \left(\frac{U_e \eta_0}{E' R'}\right)^{0.68} (\alpha E')^{0,49} \left(\frac{F_n}{E' R'^2}\right)^{-0.073} (1 - e^{-0.68k}) \; R' \quad [\mu m] \tag{7}$$

where U_e is the sliding velocity, η_0 is the dynamic viscosity of the lubricant at 30 °C, and k is the ellipticity parameter, which is equal to 1 for a circular contact. By varying the load F_n of sliding, various thicknesses of the lubricating film h_{min} are obtained, which are related to the friction. The behavior of the friction coefficient is represented by the Stribeck curve (Fig. 4.3), which is related to the lubrication regime via the Hersey number and is calculated via Eq. 8 [17]. The RMS roughness values, which depend on the equivalent amplitude of roughness (σ_{RMS}), are calculated from ${S_{q1}}^2$and ${S_{q2}}^2$which are the average roughness of the disk and sphere, respectively, via Eq. 9.

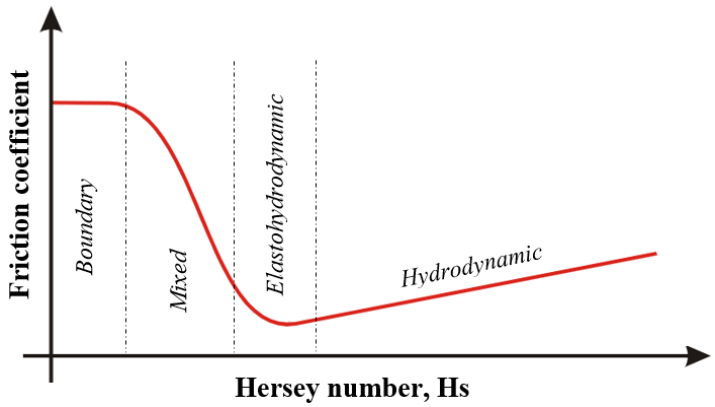

Figure 4.3 - Stribeck curve: The friction coefficient µ versus the Hersey number *Hs*.

$$Hs = \frac{\eta_0 U_e}{P_{mean}\, \sigma_{RMS}} \quad [non - dimensional] \tag{8}$$

$$\sigma_{RMS} = \sqrt{{S_{q1}}^2 + {S_{q2}}^2} \ [\mu m] \tag{9}$$

A total of three disks and 36 spheres were used for the sliding tests. In Test 1 (radius of 18 mm), one disk and seven spheres were used for each lubricant, and the tests were repeated two times for each load to ensure repeatability. In Test 2, the disk of the previous test (radius of 20 mm) was used, but with a set of five new spheres for each lubricant, and the wear of the sphere was evaluated every hour of test. The roughness (Ra) of the surfaces of the disks was measured using a roughness tester and the roughness of the sphere was defined by ISO 3290-1. In addition, a microhardness tester was used to measure the hardness of the specimens.

The film parameter (λ) relates the film thickness and the RMS value of the roughness amplitude, namely σ_{RMS}. λ is also known as the "Lambda factor," and its value depends on the lubrication regime and the Stribeck curve in the range of values that were obtained experimentally. The parameter of the film is calculated via Eq. 10:

$$\lambda = \frac{h_{min}}{\sigma_{RMS}} \ [non - dimensional] \tag{10}$$

4.2.5 *Determination of the coefficients of friction and wear*

The coefficient of friction was calculated from the measurement of the instantaneous friction force that was provided by the tribometer, which was divided by the normal force that was exerted by the pin, using the concepts that were proposed by Amontons and Coulomb [39]. The diameter of the wear scar (WSD), which is denoted as d, was measured using an optical microscope in the directions of the ordinate and abscissa at the end of each test. To calculate the volume that was removed from the sphere surface, it was necessary to calculate the height that was removed from the volume, namely, h, via Eq. 11, from the radius r of the sphere and the diameter d of the scar that is shown in Fig. 4.4. The removed volume, which is denoted as Q, is calculated via Eq. 12, which depends on the hemispherical geometry [40]:

$$h = r - \left(r^2 - \left(\frac{d}{2}\right)^2\right)^{\frac{1}{2}} [m] \tag{11}$$

$$Q = \pi h^2 \left(r - \frac{h}{3}\right) \ [m^3] \tag{12}$$

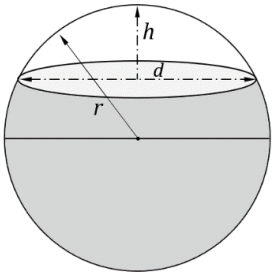

Figure 4.4 - Scar wear and parameters to calculate the removed volume of the sphere (Li, et al. (41)).

where *d* is the wear scar diameter, *r* is the radius of the half-sphere, and *h* is the height of the wear volume. To determine the coefficient of wear, namely, K, the wear model that was proposed by Archard is used, as expressed in Eq. 13 [42].

$$\sum_{i=1}^{n} Q_i = K\left(\sum_{i=1}^{n} F_{n_i} S_i\right) [mm^3] \tag{13}$$

where S_i is the sliding distance of each test in m, K is the wear coefficient in mm^3/Nm, and F_{n_i} is the normal load in N. The removed volume Q_i is cumulative over all tests and is represented by a linear equation.

After the lubricated sliding tests were conducted, the track surface failure mechanisms were evaluated via scanning electron microscopy (SEM) with dispersive energy spectrometry (EDS) analyses.

4.3 Results and analysis

An analysis was conducted for each test condition to evaluate the lubrication regimes of each lubricant and the damages on the surfaces of the disks and of the spheres that were used in the tests. Thus, it is possible to simulate the sliding of materials that are commonly used on the surfaces of hydraulic components. With these results, it was possible to evaluate the tribological behaviors of the biodegradable hydraulic oils.

4.3.1 *Viscosity*

To determine the lubrication regimes and the film thicknesses, it was necessary to determine the viscosity behavior of the lubricants, mainly at the mean temperature of 30 ± 3 °C of the test. The coefficients, namely a and b, of the Reynolds equation (Eq. 1), its

experimental correlation, and the dynamic viscosity that were obtained for the exponential viscosity versus temperature variation are listed in Table 4.6. These coefficients were obtained in the range of 10 to 70 °C.

Table 4.6 - Fitting parameters according to the Reynolds equation for the viscosity at 30 ºC.

Lubricants	***a***	***b***	R^2	η_0 **[Pa.s]**
HEES - Ester	-0.035	0.1726	0.97	0.060
HLP - Mineral	-0.036	0.1678	0.98	0.057
HEPR - Hydrocarbon	-0.029	0.1221	0.98	0.051

According to the viscosity data that were obtained in the laboratory after the tests, the values of coefficients a and b are lower for the biodegradable hydraulic oil (HEPR); hence, this fluid is of lower viscosity. In addition, higher similarity of this property is observed for HEES and HLP oils.

4.3.2 *Lubrication regimes and film thickness*

The performance of the lubricant in various lubrication regimes is typically characterized using the Stribeck curve, which relates the coefficient of friction μ with the variables of contact pressure, sliding velocity, dynamic viscosity, and RMS roughness using the Hersey number, which is named as Hs [17, 43]. In the tests, Stribeck curves were obtained for various loads and a single sliding speed according to the parameters that are specified in Table 4.1 (Test 1) via Eq. 8. The tests were conducted at a total sliding distance of 125 m for each load. Figure 4.5 presents the results of the lubrication regimes for the sliding of the brass/WC–CoCr surfaces.

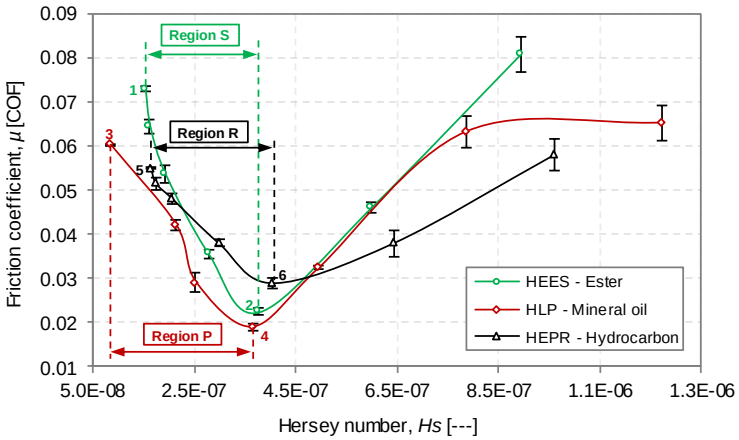

Figure 4.5 - Stribeck curve: The coefficient of friction versus the Hersey number for each lubricant and applied load.

As shown in Figure 5, the coefficient of friction ranged from approximately 0.02 to 0.08 within the Hs range of 1.38E-8 and 1.17E-6. The lowest values of the coefficient of friction for the lubricants were between 0.02 and 0.03, and this region is characterized by a change in the regime of elastohydrodynamic lubrication. For a higher coefficient of friction and a low Hersey number (smaller than 1.38E-8), the regime is mixed lubrication. For higher values of the coefficient of friction, namely, greater than 3.7E-7 Hs, the trend is to modify to the hydrodynamic regime, but with the challenge that a punctual contact of the sphere would have to form a lubricating film. Under this condition, the roughness without deformation by the medium pressure predominates, which is a requirement that characterizes the hydrodynamic regime.

The behaviors of the lubricating oils with decreasing loads and increasing Hersey number were analyzed and compared, and the following results were obtained: In the range that was defined as "Region S", the value of the coefficient of friction μ from point 1 to point 2 decreased from 0.073 to 0.022 with biodegradable oil HEES. For the mineral oil, namely, HLP (Region P), the coefficient of friction from point 3 to point 4 had a variation of 0.060 to 0.019. In the region R that was defined for biodegradable oil HEPR, the coefficients of friction ranged from 0.055 to 0.030 between points 5 and 6 of Fig. 4.5. By evaluating the region of mixed lubrication and elastohydrodynamics, it was observed that during the tests, oil HEES corresponded to higher values of the coefficient of friction for most of the evaluated loads, compared to the other lubricants. In the hydrodynamic lubrication regime for the higher Hersey value of the HEES oil, which corresponds to a load of 0.3 N, the highest value of the coefficient of friction is observed. While the HLP oil corresponds to lower loads and higher Hersey numbers, the coefficient of friction tends to maintain the same value because the film thickness remains the same. This phenomenon of lubrication, which is known as starvation, can occur in the regime of hydrodynamic lubrication [44]. The authors further state that the lubricant film is not only related to the pressure, speed, and viscosity as independent parameters but also to the level of oil filling during sliding of the surfaces.

The friction depends on the film thickness, the roughness contact, the temperature increases and the structural deformations of the components [45]. The film thickness is calculated via Eq. 7. The following values were obtained for the dynamic viscosity (η_0) and the viscosity-pressure coefficient (α): $\eta_0 = 0.060$ and $\alpha = 1.38 \times 10^{-8}$ for HEES oil, $\eta_0 = 0.057$ and $\alpha = 1.82 \times 10^{-8}$ for HLP oil, and $\eta_0 = 0.051$ and $\alpha = 1.58 \times 10^{-8}$ for HEPR oil. Therefore, the values of the minimum film thickness of HEES oil and HEPR are lower than that of HLP. The viscosity and viscosity-pressure coefficients values affect

the film thickness. These properties depend on the molecular structure of each lubricant. Fig. 4.6 compares the calculated film heights for the various mean contact pressures (P_{mean}) that were applied in the tests, and the coefficient of friction and the film parameter λ as functions of the Hersey number.

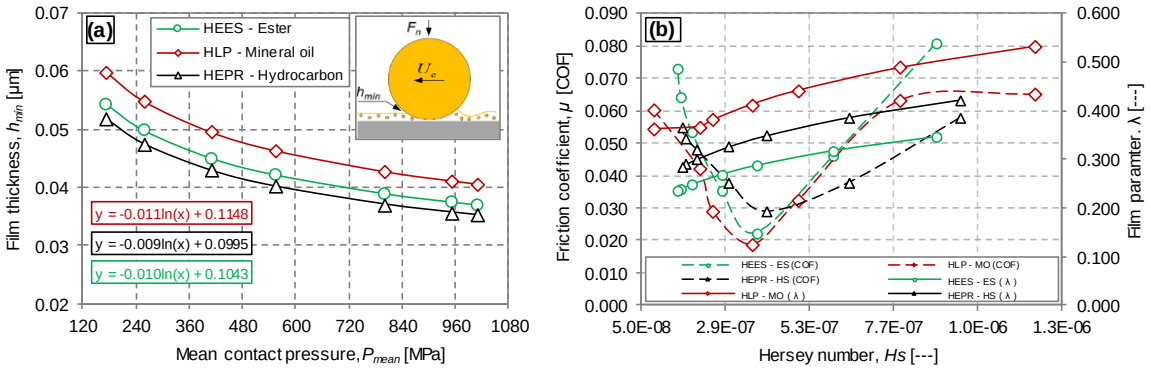

Figure 4.6 - Lubrication film evaluation. (a) The film thickness with respect to the mean contact pressure and (b) the film parameter and coefficient of friction as functions of the Hersey number.

Fig. 4.6 (a) shows that the result of the film thickness as a function of the mean contact pressure has a logarithmic characteristic that was modeled by the experimental data, which corresponds to a curve quality estimate of over 99 %. Fig. 4.6 (b) shows the relation of the Stribeck curve with the film parameter, λ, whose units are represented in the secondary axis of the graph. In this result, differences of 9 and 13 % of the thickness of the HLP lubricant film for the HEES and HEPR lubricants, respectively, were identified.

The values of the friction coefficient and the film parameter (λ) as functions of the Hersey number are presented in Table 7, which analyzes the behavior of the coefficient of friction and the modification in the lubrication regime, along with the values of the film parameter for the ecological and mineral lubricants.

The film parameter expresses the severity of the contact roughness during the sliding. In previous lubricated sliding tests of a sphere on a disk that was coated with three metallurgical powders, values of $\lambda \cong 0.5$ for tests with 0.5 m/s speed and $\lambda \cong 2.2$ for tests with 4 m/s speed were obtained [41]. It was defined that if $1 > \lambda > 3$, there is a mixed lubrication regime, and the lubrication limit would be $\lambda = 0.5$.

The divisions of the mixed, elastohydrodynamic and hydrodynamic lubrication regimes are identified based on the changes in the values of the coefficient of friction, which are mainly near the upwardly concave point, according to the tests that were conducted [45]. However, other research indicates that these results would have acceptable precision for light and moderate loads, but not for high loads [46]. In the sliding test, the lowest coefficient of

friction is found in the region of concavity that is identified in Table 4.7. The friction coefficient for HEES biodegradable oil is $\mu_{HEESmín} = 0.022$, which corresponds to the film parameter value of $\lambda_{HEESi} = 0.29$. The friction coefficient of the mineral oil HLP, namely, $\mu_{HLPmín} = 0.019$, corresponds to a film parameter value of $\lambda_{HLPi} = 0.41$. For biodegradable oil HEPR, the coefficient of friction was $\mu_{HEPRmín} = 0.029$, which corresponds to $\lambda_{HEPRi} = 0.35$. The Stribeck curve shows that in the hydrodynamic regime, the HEPR oil had the lowest coefficient of friction, which is recommended for moderate loads and medium speeds. However, HLP and HEES outperform it in the elastohydrodynamic regime, as they are more suitable for higher loads and speeds than HEPR.

The values of the film parameter λ that are presented in Table 4.7 does not accord with previous research [41]; this is because the WC-10Co4Cr coating material had high porosity, as shown in Fig. 4.2 (b), and a substantial roughness difference due to the surface preparation process of the disk. This type of surface has small reservoirs for lubricating oil that are not considered in the film thickness calculations; however, it performs well for lubrication and yields smaller values for λ.

Table 4.7 - Coefficient of friction and film parameter (λ) as functions of the Hersey number for each lubricant.

	HEES - Synthetic Esters							
01	Lubrication regime			Mixed		Concavity	Elastohydrodynamic	
02	Applied load, F_n (N)	60	50	30	10	4	1	0.3
03	Hersey number, Hs	1.53E-07	1.63E-07	1.93E-07	2.78E-07	**3.77E-07**	5.99E-07	8.94E-07
04	Coefficient of friction	0.073	0.064	0.054	0.036	**0.022**	0.046	0.081
05	Lambda, λ	0.24	0.24	0.25	0.27	**0.29**	0.32	0.35

	HLP – Mineral oil							
01	Lubrication regime		Mixed			Concavity	Elastohydrodynamic	
02	Applied load, F_n (N)	60	50	30	10	4	1	0.3
03	Hersey number, Hs	8.38E-08	2.14E-07	2.53E-07	**3.65E-07**	4.96E-07	7.87E-07	1.17E-06
04	Coefficient of friction	0.060	0.042	0.029	**0.019**	0.032	0.063	0.065
05	Lambda, λ	0.36	0.37	0.38	**0.41**	0.44	0.49	0.53

	HEPR - Synthetic Hydrocarbons							
01	Lubrication regime			Mixed		Concavity	Elastohydrodynamic	
02	Applied load, F_n (N)	60	50	30	10	4	1	0.3
03	Hersey number, Hs	1.64E-07	1.75E-07	2.07E-07	2.99E-07	**4.05E-07**	6.43E-07	9.611E-07
04	Coefficient of friction	0.055	0.051	0.048	0.038	**0.029**	0.038	0.058
05	Lambda, λ	0.29	0.29	0.30	0.33	**0.35**	0.39	0.42

The average roughness of the brass sphere was $S_{q_{pin}} = 0.015\,\mu m$, whereas the roughness of the disk that was used with the HEES lubricant was $S_{q_{HEES}} = 0.135\,\mu m$; hence, the roughness of the disk was 9 times larger than of the sphere. The disk that was used for testing with the HLP lubricating oil has a HLP roughness of $S_{q_{HLP}} = 0.121\,\mu m$, and the sphere maintains the same value, in which case the roughness of the disk is approximately 8 times greater. For the HEPR oil, the value of the roughness of the disk, namely, $S_{q_{HEPR}} = 0.105\,\mu m$, corresponds to 7 times the difference of the sphere. The roughness values influence substantially the calculation of the film parameter $\lambda = h_{mín}/\sigma_{RMS}$. Since the disc roughness is approximately 7 to 9 times greater than the sphere, the high value of roughness in the denominator promotes low values of the film parameter. The results of other studies that were conducted on a lubricated test machine demonstrate that for values of $\lambda > 5$, the friction does not increase indefinitely; with higher speeds, the friction begins to decrease again [47]. This is because with a high shear rate, the lubricant begins to heat, which decreases the viscosity and, therefore, causes a decrease in the friction. The friction is not affected by the longitudinal roughness but depends strongly on the peak-to-valley height, namely, the equivalent roughness [48]. In Fig. 4.5, at the last point for the HLP oil, which corresponds to the highest Hersey number value, stabilizing behavior of the coefficient of friction was also observed, which was due to the lubrication-starved conditions.

Other studies show that high pressure, antifriction, and anti-wear additives substantially decrease the value of the coefficient of friction and, consequently, the value of the coefficient of wear [49]. In this study, the authors identified high concentrations of zinc, phosphorus, and molybdenum, which are usually used in lubricant formulations as extreme pressure and anti-wear additives. Table 4.8 show the concentrations of elements in lubricants HEES, HLP, and HEPR, which were determined via inductively coupled plasma atomic emission spectrometry (ICP).

Table 4.8 - Concentrations of the elements that were used as additives in the lubricants.

No.	**Lubricants**	**Elements (mg/l)**			**Compared to HEES**		
		Zinc Zn	Phosphorus P	Sulfur S	Ratio Zn	Ratio P	Ratio S
1	HLP - Mineral oil	290.3	238.6	1027.9	29.3	3.2	1.1
2	HEPR - Synthetic hydrocarbons	117.1	174.8	1091.3	11.8	2.3	1.1
3	HEES - Synthetic esters	9.9	74.4	938.4	1.0	1.0	1.0

According to the concentrations of the elements that were used as additives that are presented in Table 4.8, the synthetic biodegradable oils, namely, HEES and HEPR, have lower concentrations of Zn and P, which are used as anti-wear additives. The results demonstrated that there was 29.2 times more Zn in HLP than in HEES oil and 11.8 times more in HEPR. For phosphorus (P), the values were 3.2 times that in mineral oil for HEES and 2.3 times for HEPR. These higher concentrations of zinc and phosphorus in the mineral oil increase its capacity to withstand higher loads without affecting the contact of the surfaces, which, consequently, reduces the coefficient of friction compared to the evaluated biodegradable oils. The lubricants are often mixed with zinc dialkyldithiophosphate (ZDDP) as a multifunctional additive [49]. Zn and P adhere to the surface of the steel and protect this surface against abrasive and adhesive wear mechanisms, thereby reducing the friction and wear during the sliding. Table 4.8 also presents the differences in sulfur concentrations, which, in combination with other elements, is used as an extreme-pressure additive. The lowest concentration was identified for HEES and the highest for HEPR oil, thereby revealing the effect of this element on the stabilization of the friction coefficient for the HEPR oil, as shown in Fig. 4.6b. The results of other studies support the effect of sulfur as a wear-inhibiting element and the reduction in the coefficient of friction [50]. In this study, the authors evaluate the wear and friction behavior in the sliding of spheres that were manufactured from AISI 52100 and steel disks.

4.3.3 *Results of friction and wear mechanisms - Test 1*

The wear and friction tests were conducted with loads of 0.3, 1, 4, 10, 30, 50, and 60 N, at a total distance of 125 m. To evaluate the wear of spheres after lubricated sliding, it was necessary to measure the wear scar diameter (d) at the end of each test. From the measurements of the scar diameter, the removed height (h) of the pin (sphere) was determined via Eq. 11, from which the volume loss of the sphere (Q) was calculated via Eq. 12. Figure 4.7a shows nonlinear behavior for the wear scar (WSD) for each load and a scar morphology that indicates higher wear for the spheres with HEES biodegradable oil. The differences in the wear scars are visible after sliding, as shown in Fig. 4.7b-d.

The largest difference was observed for the WSD with the load of 60 N. With this load, the average WSD with HEES was 1.301 mm (Fig. 4.7b), compared to 0.996 mm for HLP (Fig. 4.7c) and 0.696 mm for HEPR (Fig. 4.7d). According to the values of the average friction coefficient for all loads during sliding, the mineral oil presented a mean value of the

friction coefficient of $\mu_{HLP} = 0.044$, compared to $\mu_{HEES} = 0.054$ and $\mu_{HEPR} = 0.043$; hence, the biodegradable oil HEES has difficulty maintaining a lubricant film between the sliding materials.

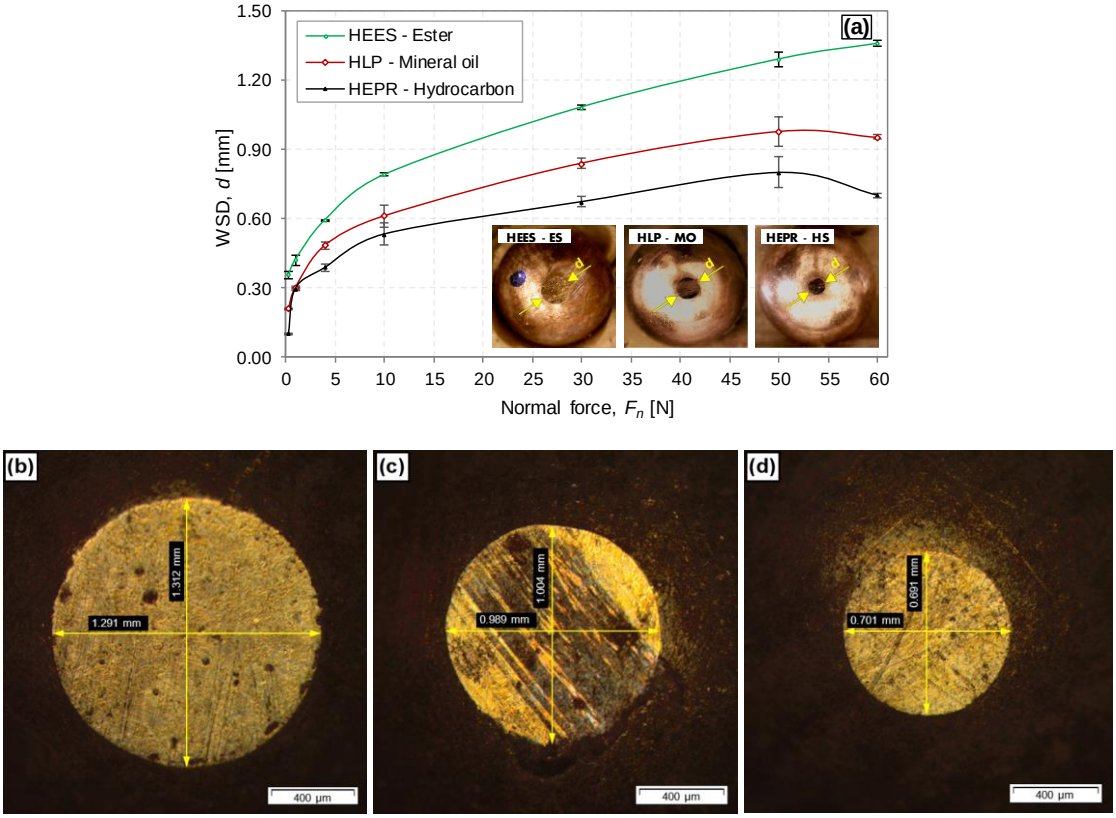

Figure 4.7 - Wear of the spheres: (a) The evolution of a wear scar (WSD) for each load and (b), (c) and (d) sliding with HEES, HLP and HEPR, respectively, for the load of 60 N.

From the data on the removed and accumulated Q volumes of the sphere as functions of the load and the distance traveled, the dimensional wear coefficient K is calculated via Eq. 13. The wear behavior of the spheres that were used as pins in the sliding test for each lubricant is presented in Figure 4.8.

The coefficient of wear (K), which was obtained via Eq. 13, for the sphere of Cu-35Zn shows linear behavior for the three lubricants. For the HEES biodegradable oil, the value is $K_{HEES} = 6.90 \times 10^{-5} mm^3.m/N$ with a correlation coefficient of R^2 = 99.7 %. With the mineral oil, $K_{HLP} = 2.12 \times 10^{-5} mm^3.m/N$ with R^2 = 99.8 %. For the biodegradable HEPR oil, $K_{HEPR} = 8.62 \times 10^{-6} mm^3.m/N$ with a correlation of 99.6 %; hence, in all cases, the quality of the data that were used in the linear regression is satisfactory. The differences in wear among the lubricants are substantial, namely, the removed volume accumulated and Qi with use of the HEES biodegradable oil was 1.34 mm^3, compared to 0.4 mm^3 with the mineral oil. Comparing the HEPR and the HLP,

the removed volume of the biodegradable oil was lower, with a value of 0.16 mm^3. In the end, the sphere wear coefficient with the HEES biodegradable oil was 3.2 times higher than that with HLP and 8.3 times that with HEPR.

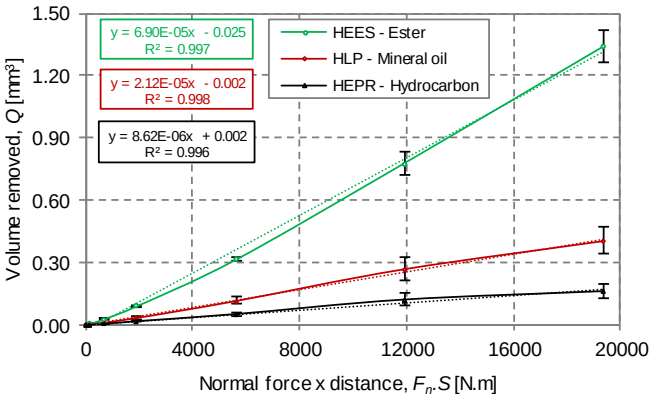

Figure 4.8 - Results for the wear coefficient K in mm^3/N.m for each lubricant

The lubrication regimes and partial wears in the short-term tests are compared in Fig. 4.9 for sliding with the HEES, HLP and HEPR oils.

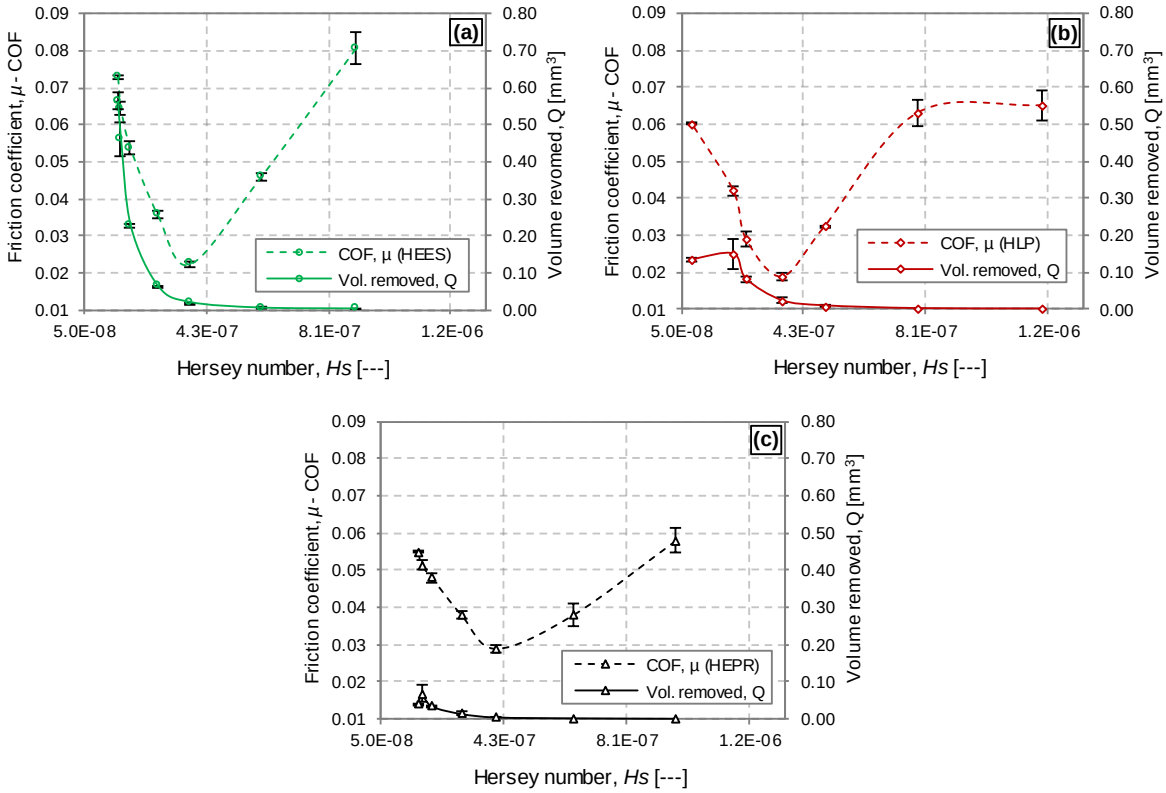

Figure 4.9 - Comparison of the coefficient of friction and the removed volume from the sphere versus the Hersey number. (a) HEES - esters, (b) HLP - mineral oil, and (c) HEPR - hydrocarbon.

The Hersey number is compared with the coefficient of friction and removed volume from each test. For all lubricants, in low loads and in the elastohydrodynamic regime, small

and negligible wear occurred prior to satisfying the concavity condition of the Stribeck curve. In this regime, there is no contact between the asperities of the surfaces. If the Stribeck curve satisfies the concavity condition, small but noticeable wear occurs. Hence, wear could be avoided with larger values of the Hersey number than the value that defines the concavity condition. For the HEES oil, the lowest coefficient of friction was attained with the load of 4 N. However, with smaller loads (greater than 1 N), a lower coefficient of friction and likely less severe wear could be realized, as detected in the boundary lubrication regime. Additionally, under the concavity condition, the lowest coefficient of friction with the HEPR oil was with attained the load of 4 N; however, with this oil, lower wear was realized compared to the HLP mineral oil and the biodegradable HEES oil. In all tests, it was observed that the HEPR oil corresponded to less variation of the friction coefficient in the lubrication regime. After leaving the range that is defined by the concavity condition, the wear differs substantially among the oils; it is mild for HLP (mineral) and HEPR (hydrocarbons) and highly severe for the biodegradable HEES (ester) oil. In the mixed lubrication regime, contacts will occur between the highest peaks of the roughness. For all sliding conditions of the lubricants, the additives have affected HEPR and HLP strongly and positively due to the high concentrations of Zn and P, which are specified in Table 4.8. At the point of the largest load of 60 N, which corresponds to the smallest Hersey number for HLP and HEPR (Figures 4.10b-c), the wear was slightly reduced compared with the load of 50 N. This is due to a reaction of the anti-wear and extreme pressure additives that operate optimally under these conditions.

In other lubricated sliding tests of a copper block under an SAE 52100 steel wheel, with elastohydrodynamic lubrication, the coefficient of friction, the wear rate, and the temperature exhibited low and constant values [51]. In contrast, mixed lubrication is characterized by a higher coefficient of friction. Consequently, the wear would occur due to the lack of lubricant film, thereby causing scratching, removal, deposition, and crushing of particles in the wear track; if the material is of high ductility, the wear would be caused by successive passages of the sphere on the track. the track.

After the analysis of the wear on the sphere and disks, the results regarding the contamination of the lubricants, which was due to the wear of the bronze sphere, are presented, which were obtained according to ASTM D5185. Additionally, particle count results were obtained for each lubricant according to ISO 4406. Table 4.9 presents the results for each hydraulic oil before and after the wear tests.

Table 4.9 - Amounts of copper that were detected in the lubricants in parts per million (ppm) via spectrochemical analysis and particle counting according to ISO 4406 before and after the wear tests.

Element (mg/l) and Standard	HEES - Ester		HLP – Mineral oil		HEPR - Hydrocarbon	
	Before	After	Before	After	Before	After
Copper	0.10	9.11	0.10	0.86	0.10	0.31
ISO 4406	17/16/11	18/17/13	16/16/13	17/16/13	19/17/12	19/17/13

Table 4.9 presents the concentration of copper particles for each lubricant after the sliding tests. The results demonstrate that the number of particles that resulted from the wear of the sphere after the tests was higher for the HEES biodegradable oil, which corresponds to an increase of approximately 91 times, compared to 8.6 and 3.1 times for HLP and HEPR, respectively. Previous studies identify the elements (Fe, Cu, and SiO_2) that are the main contaminants in a lubrication system and demonstrate that high concentrations of these elements increase the coefficient of friction and the wear of the surfaces in contact [52]. Table 9 also supports the evolution of the number of solid particles, in which the mineral oil presented with lower contamination than the biodegradable lubricating oils, which is due to the changes of the three codes of the standard. Particle quantification with this standard is typically conducted with sizes ≥4, 6 and 14 μm, which are identified by codes 9 to 28. In the results that were obtained after the tests, greater contamination in the biodegradable oils is observed since the codes underwent greater modifications, compared to without oil use. The concentration of copper as a contaminant in biodegradable oils also substantially impacts the increase in the viscosity, the oxidation, and the aging of the lubricating oil [53].

4.3.4 *Results of friction and wear mechanisms - Test 2*

In most studies on the tribological conditions of lubricated surfaces, short-term tests are conducted. However, via short-term tests, it is not possible to identify a trend in the coefficient of friction or to predict the damage that was caused to the surface by its modification. In this study, the results of the friction coefficient throughout the test for each lubricant are primarily presented separately for each hour of the test. In the tests, three disks were coated in WC-CoCr, namely one for each lubricant. The objective of this test was to simulate the sliding of hydraulic components that are not replaced after a period of use and to evaluate their behavior under critical conditions. Figure 4.10 presents the results of the coefficient of friction for long tests with a load of 30 N. Under these load and speed conditions, the mixed lubrication regime was observed, as shown in Fig. 4.5.

The friction force signals that were provided by the load cell have been filtered at low-pass frequencies so that the electrical noise and machine vibrations do not affect the frictional forces. If the normal force is constant and the friction force consists of only force values, the coefficient of friction has small amplitudes under stable and differentiated conditions and under floating conditions.

In all tests, the coefficient of friction for the HLP mineral hydraulic oil is the most stable, followed by HEES oil and HEPR oil. The coefficient of friction, which is plotted in Fig. 4.10, is analyzed as follows for each test time.

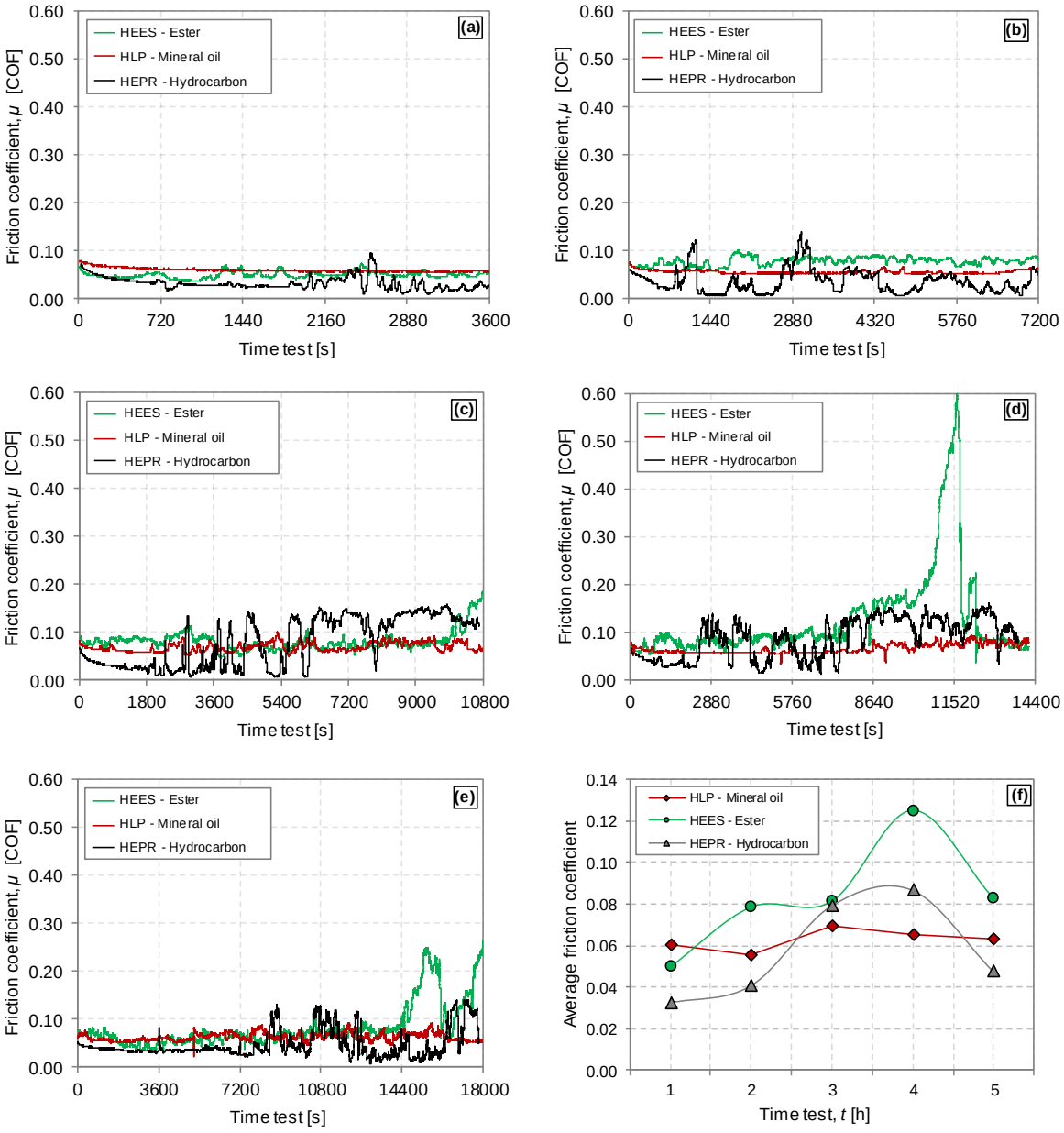

Figure 4.10 - Results of the coefficient of friction at various test times: a) 1 h, b) 2 h, c) 3 h, d) 4 h, and e) 5 h, and f) the trend of the coefficient of average friction at each test time.

In the tests that were conducted for a duration of 3600 s, the average values of the friction coefficient for the lubricating oils were $\mu_{HEES} = 0.050$, $\mu_{HLP} = 0.060$ and $\mu_{HEPR} = 0.032$. In this test, low instability for the HEPR was observed from 2000 s. In the second test, which was 7200 s in duration, a higher average value of the coefficient of friction for HEES oil was observed, along with instability of HEPR, compared to mineral oil HLP. The values of the average coefficient of friction were $\mu_{HEES} = 0.078$, $\mu_{HLP} = 0.056$ and $\mu_{HEPR} = 0.041$. It is also found that from this test that the stick-slip behavior becomes more evident throughout the HEPR oil sliding test. The frictional force changes with the elasticity of the dynamic system and the speed, which would be close to the critical speed of the mass-spring microsystem. This change occurs due to the transition from mixed lubrication to boundary lubrication, which influences the friction and changes the speed from highest to lowest, thereby approaching dry friction [54]. According to previous research, the maximum amplitude of the stick-slip is proportional to the difference between the static and kinetic friction forces [55]. However, in the experimental results that are presented in Fig. 4.10 for HEPR oil, higher values were observed for the coefficient of static friction. In the 3-hour (10800 s) tests, the mean coefficient of friction for the HEES was higher than for the other lubricating oils. In this test, the instability for the HEPR oil started at approximately 1800 s, and this behavior was maintained until the end of the test, with an increasing trend throughout the test. In these tests, the average COF values for the oils were $\mu_{HEES} = 0.081$, $\mu_{HLP} = 0.069$ and $\mu_{HEPR} = 0.079$. In the fourth test, which was conducted for a duration of 14400 s, the HLP oil again presents better stabilization, and an increasing trend is observed for the HEES oil, in addition to a sudden increase in the coefficient of friction at approximately 11000 s for this fluid. This result is explained by the adhesion mechanism on the surface of the disk, which demonstrates the low performance of the friction and wear additives for this biodegradable ester-based oil. The adhesion mechanisms result in metal-to-metal contact and likely increase the coefficient of friction. As the wear is developing, debris is released and slightly increases the roughness of the surfaces in an indirect way; a transitorily decreasing in the film parameter (λ) is observed [41]. The results of the tests that were conducted at 5 hours were similar to the previous results. In these tests, the average COF values that were obtained for the three oils were $\mu_{HEES} = 0.083$, $\mu_{HLP} = 0.063$ and $\mu_{HEPR} = 0.047$. In all the tests, the values that were obtained for the coefficient of friction for the HEPR oil were lower than those for the other lubricants. Fig. 4.10 (f) shows the behavioral trends of the average friction coefficients for each test time. The linear regression yields coefficients of 0.0112, 0.0015 and 0.0076 for

HEES, HLP, and HEPR, respectively. According to these values, the coefficient of friction for the biodegradable HEES oil is the highest, followed by that for the biodegradable HEPR oil and, finally, that for the HLP mineral oil, thereby demonstrating the performances of the lubricants during the sliding of the WC-CoCr/Cu-Zn tribological pair.

The long-term tests were used to evaluate the volume that was removed from the sphere via Eqs. (11) and (12) and to obtain the coefficient of wear via Eq. (13) for each lubricant. Figure 4.11 shows the comparison of the accumulated wear coefficients for the 5 evaluated times.

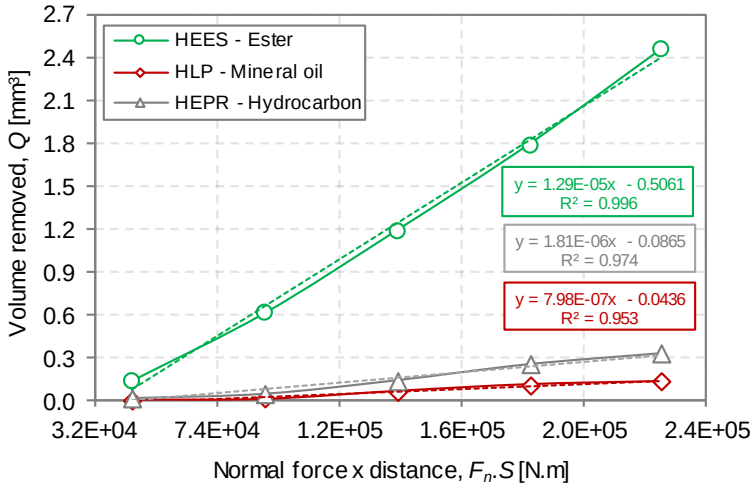

Figure 4.11 - Wear coefficient K in mm^3/N.m for each lubricant with a one-hour interval between tests.

The comparison of the performances of the lubricants with respect to the wear resistance shows the following: The HPL oil showed a lower coefficient of wear, which was on the order of $K_{HLP} = 7.98 \times 10^{-7}$ mm^3/ (N.m), and its removed volume was lower compared to HEES. The linear correlation of 95.3 % for HLP demonstrates that its trend is to maintain its wear resistance. The HEPR oil performed well with a wear coefficient of $K_{HEPR} = 1.81 \times 10^{-6}$ mm^3/ (N.m), and the ratio of the HEPR wear coefficients with HLP is 2.27. The HEES oil did not provide satisfactory wear resistance during the sliding of materials. The wear coefficient that was obtained for the sphere while using this lubricant was $K_{HEES} = 1.29 \times 10^{-5}$ mm^3/ (N.m), and its distance, which is plotted in Fig. 4.11, shows that the wear was greater and evident. The ratio of the HEES wear coefficients with HLP is 16.7 and that with HEPR is 7.13.

The performance results of the lubricating oils with respect to wear and friction are compared in Fig. 4.12. These results consist of the removed volume for each test time and the behavior of the coefficient of friction.

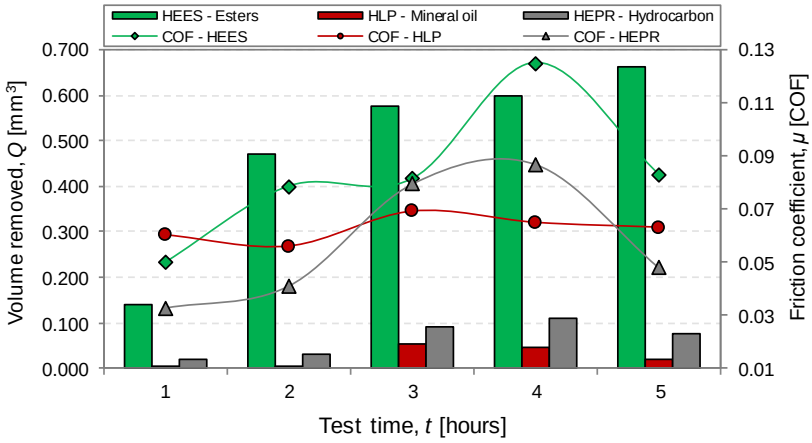

Figure 4.12 - Relationship between the removed volume Q in mm^3 and the coefficient of friction μ versus the test time t in hours.

According to Fig. 4.12, the trends are not linear in any case and the behavior can be summarized as follows: For the first three hours, there is a tendency for increased friction and wear for all lubricants. The increase in wear in the first three hours is not proportional, and although the coefficient of friction decreased slightly in the second hour for the HLP oil, its increase in the third hour is approximated by the average of the other oils. For the HEES oil, in the third hour, a slight decrease was observed. In the fourth hour, the coefficient of friction was higher for the HEES and HEPR oils, whereas that for the HLP oil decreased slightly. The greatest wear of HEPR occurs the fourth hour. The coefficient of friction of the HEES oil was much higher than those of the other oils due to the abnormal behavior of the coefficient of friction, which is shown in Fig. 4.10d, which reaches the value of the coefficient of dry friction. This is due to the decrease in lubrication at this time. In the fifth hour, the coefficients of friction decrease with all lubricants; the decreases are substantial for HEES and HEPR but almost imperceptible for HLP. Although the wear of the spheres with the use of HEES is higher than for the other lubricants, the trend shows a decrease in the wear rate. The trend of increasing wear was prevented by the changes in the coefficient of friction, as shown in Fig. 4.10 (e). The changes in friction and wear for the brass in the limit lubrication regime occur due to a strong plastic deformation of the debris, with intragranular sliding in the α phase, and appear with localized deformation in shear bands, with an increase in hardness after the tests [51]. According to the experimental results of Fig. 4.12, the changes in the coefficient of friction and wear would be affected by the detachment of the brass over the disk track, thereby filling a portion of the pores of the disk coating. This third body, which is added instantly by debris and crushing with adhesion to the disk surface, has modified the initial characteristics of the surfaces, thereby reducing the friction and wear.

With the increase in the number of passes or repeated sliding, the coefficient of friction for copper alloys gradually decreases [56]. Several mechanisms of wear have been evaluated and discussed for mechanical systems, such as abrasive wear, adhesive, and fatigue. In the tests that were conducted in this study, mostly in the mixed lubrication regime, abrasive wear and adhesive mechanisms were identified after the sliding on the tracks. Figs. 13, 14 and 15 present the micrographics that were obtained via SEM of the worn surfaces of the disk after the Cu-Zn alloy sliding, in addition to the chemical compositions that were made by EDS outside and within the wear track.

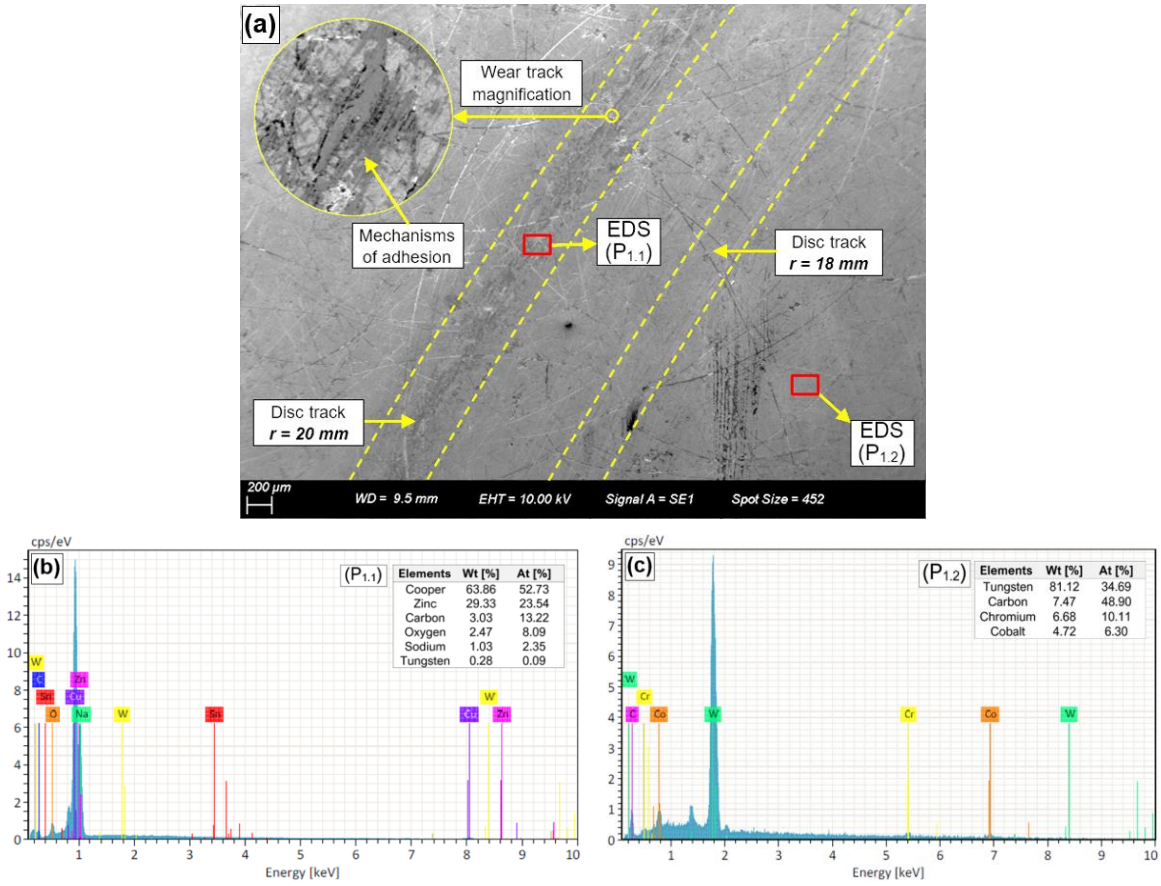

Figure 4.13 - SEM-EDS micrograph and chemical compositions of a WC-CoCr surface that was lubricated with HEES.

Figure 4.13a shows a micrograph of the wear track that was produced by the sliding of the Cu–Zn sphere against the disk that was made of WC–CoCr and lubricated with HEES hydraulic oil. In the magnified view of the track surface, a material that has been deposited on the disk is identified in darker color, thereby demonstrating the adhesive wear mechanism, which was subsequently supported by the chemical composition. Figure 4.13a still shows grooves that are aligned in the direction of sliding, which are characteristic of an abrasive wear mechanism. Then, the adhesion of the sphere material on the disk was

supported by the analyses that were conducted via EDS (Fig. 4.13b). High concentrations of copper (63.86 %) and zinc (29.33 %) elements from the sphere material, which were higher than those of the other elements of the WC–CoCr alloy, were identified. In Fig. 4.13c, the chemical elements that are present on the surface of the disk outside the wear track (P1.2) are identified for comparison with the worn surface (P1.1), for evaluating the mechanisms. The adhesive wear occurs with the sliding of the metals when the surfaces are in contact [57]. During the sliding, it is possible that micro-soldering occurs between the metals, with a subsequent detachment of these materials. The more compatible the metals, the more severe the adhesive wear. Metals are considered compatible when their weldability is between 0.1 and 1%. If it is below 0.1 %, the metals are considered partially incompatible. If it is outside this range, the metals are characterized as not compatible.

In the tests, the predominant material on the disk surface is tungsten (W - 70.2%), whereas in the sphere, it is copper (Cu - 62.3%). The tungsten carbide alloy and brass that were used in the tests are partially compatible; therefore, adhesive and abrasive wear occur [58].

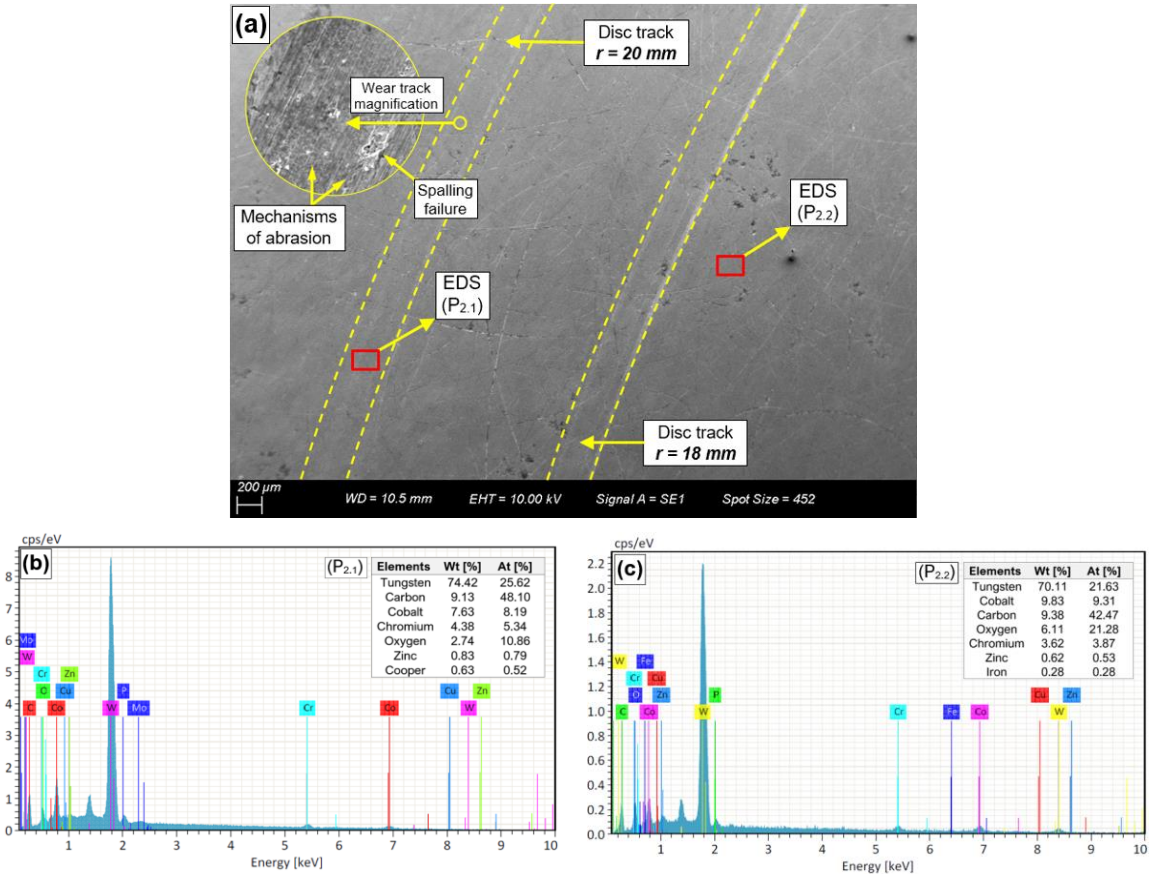

Figure 4.14 - SEM-EDS micrograph and chemical compositions of a WC-CoCr surface that was lubricated with HLP.

Figure 4.14a presents the same information for the lubricated sliding but with the HLP oil. In this result, the mechanism of abrasive wear on the track was more evident after the tests. In the magnified view of the track region, it is possible to better identify the alignment direction of the grooves and the mechanism of surface damage, such as chipping failure in the coating. Figure 4.14b presents the amounts of Cu (0.63 %) and Zn (0.83 %) on the surface, which are much lower than in the wear track with HEES oil; hence, HLP mineral oil presents superior tribological performance for surfaces. Additionally, in Fig. 4.14c, the elements that are present outside the wear track are compared. As the surface of the disk is coated with the WC-10Co4Cr alloy, whose average microhardness is 1256 $HV_{0.02}$, against a sphere that is made of the Cu-35Zn alloy with 172 $HV_{0.02}$, the sphere wear is abrasive and severe. Even with the high-hardness tungsten carbide, abrasive wear occurred on the disk, thereby demonstrating that the debris that was detached from the disk hard surface was embedded in the surface of the sphere and remained attached to the sphere. Via this mechanism, the sphere behaved as a cutting tool for the disk, and the lubrication film did not prevent the scratching of the surface.

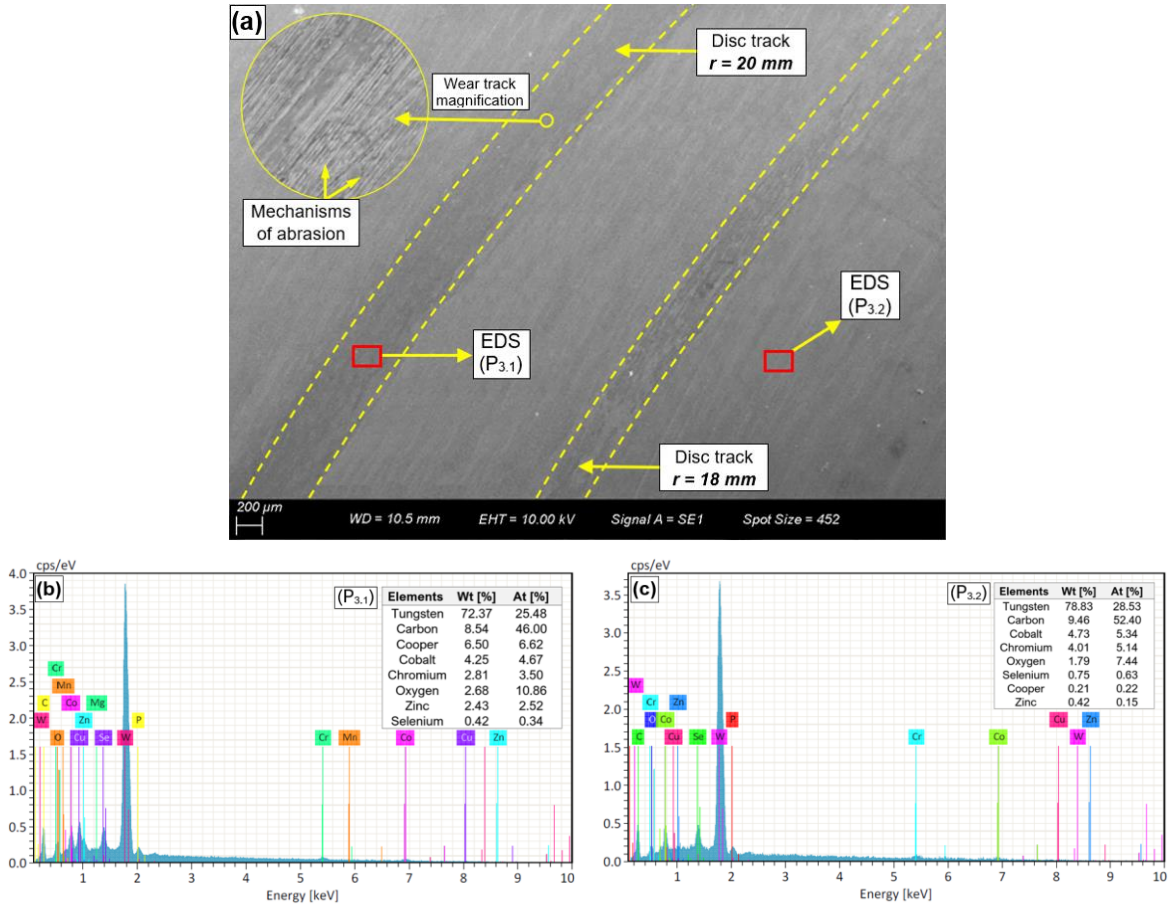

Figure 4.15 - SEM-EDS micrograph and chemical compositions of a WC-CoCr surface that was lubricated with HEPR.

A micrograph of the wear track that was produced while using HEPR biodegradable oil is shown in Fig. 4.15a. The occurrence of abrasion mechanisms is also observed in the magnification of the wear track, similar to those that were observed with HLP oil, but with more grooves and microcuts along the wear direction. In these tests, measurements were also made via EDS (P3.1 and P3.2) to evaluate the mechanisms of wear. In Fig. 4.15b, 6.5 % copper elements (Cu) and 2.43 % zinc elements (Zn) were identified; hence, the concentrations of these materials are higher in this case. A decrease in the thickness of the lubricating film enables the surfaces to approach each other, thereby resulting in more severe wear [32]. Abrasive wear occurs when the hard surface (disk) directly cuts of the ductile surface (sphere), which causes grooves and scratches to form on the surface [59]. In this case, an inadequate amount of lubricant and the formation of a lubricant film directly influence the abrasive wear, along with the concentrations and the combination of antifriction, anti-wear and extreme-pressure additives in each oil.

4.4 Conclusions

From the results that were obtained in the theoretical and experimental studies, the following conclusions are drawn:

- The comparison of the mixed and elastohydrodynamic lubrication regimes demonstrated similarities in the coefficient of friction between HLP and HEES, which differed substantially from that of HEPR oil. The variations in the boundary lubrication and elastohydrodynamics were smaller in HEPR; hence, it is suitable for applications in the reciprocating sliding process. The smaller variation of the coefficient of friction influences the energy consumption of the hydraulic equipment. Additionally, the starvation phenomenon in the HLP oil was identified from the change in the coefficient of friction with the thickness of the film.
- The rheological properties of the fluids, such as the pressure-viscosity coefficient, along with the dynamic viscosity, influenced the formation of the lubrication film. The Lambda parameter (λ) did not accord with the values that were obtained in other studies. This difference is due to the high porosity and the surface finish of the WC–CoCr coating, which provides a high value of roughness of the disk, which is 11 times greater than that of the sphere.
- The concentrations of the Zn and P additives influence the friction results and the wear mechanisms. Furthermore, a larger proportion of sulfur (S) is used for the HEPR oil.

Typically, sulfur is used as an extreme-pressure additive, which also explains the satisfactory performance in short- and long-term sliding tests.

- In the short-term wear tests, the coefficient of wear *K* was approximately 3.2 times greater with the HEES oil than with the HLP oil; with HEPR, the coefficient of wear K was approximately 8 times lower than that with HEES.
- Contamination of the lubricants with copper particles was identified in higher concentrations in the HEES oil. A portion of these particles that detached from the sphere also adhered to the disk track, thereby changing the coefficient of friction and the wear of the surfaces.
- In the long-term tests, as the number of hours increased, the stability of the coefficient of friction changes. For the HEPR, the instability exhibited the stick–slip phenomenon. For the HEES oil, the mixed lubrication regime changed for the limit lubrication, sometimes reaching the values of the coefficient of dry friction.
- The long-term tests showed that the wear coefficients differed from those that were obtained in the short-term. The wear coefficient ratio of HEES/HEPR was 7.1, compared to the HEES/HLP ratio of 16.2. The HEPR/HLP ratio was 2.3. The performance of HLP is due to the concentrations of zinc and phosphorus elements in the additives. However, the HEPR oil showed satisfactory performance in the long-term tests.
- The adhesion phenomenon of the sphere on the disk was more evident in the sliding with the HEES oil. According to the EDS results, 93% of the copper and zinc elements were deposited on the disk surface with the use of the HEES oil, whereas for sliding with the HLP and HEPR oils, 1.46 and 8.93%, respectively, were deposited.
- Due to the higher concentrations of extreme-pressure and anti-wear additives and the higher value of the coefficient of pressure-viscosity, the HLP oil realized a superior performance. The HLP oil avoided the adhesion of the sphere on the disk and, consequently, realized lower wear rates in the tribological system.
- At the end of this study, the need was identified to increase the concentrations of additives in biodegradable oils, especially ester-based oils (HEES), to increase their performance and to improve the wear resistance of the surfaces in contact.

4.5 References

[1] STACHOWIAK, G. W. **How tribology has been helping us to advance and to survive**. Friction, 5(3): 233-247, 2017.

[2] ZHANG, S. W. **Green tribology: fundamentals and future development.** Friction, 1(2):186-194, 2013.

[3] SASAKI, S. **Environmentally friendly tribology (eco-tribology).** Journal Mechanical Science Technology, 24(1):67-71, 2010.

[4] ANAND, A.; HAQ, M. I. U.; VOHRA, K.; Raina, A.; WANI, M. F. **Role of green tribology in sustainability of mechanical systems: a state-of-the-art survey**. Material Today, 4(2):3659-3665, 2017.

[5] JURAJ, T.; ĽUBOMIR, H.; JAN, K.; JURAJ, J.; MICHELA, J. **Evaluation of new biodegradable fluid on the basis of accelerated durability test**, FTIR and ICP spectroscopy. Research in Agricultural Engineering, 63(1):1-9, 2017.

[6] Mendonza, Y. E. A. **Sistematização do Projeto de Circuitos Hidráulicos para o Emprego de Fluidos Biodegradáveis**. Ph.D. thesis, UFSC – Federal University of Santa Catarina, Mechanical Engineering, Florianópolis, 2013.

[7] JOHN DEERE. http://www.deere.com. Accessed 12 Oct 2018.

[8] MADANHIRE, I.; MBOHWA, C. **Mitigating environmental impact of petroleum lubricants**. New York, Springer, 2016. 239 p.

[9] SAPAWE, N.; SYAHRULLAIL, S.; IZHAN, M. I. **Evaluation on the tribological properties of palm olein in different loads applied using pin-on-disk tribotester**. Jurnal Tribologi, 3:11-29, 2014.

[10] REGUEIRA, T.; LUGO, L.; FANDINO, O.; LÓPEZ, E. R.; FERNÁNDEZ, J. **Compressibilities and viscosities of reference and vegetable oils for their use as hydraulic fluids and lubricants**. Green Chemistry, 13:1293-1302, 2011.

[11] MANG, T. **Encyclopedia of lubricants and lubrication**., New York, Springer, 2014. 2403 p.

[12] MAJDAN, R.; TKÁČ, Z.; KOSIBA, J.; ABRAHÁM, R.; JABLONICKÝ, J.; HUJO, L.; MOJŽIŠ, M.; ŠEVČÍK, P.; RÁŠO, M. **Evaluation of tractor biodegradable hydraulic fluids on the basis of hydraulic pump wear**. Research in Agricultural Engineering, 59:75-82, 2013.

[13] SYAHIR, A. Z, ZULKIFIM N. W. M.; MASJUKI, H. H.; KALAM, M. A.; ALABDULKAREM, A.; GULZAR, M.; HARITH, M. H. **A review on bio-based lubricants and their applications**. Journal of Cleaner Production, 168:997-1016, 2017.

[14] KUČERA, M.; BUJNA, M.; KORENKOVÁ, M.; HAAS, P. **Possibilities of using ecological fluid in agriculture**. Advanced Materials Research, 1059, 61–66, 2014.

[15] TKÁČ, Z.; ČORŇÁK, S.; CVIKLOVIČ, V.; KOSIBA, J.; GLOS, J.; JABLONICKÝ, J.; BERNÁT, J.; **Research of biodegradable fluid impacts on operation of tractor hydraulic system**. Acta Technologica Agriculturae, 20:42-45, 2017.

[16] PIRRO, D. M.; WEBSTER, M.; DASCHNER, E. **Lubrication fundamentals**. Florida, CRC Press, 2017. 578 p.

[17] DIEW, M.; ERNESTO, A.; CAYER-BARRIOZ, J.; MAZUYER, D. **Stribeck and traction curves under moderate contact pressure: from friction to interfacial rheology**. Tribology Letters, 57:1-10, 2015.

[18] HU, Y.; WANG, L.; POLITIS, D. J.; MASEN, M. A. **Development of an interactive friction model for the prediction of lubricant breakdown behaviour during sliding wear**. Tribology International, 110:370-377, 2017.

[19] BLAU, P. J. **Friction science and technology: from concepts to applications**. 2. ed. Florida, CRC Press, 2009. 436 p.

[20] Bayer, R. G. **Mechanical wear prediction and prevention**. Nova York, Marcel Dekker, 1994. 657 p.

[21] BHUSHAN, B. **Principles and applications of tribology**. 2. ed. Hoboken, Wiley, 2013. 1006 p.

[22] HOLMBERG, K.; ERDEMIR, A. **Influence of tribology on global energy consumption, costs and emissions**. Friction 5(3):263-284, 2017.

[23] AL-SAYED S. R. A.; HUSSEIN, A. H. A, NOFAL, A. A. M. S.; ELNABY, S. E. I. H.; ELGAZZAR, H. A.; SABOUR, H. A. **Laser powder cladding of Ti–6Al–4V α/β alloy**. Materials 10(10):1-16, 2017.

[24] YANG, Z. **Alternatives to hard chromium plating on piston rods**. Ph.D. Thesis, Karlstads Universitet, Karlstad, Suécia, 2011.

[25] RACHIDI, R.; EL KIHEL, B.; DELAUNOIS, F.; VITRY, V.; DESCHUYTENEER, D. **Wear performance of thermally sprayed NiCrBSi and NiCrBSi-WC coatings under two different wear modes**. Journal of Materials and Environmental Sciences, 08(12):4550-4559, 2017.

[26] SILVA JUNIOR, G.; VOORWALD, H. J. C.; CIOF, M. O. H. **Evaluation of Hvof sprayed WC-13Co4Cr and hard chromium electroplated on stainless steel 15-5PH fatigue strength**. In: Proceedings of the 7th international conference on mechanics and materials in design, 7, pp 405–416, 2017.

[27] CASTRO, R. M.; ROCHA, A. S.; CURI, E. I. M.; PERUCH, F. **A comparison of microstructural, mechanical and tribological properties of WC–10Co4Cr-HVOF**

coating and hard chrome to use in hydraulic cylinders. American Journal Material Science 8(1):15–26, 2018.

[28] GENG, Z.; HOU, S.; SHI, G. L.; DUAN, D. L.; LI, S. **Tribological behaviour at various temperatures of WC–Co coatings prepared using different thermal spraying techniques**. Tribology International, 104:36-44, 2016.

[29] LIU, Y. L.; CHENG, J.; YIN, B.; ZHU, S.Y.; QIAO, Z. H.; YANG, J. (2017). **Study of the tribological behaviors and wear mechanisms of WC–Co and WC-Fe3Al hard materials under dry sliding condition**. Tribology International 109:19-25, 2017.

[30] NOORAWZI, N.; SAMION, S. **Tribological effects of vegetable oil as alternative lubricant: a pin-on-disk tribometer and wear study**. Tribology Transactions, 59(5):831–837, 2015.

[31] SAVIĆ, V.; KNEŽEVIĆ. D.; LOVREC, D.; JOCANOVIĆ, M.; KARANOVIĆ, V. **Determination of pressure losses in hydraulic pipeline systems by considering temperature and pressure**. Strojniški vestnik – Journal of Mechanical Engineering, 55(4):37–43, 2009.

[32] TOTTEN, G. E.; DE NEGRI, V. J. **Handbook of hydraulic fluid technology**. 2 ed. Florida, CRC Press, 2010. 966 p.

[33] SHARMA, B. K.; BIRESAW, G. **Environmentally friendly and biobased lubricants**. Florida, CRC Press, 2016. 450 p.

[34] MANG, T.; DRESEL, W. **Lubricants and lubrications**. Weinheim, Wiley, 2017. 1262 p.

[35] Rexroth-Bosch Group. **Environmentally Acceptable hydraulic fluids HETG, HEPG, HEES for axial piston units**. RE 90 221/01.02, Elchingen, 1993. 4 p.

[36] LINSINGEN, I. V. **Fundamentos de Sistemas Hidráulicos**. UFSC, Florianópolis. 2013, 400 p.

[37] STACHOWIAK, G.; BATCHELOR, A. W. **Engineering tribology**. Oxford Butterworth-Heinemann - BH, 2013. 832 p.

[38] HAMROCK, B. J.; DOWSON, D. **Ball bearing lubrication, the elastohydrodynamics of elliptical contacts**. New York, Wiley, 1981. 386 p.

[39] POPOVA, E.; POPOV, V. L. **The research works of Coulomb and Amontons and generalized laws of friction**. Friction 3(2):183–190, 2015.

[40] FILDES, J. M.; MEYERS, S. J.; MULLIGAN, C. P.; KILAPARTI, R. **Evaluation of the wear and abrasion resistance of hard coatings by ball-on three-disk test methods: a case study**. Wear, 302:1040-1049, 2013.

[41] LI, X, SOSA, M, OLOFSSON, U. **A pin-on-disk study of the tribology characteristics of sintered versus standard steel gear materials**. Wear, 340:31-40, 2015.

[42] ODABAS, D. **Effects of load and speed on wear rate of abrasive wear for 2014 Al alloy**. In: IOP conference series: materials science and engineering 295, pp 1-13, 2018.

[43] ERNESTO, A.; MAZUYER, D.; CAYER-BARRIOZ, J. **From full-film lubrication to boundary regime in transient kinematics**. Tribology Letters, 59(23):1–10, 2015.

[44] MULLER, M.; STAHL, L.; OSTERMEYER, G. P. **Experimental studies of lubricant flow and friction in partially filled gaps**. Lubricants 6(4):1-24, 2018.

[45] WANG, Y.; WANG, Q. J.; LIN, C.; SHI, F. **Development of a set of Stribeck curves for conformal contacts of rough surfaces**. Tribology Transactions, 49(4):526-535, 2010.

[46] DOBRICA, M. B.; FILLON, M.; MASPEYROT, P. **Influence of mixed lubrication and rough elastic-plastic contact on the performance of small fluid film bearings**. Tribology Transactions, 51(6):699-717, 2008.

[47] LAFOUNTAIN, A. R.; JOHNSTON, G. J.; SPIKES H. A. **The elastohydrodynamic traction of synthetic base oil blends**. Tribology Transactions, 44(4):648-656, 2001.

[48] GUEGAN, J.; KADIRIC, A.; GABELLI, A.; SPIKES, H. **The relationship between friction and film thickness in EHD point contacts in the presence of longitudinal roughness**. Tribology Letters, 64(3):33, 2016.

[49] THAPLIYAL, P.; THAKRE, G. D. **Correlation study of physicochemical, rheological, and tribological parameters of engine oils**. Advances in Tribology, 2017:1-12, 2017.

[50] KOMVOPOULOS, V.; DO, E.; YAMAGUCHI, S, RYASON P. R. **Effect of sulfur- and phosphorus-containing additives and metal deactivator on the tribological properties of boundary-lubricated steel surfaces**. Tribology Transactions 46(3):315–325, 2003.

[51] MOSHKOVICH, A.; PERFLVEV, V.; LAPSKER, I.; RAPOPORT, I. **Stribeck curve under friction of copper samples in the steady friction state**. Tribology Letters, 37(3):645–653, 2010.

[52] ALI, M. K. A.; EZZAT, F. M. H.; EL-GAWWAD, K. A. A.; SALEM, M. M. M. **Effect of lubricant contaminants on tribological characteristics during boundary lubrication reciprocating sliding**. Applied Physics, 1: 1-16, 2017.

[53] ASAF, Y.; DE NEGRI, V. J.; THEISSEN, H.; MURRENHOF, H. **Analysis of the influence of contaminants on the biodegradability characteristics and ageing of biodegradable hydraulic fluids**. Strojniški vestnik - Journal of Mechanical Engineering, 60(6):417–424, 2017.

[54] Baets, P.; Degrieck, J.; De Velde, F. V.; Van Peteghem, A. P. **Experimental verification of the mechanisms causing stick–slip motion originating from relative deceleration**. Wear, 243:48–59, 2000.

[55] GAO, C. **Stick-slip motion in boundary lubrication**. Tribology Transactions, 38(2):473–477, 1995.

[56] BELLEMARE, S. C.; DAO M.; SURESH, S. **Effects of mechanical properties and surface friction on elasto-plastic sliding contact**. Mechanics of Materials, 40:206–219, 2008.

[57] RABINOWICZ, E. **Wear of hard surfaces by soft abrasives**. In: International conference on wear of materials, Reston, VA, 1993.

[58] STRAFELINI, G. **Friction and wear: methodologies for design and control.** Switzerland, Springer, Cham. Tracts in Mechanical Engineering, 85, 2015. 283 p.

[59] SHAHABUDDIN, M.; MASJUKI, H. H.; Kalam, M. A.; Bhuiya, M. M. K.; Mehat, H. **Comparative tribological investigation of biolubricant formulated from a non-edible oil source (Jatropha oil)**. Industrial Crops and Products, 47(1):323–333, 2013.

5. LASER REMELTING OF WC-CoCr SURFACE COATED BY HVOF: EFFECT ON THE TRIBOLOGICAL PROPERTIES AND ENERGY EFFICIENCY

Richard de Medeiros Castro[1], Elvys Isaías Mercado Curi[1], Luiz Fernando Feltrin Inácio[1], Alexandre da Silva Rocha[2], Milton Pereira[3], Rafael Gomes Nunes Silva[4], Adriano de Souza Pinto Pereira[3]

[1]Laboratório de Engenharia de Superfícies e Tribologia - LAEST, Centro Universitário - UNISATC, Criciúma, Brazil.
[2]Laboratório de Transformação Mecânica - LdTM, Universidade Federal do Rio Grande do Sul - UFRGS, Porto Alegre, Brazil.
[3]Laboratório de Mecânica de Precisão - LMP, Universidade Federal de Santa Catarina - UFSC, Florianópolis, Brazil
[4]Belgian Welding Institute, Ghent, Belgium

Abstract

In this article, the tribological behavior and energy efficiency of surfaces coated with WC-CoCr/HVOF were evaluated after a laser remelting process, using low and high laser energy densities, respectively, 33.3 and 150 J/mm^2. The purpose of laser remelting was to adequately modify the microstructure of the coatings and promote better performance during surface sliding. Therefore, the microstructure, phase composition and microhardness of the coatings were investigated, and heat effect on the substrate. During dry and lubricated tribological tests, friction coefficient (COF), wear, and surface roughness also were evaluated. In the dry tests, friction, wear and heat dissipation energies were obtained, which were then correlated with the energy consumed by the tribometer. A HEPR-type biodegradable oil was used in the lubricated tests. The proper formation of W_2C and Co_3W_3C, obtained for the lower energy density, increased the hardness, without weakening the material, while the CrC phase acted as an anti-wear barrier. Whereas for the high energy density, thermal decomposition produced fragile phases, which were easily removed from the matrix during the wear test. The sample tested in as-sprayed condition had a high adhesion and friction compared to the remelted samples. On the remelted surfaces, greater friction stability was obtained. The lower dry friction was not linked to the lower power consumption, a result which was then attributed to the higher heat dissipation from the

surface during the tests. Finally, this study proposes a methodology for quantifying the efficiency of sliding surfaces and points to a sustainable solution for tribology.

Keywords: WC-CoCr; HVOF; Laser remelting; Friction; Energy Efficiency; Green Tribology

5.1 Introduction

High-Velocity Oxygen Fuel (HVOF) thermal spray deposition is a surface engineering technique widely used in industry to improve the performance of mechanical components, especially on the aspects of wear and corrosion [1,4]. Most surface engineering studies focus on machinery components in relative motion, such as pistons, gears, pumps, cylinders, valves, bearings, and braking systems. [4-6]. For example, hydraulic equipment for marine applications is susceptible to corrosion wear, thus, to mitigate it, coatings manufactured by HVOF with alloys based on titanium, nickel, chromium, and tungsten carbide are commonly applied [7-16]. In particular, alloy sprayed by HVOF, such as WC-CoCr is suitable where sliding wear resistance is required, but also for applications requiring the corrosion resistance promoted by the percentage of chromium in the alloy. Similar results are shown in the literature for applications with hydraulic components [17-21].

Although the state of the particles sprayed by HVOF is in the molten state before the contact with the surface, not all particles at the time of impact remain in this state. In this way, small cavities (micropores) that are distributed throughout the coating section and at the interface of the base material, are identified [22-24]. Due to these defects and the lack of metallurgical bond between the substrate and the coating, HVOF is limited to some applications, particularly those that require greater resistance to wear, corrosion and impact. Ciubotariu et al. [25], describe that under impact conditions, for example, cavitation in hydraulic machines, a poor adhesion, in combination with the presence of oxides in the pores, limits the application of the method. Murugan et al. [26] presented a study of the correlation between the hardness of the WC-CoCr coating and porosity, revealing a decrease in hardness on coatings with higher levels of porosity. Thus, it is clear that this situation reduces the lifespan of some mechanical components.

Improve the homogenization and reduce porosity of a microstructure of a coating by HVOF, and also increase impact and wear resistance, can be obtained from the laser remelting process [4,25,27-33]. These characteristics offered to the surface are obtained due

to the unique properties of laser radiation, such as high beam coherence, power availability, versatility, and a large energy density range [34]. Studies describe the use of laser remelting as an efficient technique that promote a significant improvement in the porosity content, adhesion, and tribological properties of HVOF-coatings [4,33,35-37]. This means that the characteristics of laser processing, combined with materials with good mechanical properties and the appropriate selection of the remelting parameters, can manufacture coatings with high-quality surfaces [38]. These laser remelting features demonstrate the potential of the technique to surface properties used in mechanical components.

In the literature, no detailed studies were found showing the tribological behavior of the WC-CoCr/HVOF alloy after laser remelting, in particular, relating thermal dissipation, adhesion, and deformation energies with material removal. Also, there is a lack of studies on the energy efficiency of dry, lubricated sliding surfaces in combination with the use of biodegradable synthetic oils. These oils are used in hydraulic systems when consideration is given to energy and environmental sustainability as a priority and, therefore, become linked to the concept of green tribology. This field of engineering focuses on friction and wear, which are key factors in energy conservation. Green tribology also involves environmental aspects of lubrication, new materials and alloys, and surface modification techniques [7,39], such as it is promoted in this work. It is expected that this study encourages the use of surfaces and lubricants which can improve the tribological and environmental performance of hydraulic components.

In this context, the main objective of this work is to evaluate the improvement of the surface properties of the WC-CoCr/HVOF coating by laser remelting, aiming at reducing the friction coefficient and sliding wear, and ultimately optimize the energy consumed by the hydraulic equipment. The coating was deposited on a surface of SAE 1045 steel. Then the laser remelting was carried out, changing the scanning speed and the power of the laser beam. The coatings' microstructure, phase composition and microhardness were used in their evaluation. The tribological performance of dry and lubricated sliding coatings was evaluated using a pin-on-disk tribometer. For the lubricated sliding tests, a biodegradable synthetic hydraulic oil was used. Also, an estimate of the energy efficiency of the surfaces, η_s was obtained by measuring the energy consumption of the tribometer during the dry sliding, and then correlated with the results of friction energies, W_f and, wear, U_T, and, of thermal dissipation, Q_t. The main contribution of the work is to show the impact of laser remelting on surfaces, and correlate the main performance parameters (friction, wear,

hardness, heat dissipation), to promote the use of sustainable and energy-efficient tribological systems.

5.2 Experimental procedure

5.2.1 *Materials and thermal spray deposition*

In this study, the substrates were obtained from an SAE 1045 steel rod sectioned into discs with 60 mm in diameter and 10 mm in thickness. The WC-CoCr alloy was used for coating deposition on the substrate. Previously sandblasted with aluminium oxide (Al_2O_3) particles to eliminate impurities. This procedure resulted in a target surface with an average Ra roughness of 6.4 µm.

The coating deposition was conducted with an HP/HVOF JP-5000 system by Praxair Surface. Parameter selection has been based on previous studies that mention applications for hydraulic components [12]. The HVOF spraying parameters used are shown in Table 5.1. The powder used in the deposition of the coatings was WOKA 3653 (WC-10Co4Cr), with a chemical composition (wt.%) of Co 9.74, Cr 4.11, C 5.27 and balanced by W. The density of the powder is 4.8 to 5.0 kg/m^3 with an average particle diameter of 45 ± 11 µm. The morphology and geometric characteristics of the powder particles and the cross-section of the coating are shown in Fig. 5.1.

Table 5.1 - Parameters of thermal spray used in the deposition of WC-CoCr.

Nº	Parameters	Values
1	Oxygen flow rate	0,064 ± 0.004 m^3/min
2	Powder feed rate	90 g/min
3	Gun velocity	300 mm/s
4	Spray distance	305 mm
5	Kerosene flow rate	7.57 ± 0.63 L/min

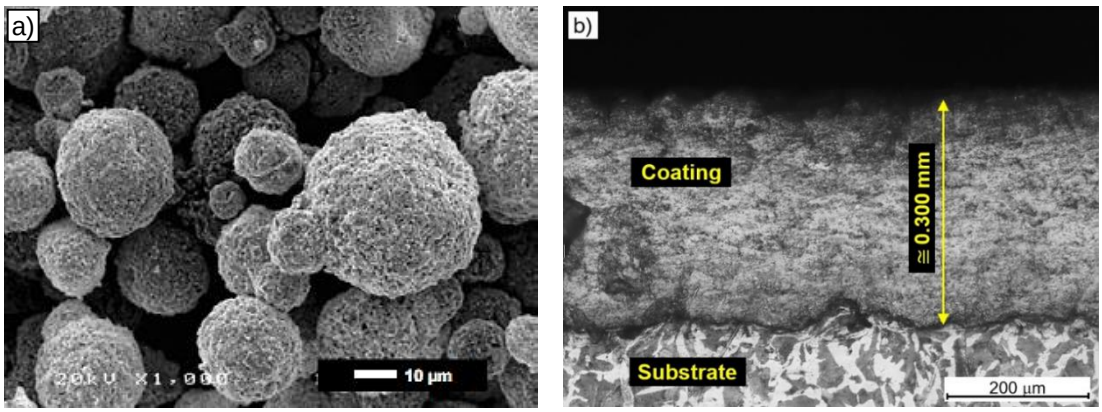

Figure 5.1 - SEM to powder morphology with 200X magnifications (a) and cross-section of the as-deposited coating (b).

HVOF deposition produced a coating with an average thickness of about 300 μm (Fig. 5.1b), which normally can be specified for the hydraulic components under study. Fig. 5.1b shows a lamellar structure and the porosities that are typical of the HVOF process. After the deposition process of the WC-CoCr alloy, the surfaces were sanded and polished to a condition usually specified in rods of hydraulic pistons, with these having an average Ra roughness of lower than 0.2 μm [40].

5.2.2 *Laser processing techniques*

The surface laser remelting (SLR) treatments were performed as shown in Fig. 5.2. A laser system composed of a YLS-10000 fiber laser source manufactured by IPG Photonics and equipped with a Precitec YW52 welding head from the laser processing head which coupled to a cartesian motion system was used for the remelting process. The nominal wavelength emitted by the source is between 1070 and 1080 nm. The remelting process was set to operate in continuous mode (CW). As for the configuration of the incident laser beam, it has a focal length of 300 mm and a theoretical focal spot of 0.8 mm in diameter. However, all remelting tests were performed with a 35 mm distance between (Zr) the beam focus and the sample surface, resulting in an estimated focal spot (di) of 1.2 mm. Two laser powers and laser scanning speed were selected, based on preliminary tests that were conducted to identify the best resulting microstructures.

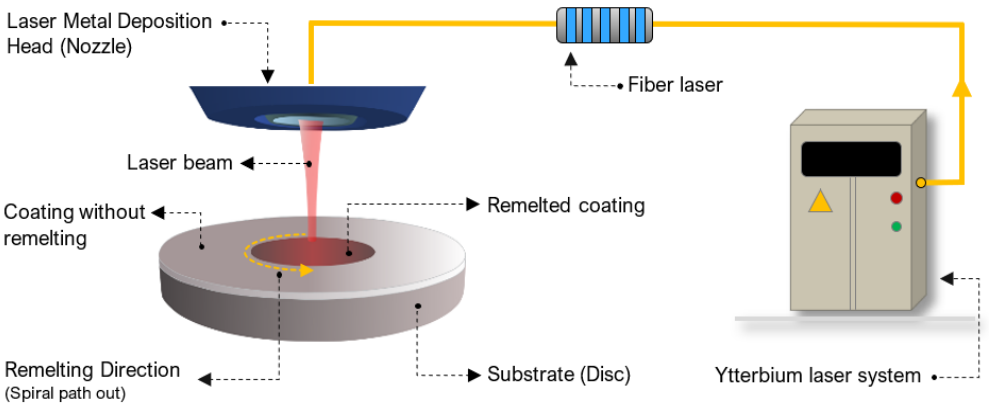

Figure 5.2 - Schematic diagram and scanning strategy of direct laser remelting process.

Fig. 5.2 shows the schematic and details of the remelting technique strategy. Note that the scanning strategy used for remelting was from the inside to the outside with the spiral strategy, as shown. The time to remelting was 4.5 and 14.6 minutes for LM1 and LM2, respectively. Maximum surface temperatures were also estimated using the thermophysical

properties of the coatings, resulting in about 1,750 K for LM1 and 2,540 K for LM2. Guo et al. provide similar results for temperatures in a laser remelting process in a WC-12Co coating [41]. In Figure 4c, it is observed that in applying the laser, the coatings have a morphology like that of a spoon, because of the typical Gaussian energy distribution of the laser process. From the values used for the scanning speed, laser power, as well as the laser beam diameter, the energy densities, E_p, (J/mm^2) were estimated. The laser energy density is expressed as $E_p = P/(v.di)$, where P is the laser beam power, v is the scanning speed (mm/s) and di is the laser beam diameter, respectively [35,42]. From previous tests using different configurations, the two optimized parameters for scanning power and speed (Table 5.2) were selected. Similar results in the literature have also indicated that the optimum parameters for coatings are obtained by the quality of the coatings after experimental testing [43,44]. Furthermore, Cui et al. [35] have related that it is important to investigate the material behavior under different parameters since the microhardness of the coatings has a non-linear result in concern to the energy density.

Table 5.2 - Parameters of laser remelting process

Nº	Parameters	Symbol	Values – LM1	Values – LM2
1	Laser Power	P	400 W	600 W
2	Scanning velocity	v	10 mm/s	3.33 mm/s
3	Laser incident diameter	di	1200 µm	1200 µm
4	Overlapping rate	---	30 %	30 %
5	Shielding gas (Ar)	---	15 l/min	15 l/min

The values of the sample maximum affected extension (z_{max}) affected by the heat source, were estimated using the mathematical models presented by equations 1 and 2 [42]. Table 5.3 shows the thermophysical properties of the surface manufactured with the WC-CoCr coating. Equation 1 was used to obtain the thermal diffusivity value (α), and the z_{max} value was calculated from equation 2.

Table 5.3 - Thermophysical properties of WC-CoCr coating

Nº	Properties	Values	Unit
1	Density, (ρ)	15800	kg/m^3
2	Specific heat, (Cp)	210	J/(kg.K)
3	Thermal conductivity, (k)	58	W/(m.K)
4	Thermal diffusivity, (α)	1.76 x 10^{-5}	m^2/s

$$\alpha = \rho Cp/k \tag{1}$$

$$z_{max} = \sqrt{\alpha ti} = \sqrt{\alpha \frac{d}{v}} \tag{2}$$

Where α is the thermal diffusivity, k is the thermal conductivity, Cp is the specific heat and, ρ is the density. To estimate the extent of the heat affected zone (HAZ), it is necessary to use the irradiation time, ti, or the laser incident diameter, di, and the scanning speed, v.

5.2.3 *Characterization of Microstructure, Phase Composition and Microhardness*

The coated samples were cross-sectioned by Wire Electrical Discharge Machining (WEDM) to assess the microstructure and microhardness of the coating layers. These samples were embedded in resin, then sanded and polished. Sanding paper (SiC) was used in up to 600 mesh, and polishing was done with 1 μm diamond paste. Etching with 2 % nital was used to reveal the microstructure of the coating in the cross-sectional area of the samples, and then evaluated using optical and scanning electron microscopy (SEM). Also, an X-ray diffractometer was used to determine the phase composition of the microstructure. The Image-J software was used to quantify the porosity of the cross-sections of coatings. A 250 × 300 μm^2 area was selected on the polished cross-section of the coating and then the image was analyzed.

Vickers microhardness tests were performed on a Shimadzu HMV-2T tester, with a 9.807 N (HV1) load for 10.0 s. Hardness measurements were made at the cross-section of the deposited coatings, as well as measurements at the top of the substrate surface. Three indentations were performed in each region analyzed, obtaining the average measure at each point. The method generated the microhardness profile of the cross-section and longitudinal measurements on the surface of the samples, as will be shown in Fig. 5.7.

5.2.4 *Tribological test of the coatings*

Tribological tests were performed using a pin-on-disk tribometer [45]. Dry and lubricated sliding tests were carried out under atmospheric conditions and at room temperature, using as-sprayed surfaces (WLR) and laser remelted ones (LM1 and LM2). In the dry tests, 6 mm zirconium oxide (ZrO_3) balls were used under unidirectional sliding on a flat disc coated with WC-CoCr. Lubricating tests, brass balls (Cu-Zn) were used, simulating the sliding of materials used in hydraulic cylinders. In the lubricated tests, a biodegradable hydraulic oil was used that uses polyalphaolefins and related hydrocarbons as the base fluid (HEPR type). This combination of laser remelting surfaces, operating on dry

and lubricated sliding, aimed to promote energy and environmental sustainability analysis. The test parameters are shown in Tab. 5.4.

Table 5.4 - Friction and wear testing parameters

Nº	Parameters	Symbol	Dry test	Lubricated test
1	Applied load	F_n	30 N	50 N
2	Pin radius	r_p	3 mm - ZrO_3	3 mm - Cu-Zn
3	Radius of wear track	R	18 mm	20 mm
4	Disc radius	r_0	30 mm	30 mm
5	Test time	Δt	62 min	124 min
6	Initial temperature	T_0	23.1 ºC	24.2 ºC

The dry tests were conducted using a load (F_n) of 30 N, at a sliding speed of 0.4 m/s, using a radius of 20 mm on the disc and a total sliding distance (Δs) of 1500 m. In the lubrication tests a load of 50 N at the same speed, a radius of 18 mm and a sliding distance of 3000 m were used. To perform the lubricated tests, the tribometer was adapted, using a cup (reservoir) with the addition of 10 ml of oil. All tests were monitored at temperature and the tests were carried out at a relative humidity of 47 ± 2 %. At each test, the used biolubricant was replaced, with a volume of 10 ml.

The friction coefficient (μ) of the tribological pairs in dry and lubricated conditions were obtained from the measurement of the frictional force (F_f), provided by the tribometer. The frictional force was divided by the normal force (applied load) exerted by the ball, $\mu = F_f/F_n$ using the concepts proposed by Amontons and Coulomb [46]. The ball wear scar diameter (WSD), which is defined as dw, was measured using an optical microscope. The volume removed (V_p), from the ball was obtained from the height, h of the worn scar, the radius r_p, of the pin (ball), by equation 3, as shown in Fig. 5.3 (section 2.6). The volume removed from the pin (ball), was calculated via equation 4 [47]:

$$h = r - \left(r^2 - \left(\frac{dw}{2}\right)^2\right)^{\frac{1}{2}} [mm] \quad (3)$$

$$V_p = \pi h^2 \left(r - \frac{h}{3}\right) \ [mm^3] \quad (4)$$

The worn volume on the disc (V_d) in the dry tests were obtained using the profile area measurement (A_d), which was measured by the roughness meter as indicated in Section 5.2.5. R is the radius of wear track. The total removed volume of the disc was obtained by equation 5.

$$V_d = 2\pi R A_d \ \ [mm^3] \tag{5}$$

Wear tracks in the coatings were observed by SEM/EDS to investigate the failure mechanisms of the sprayed and remelted coatings.

5.2.5 *Assessment of Disc Surface Properties*

Roughness is one of the main parameters used to evaluate the surfaces that will be subjected to sliding. Accordingly, using a Mitutoyo SJ 310 roughness meter, the discs' surface roughness was obtained. Five measurements were performed every 72 degrees of the disc perimeter and the average of these measurements was obtained. Table 5.5 shows surface conditions prior to tribological testing at parameters Ra, Rz and Rmr, commonly used to assess hydraulic cylinders surfaces.

Table 5.5 - Measurement of initial roughness of specimens. Cut-off of 0.25 mm

Nº	**Conditions**	**Ra [µm]**	**Rz [µm]**	**Rmr [%]**
1	LM1	0.085 ± 0.006	0.911 ± 0.057	77.9 ± 0.4
2	WLR	0.089 ± 0.002	1.440 ± 0.101	77.1 ± 0.6
3	LM2	0.112 ± 0.021	1.125 ± 1.172	79.1 ± 0.2

The evaluation of the coating's worn surfaces after the sliding tests were done by two methodologies: SEM and roughness profile measurement. This procedure was used to calculate the volumetric loss of discs. To obtain the average profile of the worn area of each sample, five measurements were taken along the perimeter of the track. Then, the concepts of numerical integration were used to evaluate the worn area, obtained in μm^2. Finally, an arithmetic mean of these segments was taken and the total sliding length of the track was estimated.

5.2.6 *Methodology for Estimating Energy Efficiency of Sliding Surfaces*

The evaluation of the energies manifested on the surfaces during the sliding of the disc against the ball was carried out by measuring the following quantities: frictional force, temperature, rotation speed, and electric current of the tribometer drive motor. A non-invasive meter was installed in the electric motor supply to measure the electric current. The friction force (F_f) was measured by a load cell of the tribometer and the friction coefficient

was obtained for the normal load applied, F_n, recorded at each sampling time. The temperature was measured using an infrared sensor, installed in the direction of the sliding contact between the ball and the disc.

The analysis of the energy of the surfaces was conducted using the concepts of the first and second law of thermodynamics, proposed by Rymuza [48]. The total energy of friction (E_{Tf}) is changed into the thermal energy (Q_t), energy stored in the rubbing materials (W_f) and wear debris (U_T), by equations 6 and 7.

$$E_{Tf} = Q_t + W_f + U_T \quad [J] \tag{6}$$

$$W_f = \int_0^S F_f \, ds = \int_0^S F_f \, v dt \quad [J] \tag{7}$$

An analytical model that estimates the heat of friction in the region of contact between ball and disc is proposed by Rymuza [48], Kennedy et al. [49] and Federici et al. [50]. Equation 8 shows the model, where q_t is the total heat dissipation due to friction per unit area, generated by the sliding contact. While the heat dissipated by the pin and disc, is represented by q_{pin} pin and q_{disc}, respectively. Equation 9, the total specific heat dissipated is converted into thermal energy, when is multiplied by the nominal contact area (A_n) between the pin (ball) and the disc. Na Fig. 5.3 shows the schematic diagram of a typical pin-on-disk contact and its main properties.

$$q_t = q_{pin} + q_{disc} = k_p \frac{T_s - T_0}{l_p} + h_d \frac{T_s - T_0}{\left(\frac{a}{r_0}\right)^2} \quad [W/m^2] \tag{8}$$

$$Q_t = q_t . \frac{A_n}{\Delta t} = q_t . \frac{2\pi . a^2}{\Delta t} \quad [J] \tag{9}$$

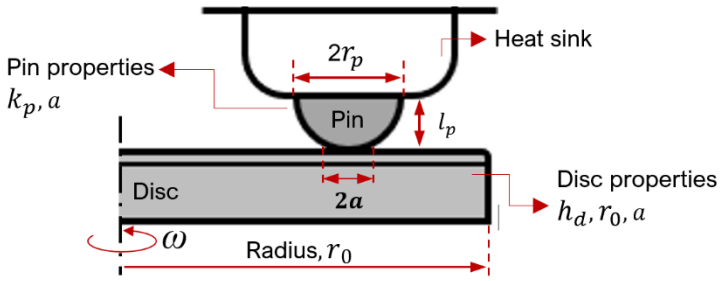

Figure 5.3 - Schematic diagram of a typical pin-on-disk contact and its main properties

Where k_p is the thermal conductivity of the pin, l_p is the length of the heat paths, T_s and T_0 are the final and initial surface contact temperature, respectively. The portion of heat

in the disc is defined by h_d which represents the thermal convection coefficient, a is circular contact radius of the pin on the disc and r_0 is the external radius of the disc. The temperatures T_s and T_0 were obtained with experimental measurements. If the pin end is hemispherical, the contact zone could be determined by elastic (Hertzian) contact analysis, with the parabolic pressure distribution within the contact zone.

Kennedy et al. [49], described that the propagation of heat from the disc should be considered only by convection because by conduction it is quite questionable since the heat in the disc is released mainly from the exposed surface that is in a rotating motion. While the transfer of heat by conduction prevails on the pin. However, considering a pin with spherical geometry, sliding in a plane, the effective value of l_p, shown in Fig. 5.3, can be obtained considering that the heat flow is not unidirectional, but in all directions. The following relationship showed in equation 10, was proposed by Ashby et al. [51].

$$l_p = \frac{\sqrt{\pi}}{2}.r_p = 0.89.r_p \quad [m] \tag{10}$$

The deformation produced between the pin and the disc generates a contact area, which is calculated using Hertz pressure concepts, where $R'$and E' are the radius of curvature and the equivalent Young's modulus, respectively. The radius of curvature can be defined by $R' = r_p/2$ and E' is obtained by equation 12. $E_{1,2}$ is the Young's modulus and $v_{1,2}$ is the Poisson's coefficient for the pin and the disc, respectively [52].

$$a = \sqrt[3]{\frac{3F_n R'}{E'}} \quad [m] \tag{11}$$

$$E' = \frac{E_1.E_2}{E_2(1-v_1^2)+E_1(1-v_2^2)} \; [N/m^2] \tag{12}$$

The friction dissipation energy occurs not only in the form of total heat dissipation (Q_t), but also due to the deformation, adhesion, and the applied load's potential energy. According to Johnson et al. [53], the total energy in that of the sliding system, is calculated by equations 13 and 14.

$$U_T = U_s + U_E + U_P \quad [J] \tag{13}$$

$$U_T = -\pi a^2 W_a - \frac{(1-\nu^2)F_n^2}{4Ea} + A + B \quad [J] \tag{14}$$

The terms A and B are arbitrary constants for stored elastic energy and, the potential energy of the load, respectively. Makkonen [54] indicates that the energy of deformation and adhesion named W_a, is estimated by equation 15.

$$W_a = \mu 2dH \quad [J/m^2] \tag{15}$$

Where μ is the friction coefficient (COF), d is the characteristic length of the real contacts. The length of the real contact value can be considered equal to 1 nm. This constant value is validated by previous studies, obtaining 0.96 for the linear correlation coefficient between the theoretical and measured COFs, and confirmed this constant value for different materials [54]. The surface hardness of the most ductile material (disc surface) is represented by H. In the dry tests, a Al_2O_3 ball with an average hardness of 1500 HV was used. Tabs. 5.6 and 5.7 the input values are presented for each quantity mentioned in the equations for the disc and pin surfaces.

Table 5.6 - Mechanical and thermal properties of surfaces for use in equations

Nº	**Properties of surfaces**	**Symbol**	**Disc - surface conditions**			**Pin (ball)**
			LM1	**WLR**	**LM2**	
1	Young's modulus, GPa	E	580	580	580	303
2	Poisson's ratio	ν	0.23	0.23	0.23	0.21
3	Average microhardness, HV_1	H	1313 ± 42	1107 ± 16	906 ± 21	1500 ± 16
4	Thermal conductivity, W/(m·ºC)	k_p	---	---	---	25
5	Thermal convection, W/(m².ºC)	h_d	44.8	44.8	44.8	---

There are two approaches to evaluate the efficiency in a sliding process, which are: the energy efficiency of the equipment under analysis (Zhou et al. [55]) and that of the sliding surface (Wu et al. [56]). In both cases, the yield is evaluated by the ratio between useful energy and delivered energy. In machines, the electrical energy has two parameters, the voltage, and the electrical current. Normally a constant voltage is considered, and the current would be changing as a function of the instantaneous energy consumption. As for surface energy, Wu et al. [56], defines that the input energy E_{in}, is calculated by equation 16, and the wear energy, E_w, is obtained by equation 17.

$$E_{in} = W_f + E_w \quad [J] \tag{16}$$

$$E_w \cong E_c + E_s \quad [J] \tag{17}$$

Where, E_c is the thermal energy dissipated by the wear parts, and E_s corresponds to the increase in the surface energy that was generated as the wear parts became abrasive particles.

Table 5.7 - Values for the parameters of surfaces – dry test

Nº	Parameters of surfaces	Symbol	Pin and Disc		
			LM1	WLR	LM2
1	Final test temperature, ºC	T_s	23.1 ± 0.4	25.2 ± 0.5	26.6 ± 0.6
2	Friction coefficient - COF	μ	0.11	0.44	0.10
3	Circular contact radius, m	a		8.65×10^{-5}	

If the input energy dissipated by the surface corresponds to that produced by friction, wear, and heat energy, then the surface efficiency, η_s can be determined by the following relationship, according to equation 18. Where W_f is energy stored in the rubbing materials, Q_t is thermal energy and U_T is the total wear energy.

$$\eta_s = \frac{W_f}{W_f + Q_t + U_T} \times 100 \ [\%] \tag{18}$$

5.3 Results and Discussion

5.3.1 *Microstructure and Phase Composition of WC-CoCr Coatings*

The achievement of a more suitable microstructure and the prediction of the heat-affected zone (HAZ) in a process of heat treatment or remelting, requires an optimization of the laser energy parameters. This optimization is usually obtained by numerical finite element simulation (FEM) or by a set of experimental tests [25,26,43,57,58].

Energy densities E_p of 33.3 and 150 J/mm^2 were obtained from the laser power of 400 and 600 W for LM1 and LM2 (Table 5.2), respectively. Fig. 5.4 shows the micrographs of the coatings cross-sections and highlights the HAZ. The layer thickness of the coating applied for LM1, and WLR was about 300 µm. However, only in the LM2, geometric dilution of the coating was identified, increasing its thickness. As seen in Fig. 5.4c, the higher energy density, increased thermal diffusion along the sample cross-section.

The value of the HAZ maximum depth, (z_{max}) da HAZ, was obtained from equations 1 and 2. The estimated values of the coating layer thickness for samples LM1 and LM2 were calculated as 1.45 and 2.52 mm. However, in Figs. 5.4a and 5.4c the effect of heat at reduced

dimensions, i.e., half of the calculated values, being 0.65 mm for LM1 and 1.25 mm for LM2, are noticeable. Śloderbach and Pająk [59], show that the HAZ is classified into several regions of the cross-section, with each depth and temperature, corresponding to the boundaries represented in the phase diagram of the material. In this study, performed for steel alloys, the authors show that the maximum irradiation depth would be near 600 ºC. However, only near 880 °C, would be at the grain refinement limit that would correspond to the approximate depth values that were presented in Figs 5.4a and 5.4c. Problems related to high dilution with extensive HAZ and the lack of metallurgical bonding between the coating and the substrate still need to be addressed, as highlighted by the literature [4,6,9,12]. Also, selecting an alloy with suitable properties for some specific applications is still a complex task.

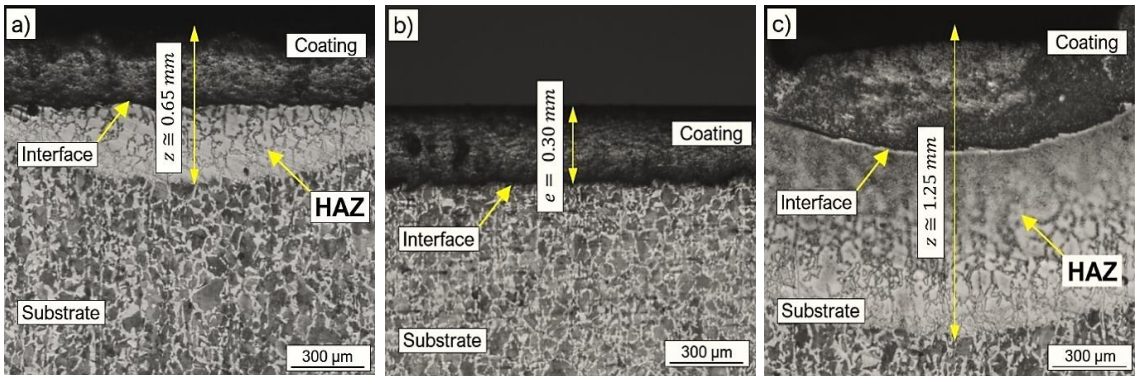

Figure 5.4 - Low-magnification OM microstructure of the cross-sections of the coatings. LM1: a) remelted 400 W, (b) WLR: detailing of the microstructure sprayed, c) LM2: remelted 600 W.

Fig. 5.5 shows the SEM micrographs at low and high magnification of the cross-section and of the coated surfaces, as well as the remelted laser coatings. The LM1 and WLR samples (see Fig. 5.5a-b), show a typical lamellar and under-layered microstructure produced by HVOF thermal spray, homogeneously formed, crack-free, high density, and with a low degree of porosity [60,61]. At the highest magnifications shown by SEM, these microstructures reveal the presence of only thin layers of oxides or micropores inside the coating.

The lowest remelting energy (LM1) produced a partial heat treatment of the coating, but it was likely insufficient to establish a good metallurgical bond with the substrate. However, in LM2, a significant modification in the microstructure of the coating and substrate was observed. These changes in the substrate also influenced its microhardness and the decrease of voids (highlighted by a yellow circle - Figs. 5.5). In cross-section, no significant change was observed in the microstructure of the WLR for LM1, which affected

the porosity differentiation, but for LM2, the decrease in porosity was clear. In an analyzed area of 350 x 250 µm in the cross-sections of the samples, approximately the following percentages of porosities were obtained: 1.74, 1.63, and 0.44 % for LM1, WLR, and LM2, respectively. However, in the top images of the surfaces at 5000 X magnification (Fig. 5.5d-e), the changes in microstructure are better evidenced, especially with the change in the homogenization of the alloy. Other studies have also shown that the laser used as a heat source promotes the decrease of pores, the densification of the layer, as well as improving the adhesion of the coating to the substrate [38,62-65]. The impact of the dilution, as well as changes in the microstructure and chemical composition of the coatings, are revealed by X-ray analysis (Fig. 5.6).

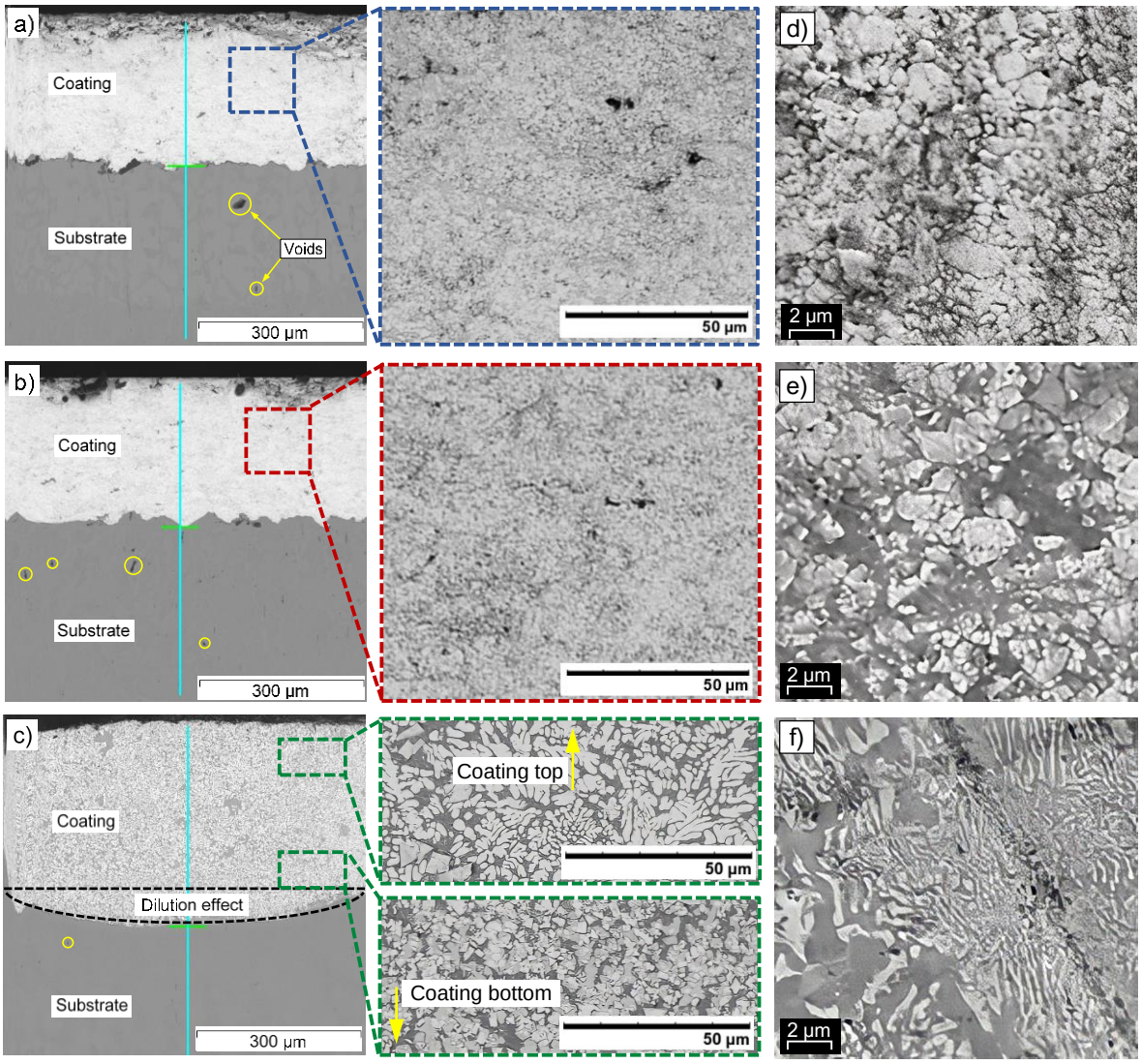

Figure 5.5 - Low and high magnification SEM microstructure of the cross-sections of the coatings: a) LM1: remelted with 400 W power and detailing of the microstructure. b) WLR: typical microstructure as-sprayed and detail of the coating thickness. c) LM2: remelted with 600 W power and microstructure for different depths. High magnification micrographs of the top of each type of surfaces: d) LM1, e) WLR and f) LM2.

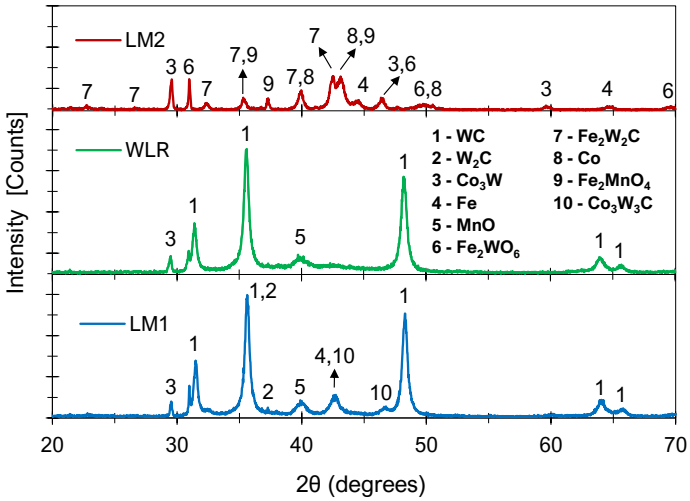

Figure 5.6 - X-ray diffraction patterns of the WC-CoCr.

The high surface temperature caused by laser beam heating promoted important changes in the microstructure of the HVOF coatings that were different for each sample. The high cooling rate resulted in a dendritic microstructure with WC agglomeration in the LM2 surface coating matrix. Although the energy density used for LM2 resulted in a good metallurgical bond between the substrate and the coating, the mechanical properties of the coating and substrate were changed. While in LM1 only a heat treatment was produced, with minor microstructural changes, in LM2 surface a remelting of the WC-CoCr coating occurred with significant microstructural changes. An analysis of the X-ray diffraction patterns identified the presence of the primary WC phase for all samples, but not clearly the CoCr phase due to the WC proportionality ratio (86% by mass). In LM1, some peaks show the formation of two new phases: W_2C and Co_3W_3C, displaced by the high temperature developed on the surface during the laser beam emission. Using the thermophysical properties of the LM1 and LM2 samples, the temperatures of 1,750 and 2,540 K were estimated, respectively, on the surfaces. The temperature reached in LM1 was close to the melting temperature of the matrix elements. These new phases (mixed carbides) formed in LM1 have a higher hardness than the monocarbon produced in the WLR. Similar studies also show that these phases are obtained after laser remelting or surface heat treatment [66-68]. In LM2, the XRD analysis identified other phases and with low energy levels obtained for WC, compared to the other samples. Although the LM2 showed an interface with a good metallurgic bond (Fig. 5.5c), the parameters used in this sample generated the formation of fragile phases or the weakening of existing phases. Furthermore, thermal decomposition identified by W_2C, shows the occurrence of decarburization of the alloy, which affected the mechanical and tribological behavior of the coatings. Also, the presence of Fe in the coating,

shows that an amount of iron was brought from the substrate to the coating, which affected the microstructure and the microhardness of the samples. Afzal et al., 2014; Afzal et al., 2015; Ghadami & Aghdam, 2019 cited that using low speeds in a laser remelting process of a surface coated with WC12%Co, the coating layer starts to melt again, and the melt depth increases with decreasing scan rates [69-71]. In this case, it was shown that the WC-Co coating remakes and begins to mix with the substrate material to form a new composite material.

X-ray analysis also identified the presence of other phases Fe_2W_2C, Fe_2MnO_4, Fe_2WO_6, MnO. The formation of these complex oxide phases occurred because of the high temperature created by the laser remelting process. Carbide formation was facilitated by improved diffusion of alloy matrix carbon. Moreover, it is suggested that these oxides were formed because laser remelting in LM2 did not provide effective gas protection, as well as the high chemical affinity of the metals of alloy with oxygen. In most cases, this chemical interaction occurs more easily than carbon in an alloy. The presence of these oxides can be beneficial during sliding, acting as a solid lubricating agent.

5.3.2 *Effect of Laser Remelting on the Microhardness*

Besides the changes in the microstructure, the effects of laser heat treatment on coatings and substrates are also identified by the microhardness of the samples. Fig. 5.7 shows the average values of Vickers microhardness (HV1) for each analysis point, with their respective standard deviation.

The microhardness measurements on both the cross-section and the surface were similar for each coating while maintaining different values between them. The parameters used for LM1 promoted an increase in the average microhardness values of the coating to 1313 HV compared to 1107 HV for the sprayed WLR sample. The increase in microhardness in LM1 was caused by the slight densification of the layer and the formation of the Co_3W_3C phase precipitated in the CoCr matrix. This precipitation occurred due to the difference in cohesive energies between the WC phases and the mixed carbide. While the cohesive energy of the WC phase is 10.64eV/atom, Co_3W_3C is 8.70eV/atom and therefore precipitated more easily in the matrix [72]. Some studies cite that W_2C and Co_3W_3C have an estimated average hardness of 3000 and 4000 HV, respectively, i.e., higher than the WC phase [72-75]. Other studies also describe that the reorganization of the CoCr matrix and the formation of new carbides improves the toughness of the material. Besides increasing hardness, greater

toughness combined with ductility, improves surface wear performance [76-79]. Fig. 5.7b further highlights the influence of the high cooling rate for LM1 on the slight increase in microhardness from the center towards the edge of the sample. (top surface, 4 to 20 mm). It is noticed that the higher cooling rate (LM1) influenced the microhardness values of this coating.

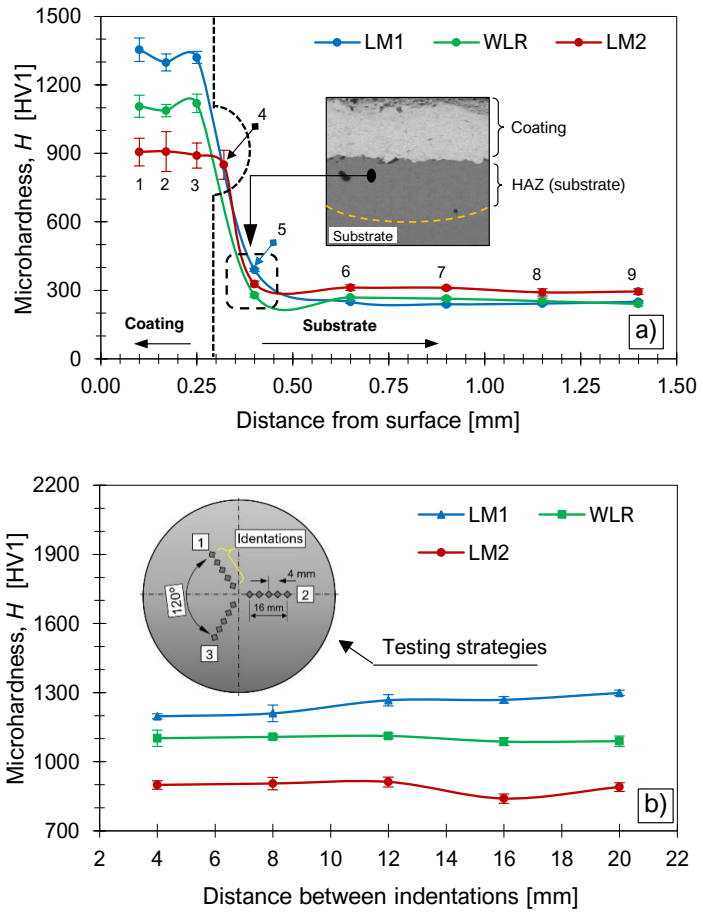

Figure 5.7 - Microhardness of the coatings: a) cross-section with detail of the heat-affected zone (HAZ) and b) top surface.

The highest energy density used for LM2 resulted in the lowest microhardness values, approximately 906 HV. In comparison to WLR, a slight increase in hardness is observed for LM1 and LM2 coatings in the HAZ region (identified - point 5). While the average in the substrate were 390 and 328 HV to LM1 and LM2, respectively, while in WLR it did not exceed 279 HV. Another important change in the LM2 sample was changed in the microhardness of the substrate across its entire measurement range, identified by points 6 to 9 (Fig. 7b). This increase in microhardness of the LM2 substrate was due to the effect of the heat treatment obtained for both conditions. Moreover, the hardness was affected by the diffusion of the alloy elements from the coating to the substrate, when the melting

temperature of the substrate material was reached. For a Fe-based alloy deposited by HVOF, Cui et al. [35] identified that the remelted thicknesses had a linear relationship with the laser energy density, within a limited range between 10 a 160 J/mm^2, while the microhardness of the remelted coatings, exhibited a parabolic relationship. In this present work, the parameters used to LM1 (33.3 J/mm^2) and LM2 (150 J/mm^2), were also similar, i.e., while a greater microhardness to LM1 was obtained, the higher energy density promoted a decrease in microhardness.

5.3.3 *Effect of Laser Remelting on Tribological Properties of Coatings*

As shown previously in the results of microstructure and microhardness, the laser can also improve the tribological properties of sliding surfaces. The results of the tribological properties are described in the following sections.

5.3.3.1 Track Profile and Dry Sliding Wear Resistance

Fig. 5.8 shows the images obtained by optical measurement, at low magnification, comparing the wear of the tracks on the discs for the dry and lubricated sliding of all samples. Fig. 5.8a (LM1) shows the wear track is not noticeable for dry tests, unlike for WLR and LM2 (Fig. 5.8b-c). Fig. 5.8d shows the average of the wear track profiles after the sliding tests in dry condition, obtained by measuring the profile. Fig. 8e shows the total volume of the disc wear (V_d), calculated by measuring the cross-section of the tracks of each sample. Also, is shown the removed pin volume (V_p), obtained with the diameter d, of the wear scar (equation 4).

The adhesion mechanism through the profile (Fig. 5.8d) and confirmed by SEM/EDS results for WLR. In Fig. 5.8c (LM2), wear tracks can also be identified, but in a smaller thickness and with the profile shown in Fig. 5.8d, showing characteristics of an abrasive mechanism, in addition to the accumulation of material, produced by plastic deformation on the surface. This deformation occurred due to the decrease in hardness, caused by the change in the material microstructure (see section 3.1). For the WLR surface, an addition of the pin material over the disk (V_d) was obtained, with estimated values of $1.57 \times 10^{-3}\ mm^3$. In LM2, the result was the other way around, i.e., with a loss of material from the disk surface occurred, resulting in a removed volume of $13.70\ \times 10^{-3}\ mm^3$. These results showed the

influence of the heat treatment process and laser remelting of the coatings' surface, as well as for the untreated WLR surface [80-83]. Also, in Fig. 8e the volumes removed from the pin after the dry tests were identified. It is possible to notice that the largest volume removed from the pin (V_p) was obtained against the sample WLR (0.87 mm^3), followed by LM1 and LM2, showing a reduction of 0.42 *and* 0.32 mm^3, respectively.

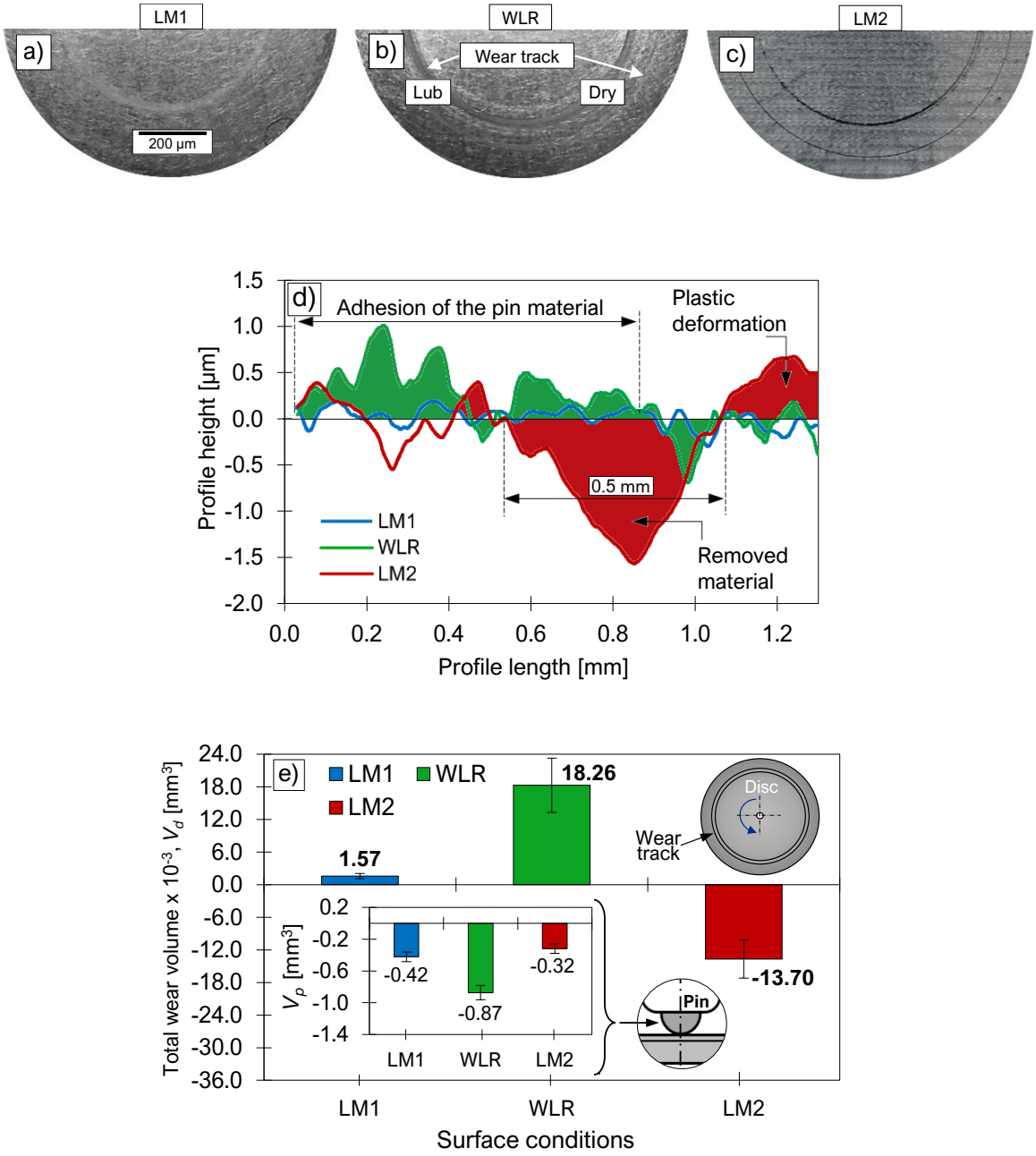

Figure 5.8 - Wear on the disc surfaces: a) LM1, b) WLR and c) LM2. d) Disc wear track detailing the area of the material adhered and removed from the surface after the dry test. e) Disc and pin wear volume after the dry test.

Figs. 5.9, 5.10, and 5.11 show the images of the wear tracks and the main micromechanisms for the three-disc coatings, obtained by SEM at low and high magnification. It is observed that the differences between the surfaces are in the concentration and types of wear mechanisms, identified as abrasive and adhesive. In order to better identify the samples in the figures, the wear micromechanisms have been specified as follows: 1 - microcuttings, microploughings, and grooves (red highlight); 2 - microcutting and grooves (black highlight); 3 - buildup effect and less compact tribolayers (yellow highlight); 4 - grooves; 5 - adhesion of the material from the ball to the disc (wear adhesive - compact tribolayers) (green highlight); 6 - the formation of oxide, splat fracture and delamination (blue highlight); 7 - oxide; 8 - delamination (purple highlight); 9 - microploughing (orange highlight) and, 10 - the accumulation of ball debris (white highlight).

For LM1 (Fig. 5.9 at high magnification), abrasion wear was noticeable, with the predominance of microcutting mechanisms, microploughings, and a slight adhesion of the ball material to the disc. The adhesive wear mechanisms predominated strongly, with a slight appearance of scratches in the WLR (Fig. 5.10), but in LM2, abrasive wear mechanisms were more evident. On this surface, the mechanisms of microcuttings and microploughings were also highlighted, which reveals the wear to two-body. As shown in Fig. 5.11, the sample remelted with the highest energy density (LM2), was more vulnerable to abrasive wear and micro-cracks formation. However, when the lower energy density was used in LM1, a slight homogenization of the microstructure and an increase in microhardness due to W_2C e CrC phases, and consequently the wear resistance was improved. Meanwhile, in the non-remelted WLR sample, the adhesive wear mechanism prevailed, with micro-cracks and the formation of oxides. The analysis of the wear tracks for LM1 and LM2 (Fig. 5.9 and 5.11) made it possible to identify mainly abrasive wear mechanisms such as microcuttings, microplates and the presence of oxides. It was noted that the difference in microhardness between the coatings and the counter-body, was one of the main causes of the abrasion wear. Fine grooves generated by ball sliding, pull-out, and delamination were observed to LM1 and LM2.

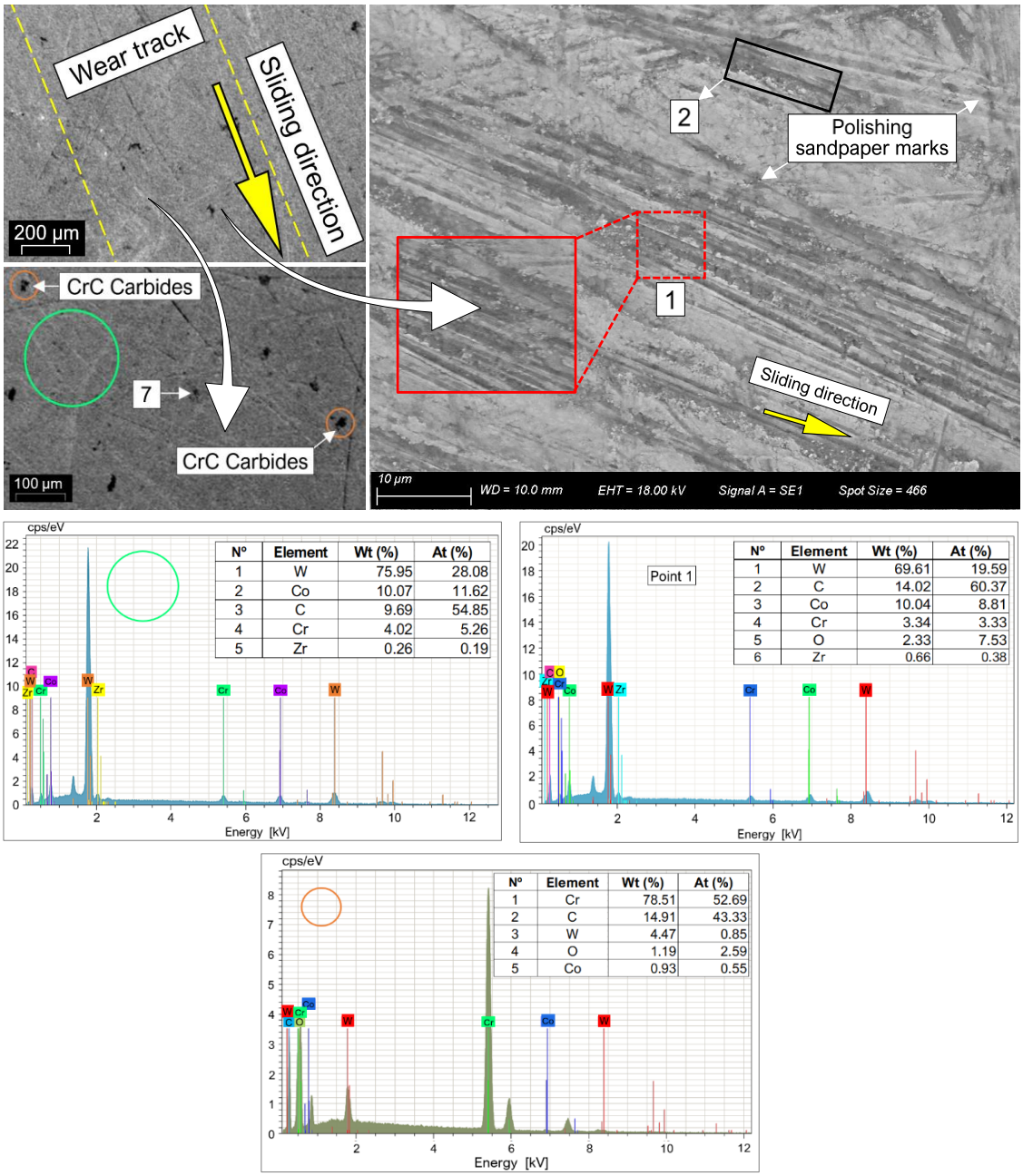

Figure 5.9 - SEM micrographs of the samples and EDS spectrum of the specified regions of the worn surfaces after the sliding wear test under the 30 N load and dry condition - LM1 surface

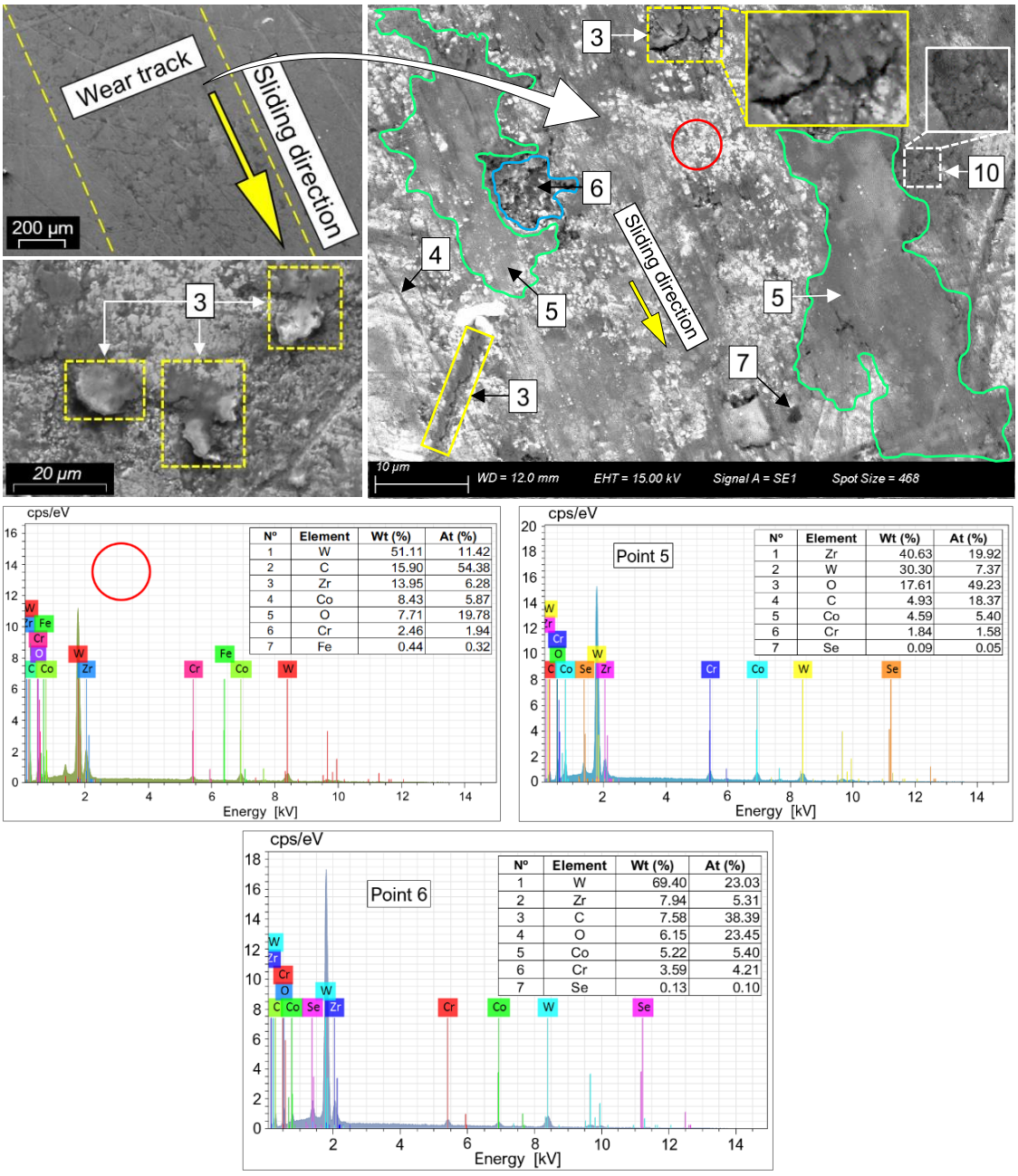

Figure 5.10 - SEM micrographs of the samples and EDS spectrum of the specified regions of the worn surfaces after the sliding wear test under the 30 N load and dry condition - WLR surface

Fig. 5.10 shows the effect of material accumulation of the pin on the disc and compacted tribolayers generated by the debris detached during the sliding process for the WLR surface. This phenomenon of strong adhesion, identified by the analysis of SEM-EDS, shows the high concentration of Zr. On this surface, there is also a slight formation of grooves and oxides. The occurrence of high adhesion for WLR is linked to the lack of homogenization of the surface coating, the difference in the geometry of the tungsten carbides, compared to the LM1 surface (see Figs. 5.5d-e). In this case of dry sliding on the

surface without remelting, the micropores are impacted negatively, acting as reservoirs for the debris generated during wear. The combination of these micropores with the accumulation of debris from the compacted ball generated an adhesion process between the tribological pair (disc and counter body), later identified by friction results. A Fe-based alloy manufactured by HVOF thermal spray was used in other studies, and then laser remelted. The results for disc wear and friction were also reduced compared to non-remelted coatings. In this study the authors reported that difference is related to the new microstructure of the coatings, the elimination of pores and cracks in the coating that was laser remelted, achieving a smooth contact interface, thus reducing the friction [80]. Park et al. [81] also report that laser heat treatment on the Stellite 1 coating, increased surface hardness, obtained microstructural homogeneity, and reduced macrosegregation and voids, resulting in wear resistance.

The EDS analyses confirmed the presence of the WC alloy, with a slight influence of the adhesion from the counter body (ball) on the disk and the formation of oxides, identified by the increment of O and C for LM1 (Fig. 5.9). From the analysis of the LM1, the presence of CrC was detected, which created a barrier against material pullout from the disc, increasing the wear resistance. According to Souza et al., (2020), laser remelting prevents the detachment of CrC, which increases the containment effect, interrupting and/or hindering the advancement of microploughings [82]. This phenomenon goes back to Zum Gahr's (1987) model of wear micromechanisms [83]. In the literature, similar results regarding the behavior of the reinforcement phases are indicated in several studies [84-90]. Another factor that contributed to increasing the wear resistance of LM1 was the formation of new phases such as W_2C e Co_3W_3C, which are high hardness compounds that in small sizes, usually attached to the WC, increase the material toughness of the material without damaging its brittleness [91]. Other studies show that a moderate degree of decarburization of WC improves wear resistance [92,93]. Although in LM2 (Fig. 5.11) the presence of W_2C was also observed, this decarbonization produced with greater energy, increased the hardness of this phase, and consequently unfavourably impacted the toughness, weakening the alloy. A study presented by Chen et al. [37] and Özkavak et al. [78], also shows that larger WC particles are more resistant to removal by small abrasive particles because the main wear mechanism of the material is preferential removal of the binder phase and subsequent detachment of the WC particles. LM2 sample, EDS-SEM analyses also confirmed a higher concentration of Fe on the surface, reducing the microhardness values. This contributed to the removal of the disc coating caused by the sliding of the ZrO_3 ball.

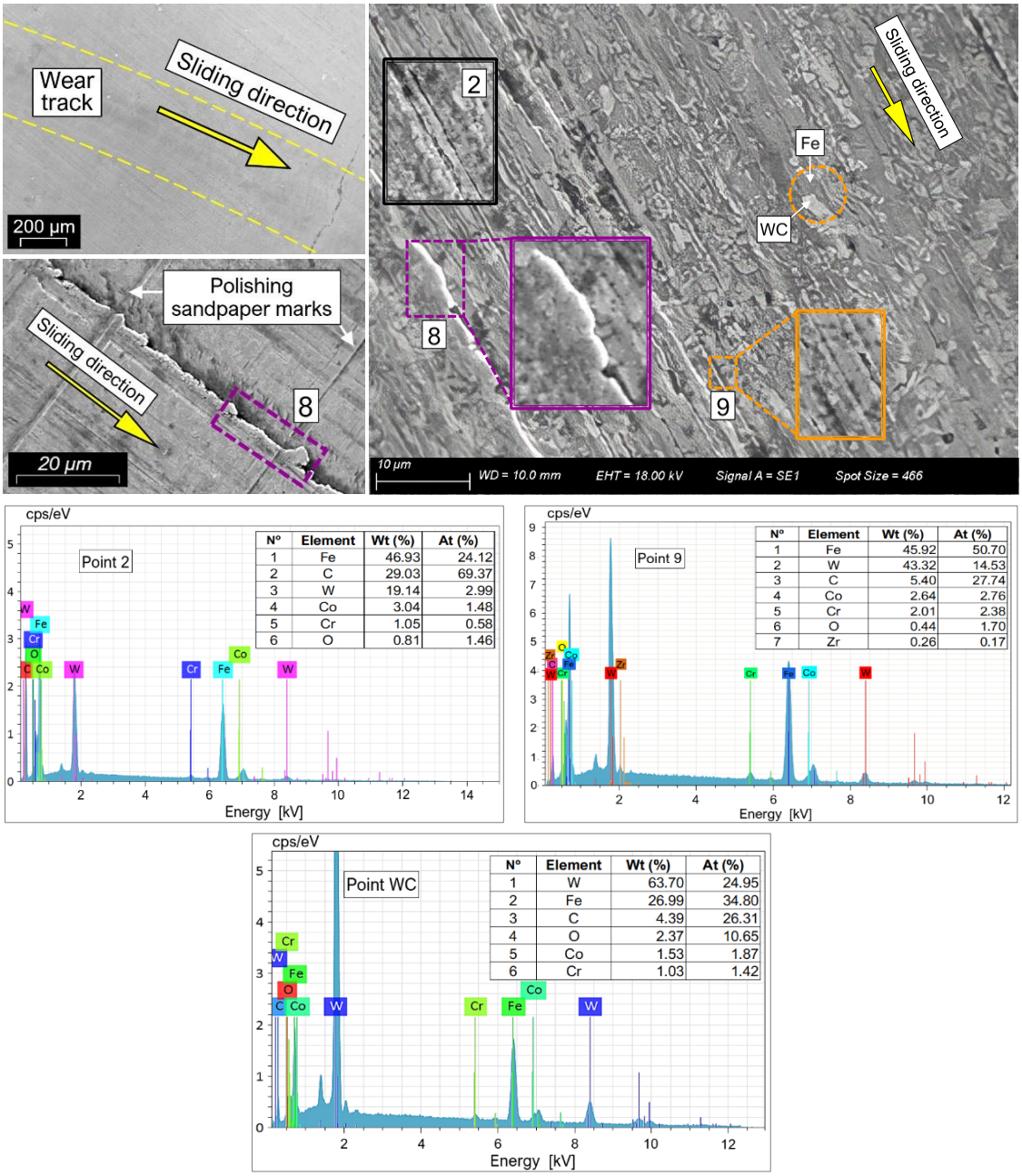

Figure 5.11 - SEM micrographs of the samples and EDS spectrum of the specified regions of the worn surfaces after the sliding wear test under the 30 N load and dry condition - LM2 surface

5.3.3.2 Friction and Roughness in the Dry Sliding Tests

Friction and roughness are also surface properties that affect the tribological behavior of mechanical components during a sliding process. These properties are connected by surface roughness and are related to the structural complexity and mechanical characteristics of the nature of the materials, as well as the preparation and its interaction with the environment [94]. Fig. 5.12 shows the evolution of the friction coefficient and the roughness comparison using the Rmr parameter (before and after the tests), for all surface conditions,

used as a comparison to investigate the laser thermal effect. The use of the roughness parameter Rmr is commonly employed for components that must operate with sealing systems, for example, surfaces of hydraulic cylinder rods, where these are characterized by a distribution of peaks and valleys, so in present work, this parameter was used.

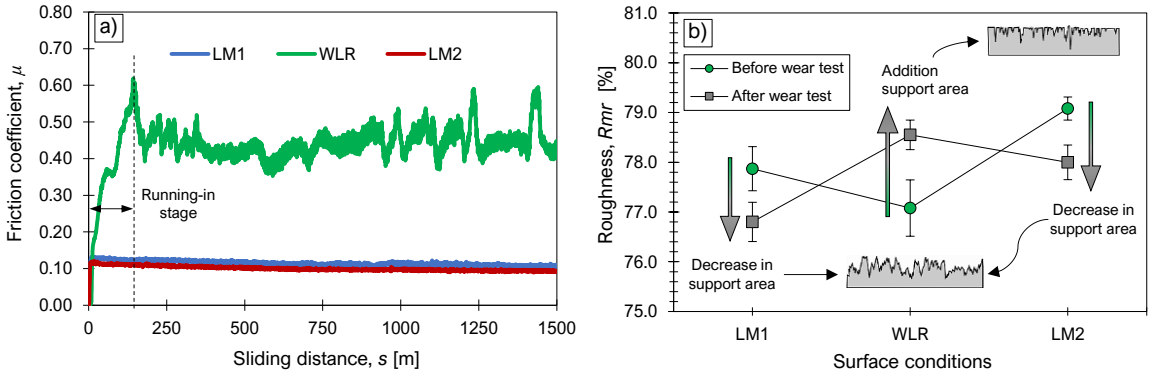

Figure 5.12 - Surface properties for coatings: a) friction coefficient as a function of the sliding distance for the sprayed coating and laser-treated coatings and b) ratio of the material length of the profile (Rmr) before and after the test.

Fig. 5.12a shows a considerable difference in the coefficient of friction between the surface of the WLR and the other samples with the same sliding distance. In the sprayed coating (WLR), a softening stage lasting approximately 150 m was observed, reaching the end of this stage with a peak of 0.65 for the COF. This indicates that from the beginning of the tests, a process of plastic deformation and adhesion between the surfaces occurs and, under the effect of shear stress, the particles are detached from the surfaces. Moreover, instability (adhesion phenomenon) is observed during the test for the WLR coating and ends the test with average values of the COF in the order of 0.44. Meanwhile, the laser-treated LM1 and LM2 surfaces had lower friction with a tendency to remain stable throughout the tests, obtaining average values of 0.10 and 0.11 for COF. These differences obtained in friction for the coatings were attributed to the different aspects of the microstructure, especially by the formation of carbides obtained with the laser treatment, in addition to the homogenization of the layers of the coatings, affecting the characteristics of the tribological system [25,80,81,95].

The highest values of the COF, obtained for WLR, were attributed to adhesion forces due to the accumulation of ball material on the surface of the disc's surface. The adhesion phenomenon was then confirmed by SEM/EDS analysis. In this sliding process, the adhesive wear occurs in three steps: the first step occurs when the pin contacts the disc, with the pin material detaching from the disc. In the second step, between 300 and 800 m, the debris

accumulates in the porosities on the surface of the disc and is then compacted on the track. Next, from the 800 to 1500 m (step 3), another phenomenon in friction is noticed, dominated by the strong adhesion between the surfaces, as they now have greater chemical compatibility, due to the layer of residue from the pin on the disc.

The tests conducted for LM1 and LM2, sliding smoothly and with low COF's, were conducted individually for two reasons: For the LM1 surface, the improvement in the layer densification of the layer, as well as the change in microstructure, caused by the thermal effect, caused the formation of a tribofilm with of higher density, preventing the pullout of the WC particles from the coating matrix. Zhang et al. [96] report that during the sliding process of surfaces coated with the WC-Cr3C2Ni alloy, manufactured by HVOF, an oxide film formed during the test has a significant influence on the adhesive wear. In LM2, the considerable change of the microstructure, with the reduction of carbides and microhardness, facilitated the removal of the disc coating material, under the action of the ball sliding. In this case, the ball acted as a cutting tool in the more ductile material, in addition, the presence of iron oxide, identified by the Fe_2MnO_4 phase, contributes to the decrease in frictional force during sliding, due to the lubricating properties of this ferrite compound.

The roughness results, performed before and after the dry sliding tests (Fig. 5.12b), using the Rmr parameter obtained through the Abbott-Firestone curve, shows the increase, or decrease of the support area of the disc surface. While there was a slight decrease from 77.9 to 77.3 % on the LM1 surface, and a similar decrease for LM2 (79.1 to 78.0 %), the results for WLR were opposite, i.e., an increase from 77.1 to 78.6 %. In this case, the sample without laser treatment (WLR) obtained the worst result, which justifies the adherence of the ball material in this sample. Jordan and Wilke [97] and Castro et al. [98] report that hydraulic cylinder rod surfaces, coated with some thermal spray process, should operate with Rmr of 70 to 90 %, thus ensuring seal integrity and the useful life of the system. Although the greatest difference was obtained in the WLR sample, the results of the sliding tests showed that the coated surfaces would still be within the established standards for this component.

5.3.3.3 Effect of Biolubricant on Wear Mechanisms

The evaluation of friction and wear resistance during lubricated sliding, becomes important for applications aimed at developing new coatings and surfaces for hydraulic components. Furthermore, promoting improvements of the tribological system of surfaces

developed from new manufacturing processes as well as the use of biodegradable lubricants is not an easy task, but it is necessary for the sustainable and long-lasting development of the industry. For this purpose, a biodegradable synthetic hydraulic oil of the HEPR type was used in the lubricated sliding tests. The selection of this type of oil was based on tests that showed important advantages in its tribological performance compared to HEES and HETG type biodegradables [98,99]. Due to the use of the lubricant in the tests, the wear of the coatings has been significantly reduced, so that only the wear micromechanisms will be presented, rather than their quantification. Fig. 5.13 shows the micrographs and chemical composition of the wear tracks obtained by SEM/EDS. It should be noted that the findings presented were quite different from those of the dry sliding tests.

The effect of lubrication on the coated surfaces had different results, showing fewer wear scars and in smaller amounts than the dry tests, especially for LM1 and WLR. In LM1 (Fig. 5.13a), a reduction in abrasive wear micromechanisms and a slight accumulation of ball material on the disc were notable. In highlighted point A, it is observed that there was deformation on the surface with the displacement of material from the disc coating, in addition to the presence of CrC, also observed in the EDS results highlighted in point B. In addition, a small concentration of Cu-Zn elements (ball material) attached to the disc was also noticed after sliding. This slight adhesion phenomenon and other abrasive wear micromechanisms on the LM1 surface indicate that there was sliding in the mixed lubrication regime. Although using HEPR oil that contains high concentrations of wear and extreme pressure additives, after 3000 m of sliding, he observed that the biolubricant was not enough to prevent wear but caused a 50 % reduction in the friction coefficient during sliding.

In WLR (Fig. 5.13b), the abrasive wear mechanism predominated during the sliding, meaning that the biolubricant partly changed the type of wear mechanism compared to the dry tests. On this surface, the distribution of coating layers, along with micropores, improved the lubrication process. These micropores served as oil micro-reservoirs, and this microtopography created appropriate conditions to generate localized pressure gradients, enhancing the efficiency of the tribological system [100]. The COF results confirm the wear mechanisms and the influence of the lubricant. When the lubricant film is not strong enough to withstand a high contact pressure, the contact between the asperities of the pin and disc is inevitable, then resulting in abrasive or adhesive wear mechanisms [101].

In both the dry and lubricated wear results, micro-cracks were observed (Fig. 5.13a/point - D). However, from the analyses previously performed on the cross-section,

these cracks are from the deposition process, followed by the grinding process, and have little influence on the performance of the coating. Point C (Fig. 5.13b) shows slight scratches on the surface with a low concentration of debris from the ball material. The chemical composition analysis (Fig. 5.13d) shows a decrease in the WC alloy concentration, compared to the other EDS analyses, identifying the presence of oxides, detected by the high content of oxygen.

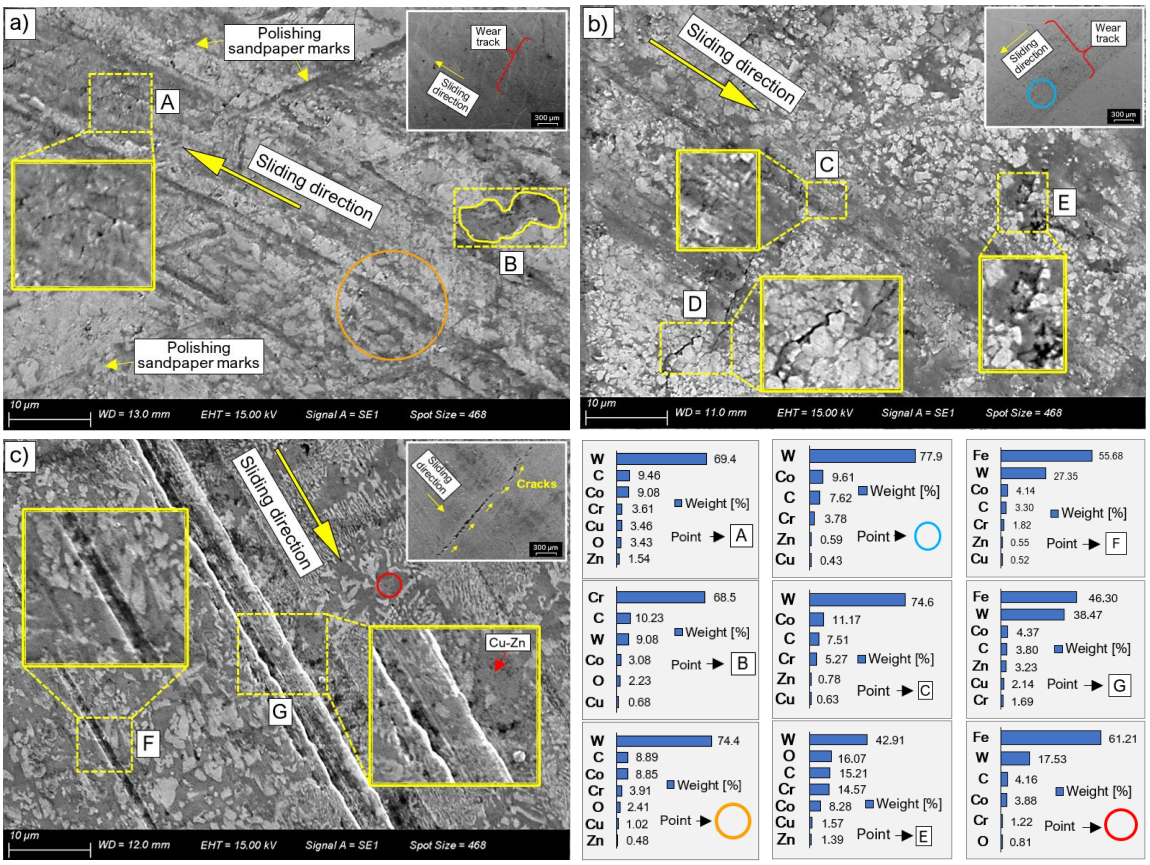

Figure 5.13 - SEM micrographs of the samples and EDS spectrum of the specified regions of the worn surfaces after the sliding wear test under the 50 N load. a) LM1, b) WLR and c) LM2.

On the surface of LM2, the micromechanisms of abrasive wear were strongly highlighted, moreover, the presence of micro-cracks was observed. These micro-cracks were caused by the high-energy density and high cooling rate after the laser remelting. As a result of this high cooling rate, tensile residual stresses were generated in the coating, and after the grinding process, these stresses were released with the appearance of micro-cracks. On this surface, in addition to microcutting, we also observe the presence of microploughings. During sliding on sample LM2, the boundary lubrication, which had low efficiency during sliding, stands out. The boundary lubrication is characterized by thin films, a low COF, but sometimes the proximity of asperities of the tribological pair can occur, increasing wear

[102]. Fig. 5.13c, the microstructural changes became more noticeable and were not homogeneous. The EDS analysis on this surface highlighted the presence of Fe in high concentrations (point F, G and highlighted in red), which, due to the lower hardness of this element, as well as the average microhardness of the top of the surface, contributed to the wear of the coating, evidenced by the track. It can be inferred that the reduction of micropores, the boundary lubrication regime, and changes in microstructure and microhardness contributed to the wear of this surface.

5.3.3.4 Frictional Behavior of Biolubricant

The evolution of the COF of the three samples is shown in Fig. 5.14, for a sliding distance of 3000 m. In addition, a comparative means and standard deviation of the COFs for dry and lubricated tests are also shown. In LM1 and WLR, it is notable that the lubricant managed to reduce the friction coefficient during sliding. Only on the surface of LM2 the effect of the lubricant was negligible. In LM1, until about 1700 m, the mean COF was 0.05, with a decrease to 0.03 at the end of the test. In WLR, from 1500 meters, a slight increase in COF was noticed. At this distance it was 0.07, reaching 2500 m with 0.09 and ending in values higher than 0.10, that is, with a tendency to increase. However, on the LM2 surface, the values were slightly unstable up to 1000 m but stabilized at 0.10 until the end of the test.

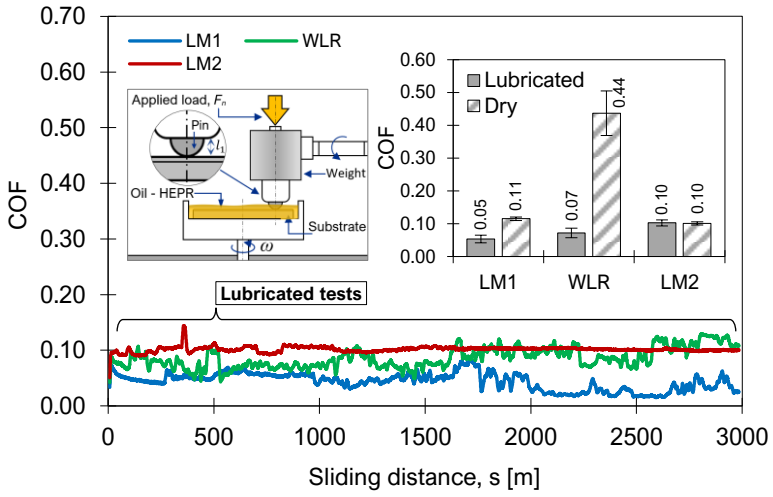

Figure 5.14 - Friction coefficient curves as a function of sliding distance for a 50 N load with comparing the average friction coefficients for lubricated and dry conditions for distinct types of surfaces.

Fig. 5.14 it was identified that the HEPR biolubricant combined with the LM1 surface was also the better combination, that is, in the dry tests, the average COF was 0.11, against 0.05 in the lubricated tests. It is emphasized here that the heat treatment parameters used for

LM1 were enough to homogenize the surface and smooth the sliding, while still leaving it with microcavities that aided in the mixed lubrication regime. Some studies also show that the addition of microcavity surfaces contributes to the reduction of COF when lubricated surfaces sliding [103,104].

A comparison of the dry and lubricated test results for the WLR sample (Fig. 5.14), indicates that surface microcavities, combined with the biolubricant, may have reduced friction. For dry tests, the average COF was 0.44, but for lubricated tests, it was 0.07, a decrease of more than six times. Tang et al. [105] and Kasem et al. [106], describe that an adequate proportion of microcavities in a lubricated sliding generate a hydrodynamic pressure to separate the surfaces, reducing friction and wear. However, in LM2, the COF results showed that it had not changed significantly, remaining close to 0.10 in the dry and lubricated tests. These friction results indicate that there was sliding in the boundary lubrication regime, which justifies the contact between the pin and the disc, and the absence of change in COF values for lubricated and dry tests. Dejun and Tianyuana [107], show that laser surface treatment after HVOF deposition, combined with the use of lubricant during sliding, change wear mechanisms, preventing premature coating failure.

5.3.4 *Effect of Laser on Surface Efficiency for Dry Sliding*

Recently, several strategies have been explored for the improvement of tribological systems, aiming at sustainability and energy efficiency in the industry, such as superlubricity regimes e new additives for lubricants, materials, composites, and high-performance alloys, as well as the use of thermal spray and laser deposition, as an alternative more efficient surface treatments [108-110].

To estimate the energy consumption during the dry sliding, the electrical current used by the tribometer was monitored. As a result of this data, power and energy consumption were calculated. The results were then correlated with the measurements of the COF and the surface temperature gradient, as reported in section 5.2.6. Fig. 5.15 shows the correlation of these physical quantities.

In Fig. 5.15a, it is observed that the COF of LM2 was lower than the other samples, however, a higher value of current consumption was obtained during the test. As opposed to the WLR, which had a higher COF. However, the results presented in Fig. 5.15b shows that energy consumption has a better correlation with the surface temperature gradient. Therefore, when analyzing the energy efficiency of a surface in a sliding process, one needs

to consider friction and heat dissipation. Equations 7 to 10 substantiate this analysis. The perception of the lower coefficient of friction would have the lowest energy consumption, which did not occur here. The temperature behavior during the LM2 test resulted in more electrical energy consumption.

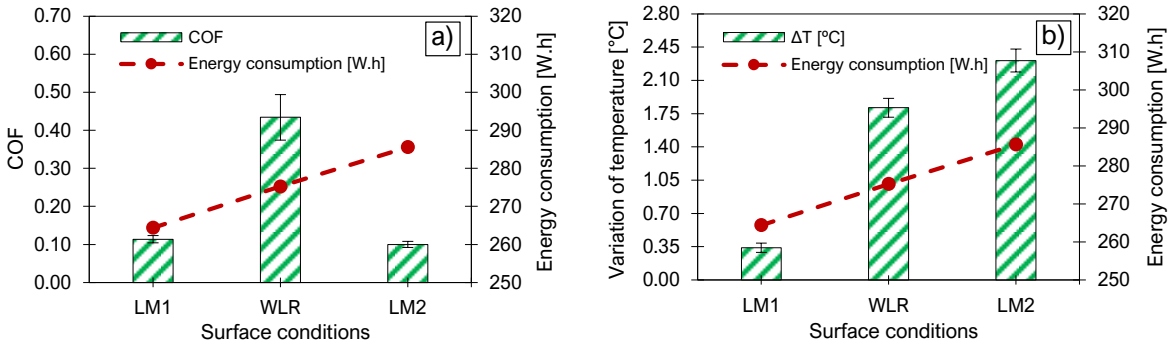

Figure 5.15 - Comparison of energy consumption under different surfaces. a) friction coefficient and b) temperature variation.

In equation 16, Wu et al. [56], separate the surface energy into two parts: the friction energy, W_f, and the wear energy, E_w. The results obtained for LM1 and LM2 showed that the friction energy was almost the same; however, they had differing values for energy consumption. This divergence of results would be attributed to the highest wear energy obtained for LM2, and the wear energy is divided into two additional parts, according to Equation 17. LM2, the thermal dissipation energy E_c, observed by the temperature change in Figure 5.15b, was higher. Conversely, surface energy, E_s, which is linked to the removal of particles, has also contributed to the increase in wear energy, E_w. Therefore, sliding that occurred in LM2 produced a higher power consumption.

Figure 5.16 shows the temperature evolution during 1500 m of sliding, equivalent to 3600 s of tests. In this result, the surface temperature of LM1 during the test remained constant at around 23.1°C. The WLR results show an increase from 2 ºC to 750 s, followed by a stabilizing trend, reaching at the end about 25.2 ºC. At the beginning of the test, the COF was high and unstable (up to 300 m – Fig. 5.12a), equal to 750 s. During this sliding time interval, it had a heat increase on the surface, in addition to the breaking of the roughness peaks, the beginning of the adhesion of two clean surfaces, and the formation of the surface tribolayer. However, for LM2, the temperature did not stabilize, increasing linearly from the beginning to the end of the tests, reaching 26.6 ºC at the end of the test. The results presented by the temperature evolution are related to the wear behavior obtained

for all samples. In LM1 and WLR, a smaller removed volume on the disc (see Fig. 5.8) was obtained. However, in LM2, increased wear was observed.

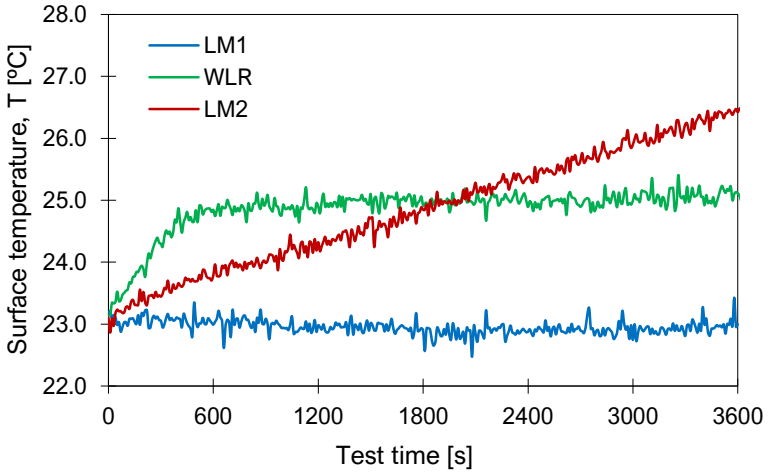

Figure 5.16 - Evolution of surface temperature during dry tests for each sample.

The energy consumption, as well as the COF and temperature gradient parameters, made it possible to assess different energy behavior of the surfaces. However, a better quantification of these energies must be made by the energy efficiency of the surfaces, taking into account the relation of useful energy (E_u) with the total energy of friction (E_{Tf}). Another method of evaluation would be to compare the current consumed by the equipment, for each type of surface. The concept of energy efficiency of the surface is obtained using frictional energy and energy dissipation using equation 18. Fig. 5.17 illustrates the results obtained after the sliding tests.

LM1 surface showed an efficiency of 99.1 %, due to the minimum wear energy and low coefficient of friction. On the WLR surface, 95.1 % efficiency was achieved. The results were affected by wear energy caused by adhesion mechanisms and moderate heat dissipation. In this case, the higher value obtained for the COF added the total energy significantly. Although a low COF was obtained for LM2, the wear energy was higher, both in the heat dissipation and in the removed volume. These conditions resulted in a 72.9 % efficiency for this surface.

Energy consumption information was linked to energy surface efficiency values, i.e., higher efficiency, lower energy consumption. The thermal energy (Q_t), energy stored in the rubbing materials (W_f) and wear debris (U_T) were used to obtain energy surface efficiency. Note that the lowest total heat dissipation (Q_t) occurred for the LM1 surface. This result is justified by its improved thermodynamic behavior, i.e., obtained low energy stored in the

coating materials (frictional phenomenon - W_f), and the low wear energy used (U_T), shown by the minimal amount of debris generated on the surface. In practice, a small volume was removed, and slight deformation occurred on the surface of LM1. In the WLR sample, the thermodynamic behavior was different, because the heat dissipation was 21 times greater than the LM1 reference surface. This is due to the higher frictional force generated by the adhesion of the tribological pair that occurred during the tests. This was justified by the increase of frictional energy (W_f) and volume in the disc, with slight deformation of the coating (see fig. 5.8e). During the LM2 surface sliding, the frictional energy (W_f) was lower than that of the WLR, but with greater heat dissipation, around 35 times higher than that of the LM1. In this case, the origin of the heat dissipation was concerned with particles breakage and surface deformations that emerged from the tests.

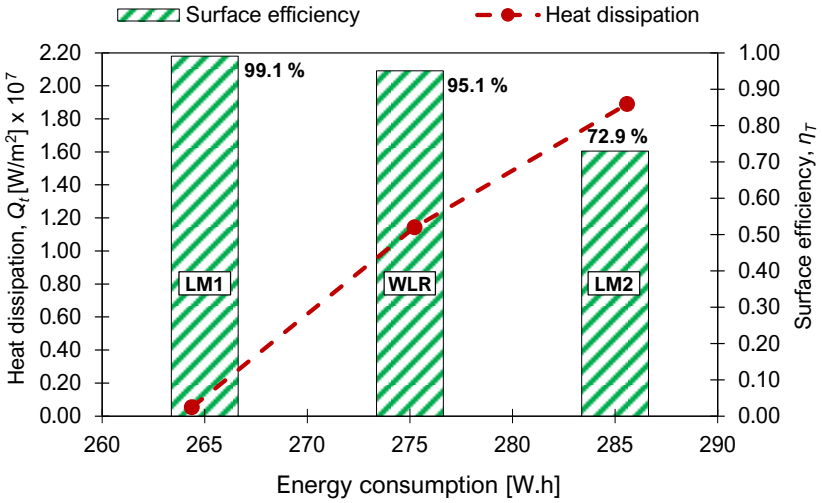

Figure 5.17 - Correlation of energy efficiency of the surfaces and heat dissipation with the energy consumption used in the tests.

Other studies support this research's findings. In a low wear regime, less than 5 % of mechanical energy is dissipated by wear, the majority of mechanical energy is converted into heat and friction [111], a fact that has increased the energy efficiency (η_s) of the LM1 surface. Yang and Shi (2018) also mention that low wear is indicative of a poor mechanical-chemical link between friction and wear [112]. For high efforts, better thermodynamic behavior is obtained, that is, with less work and less heat dissipation (Q_t), which occurs similarly to the wear rate in the plastic wear regime [113]. Recently, Aghababaei et al. (2017), have discovered a linear dependence of the debris wear volume on the frictional work (W_f) in asperity wear, which clearly shows that a portion of the mechanical work is spent on the generation of wear debris (U_T) [114]. The authors also found that friction is

generally independent of temperature or sliding velocity within a simulation range. This result of the authors reinforces the results obtained for the LM2 surfaces, in which low friction was obtained, but with a higher temperature evolution than the other samples.

In general, in published scientific studies, friction analysis is performed with a force relationship, not as an energy. The studies rarely consider heat dissipation in the results and wear is not associated with adhesion, deformation, and material removal energy. In this context, the results presented in this work have shown the importance of taking into consideration the energies of wear and friction, in addition to the energy consumption, to the tribological performances of the surfaces, especially when one aims to develop an industry that is more energy sustainable.

5.4 Conclusion

The laser remelting on HVOF coated surfaces has presented relevant features that can improve tribological contact performance. However, determining the optimum conditions for each type of application remains a challenge for the surface engineering field. As a result of this study, some conclusions can be drawn:

- The energy density of 33.3 J/mm^2 used for the LM1, promoted slight densification of the layer (seen Fig. 5d) and adequate distribution of the phases W_2C and Co_3W_3C, increasing in coating microhardness. However, for 150 J/mm^2 used in the LM2, a dendritic microstructure was formed with a built-up WC in the coating matrix. Although a good dilution and metallurgical bonding were obtained between substrate and feedstock for LM2, overheating contributed to the thermal decomposition and decarbonization of the alloy, leading to the formation of brittle phases.

- The proper formation of the W_2C and Co_3W_3C phases, with increased microhardness and CrC concentration, reduced the wear on the LM1 surface. Decarburization of the LM2 coating and a high amount of Fe was brought from the substrate to the coating, which contributed to the coating removal in tests. The lack of homogenization of the coating, combined with the micropores and the accumulation of debris from the compacted ball on the disc, induced the adhesion phenomenon of the non-remelted condition (WLR).

- In LM1, the densification of the layer resulted in the formation of a tribo-film, preventing the pullout of the WC particles. This behavior reduced friction and hence heat dissipation along the surface. In LM2, the decrease in coating hardness, the formation of Fe oxide

phases, resulted in a reduction in friction. Meanwhile, the high adhesion promoted a higher and unstable friction for the WLR sample, due to the lack of homogenization of the coating layers and the filling of the micropores with the ball (pin) debris.

- The micropores on the LM1 surface generated localized pressure gradients during the lubrication tests, which improved the performance of the tribological system and changed the wear mechanism. The low adhesion of LM1 indicates that the biolubricant HEPR did not completely prevent wear, however, the high concentrations of anti-wear additives and extreme pressure, friction has been reduced by 50%. In LM2, the reduction of micropores induced a boundary lubrication regime, maintaining the same dry friction values, but with the advantage of reduced wear.

- The quantification of various types of energy during the coating sliding was important in estimating the energy efficiency of each surface. The friction energy, W_f, was about the same for LM1 and LM2, but for WLR it was higher, due to the influence of the total wear energy caused by adhesion and moderate heat dissipation. In LM2, the lowest friction was not linked to lower electrical energy consumption, as in such cases it was higher. This divergence was caused by higher wear energy, U_T obtained for LM2, highlights the higher heat dissipation.

- The choice of a better manufacturing process for coatings, with appropriate deposition parameters, can provide an economical and environmentally sustainable benefit to the industry. Combining different methods of coating deposition with the use of biodegradable lubricants is a promising process to reduce friction and wear and improve the energy efficiency of the surface without harming the environment.

5.5 Acknowledgments

This research was funded by the Research and Innovation Support Foundation of Santa Catarina State - FAPESC, Brazil, via the project identified by #51805292 and with the support of CAPES, a Brazilian government entity focused on human resources training. A. S. Rocha acknowledges CNPq (Grant 308773/2018-7). Also, Rijeza Indústria Metalúrgica, Precision Engineering Laboratory/LMP from Federal University of Santa Catarina/UFSC and the University Center - UNISATC, which were the technical and scientific support for this work.

5.6 References

[1] LUO, X. T., SMITH, G. M., WANG, Y., GILDERSLEEVE, E., SAMPATH, S., & LI, C. J. (2019). **Cracking induced tribological behavior changes for the HVOF WC-12Co cermet coatings**. *Ceramics International*, *45*(4), 4718-4728.

[2] DING, X., CHENG, X. D., LI, C., YU, X., DING, Z. X., & YUAN, C. Q. (2018). **Microstructure and performance of multi-dimensional WC-CoCr coating sprayed by HVOF**. The International Journal of Advanced Manufacturing Technology, 96(5-8), 1625-1633.

[3] SASSATELLI, P., BOLELLI, G., GUALTIERI, M. L., HEINONEN, E., HONKANEN, M., LUSVARGHI, L., RIGON, R., VIPPOLA, M. (2018). **Properties of HVOF-sprayed Stellite-6 coatings**. Surface and Coatings Technology, 338, 45-62.

[4] GHADAMI, F., & SABOUR ROUH AGHDAM, A. (2019). **Improvement of high velocity oxy-fuel spray coatings by thermal post-treatments: A critical review**. Thin Solid Films, 678, 42-52.

[5] GHOSH, G., SIDPARA, A., & BANDYOPADHYAY, P. P. (2019). **Understanding the role of surface roughness on the tribological performance and corrosion resistance of WC-Co coating**. Surface and Coatings Technology, 125080.

[6] NAHVI, S. M., & JAFARI, M. (2016). **Microstructural and mechanical properties of advanced HVOF-sprayed WC-based cermet coatings**. Surface and Coatings Technology, 286, 95-102.

[7] ANAND, A., HAQ, M.I.U, VOHRA, K., RAINA, A., WANI, M.F. (2017). **Role of green tribology in sustainability of mechanical systems: a state-of-the-art survey.** Materials Today: Proc 4(2):3659–3665.

[8] PIOLA, R., ANG, A. S., LEIGH, M., & WADE, S. A. (2018). **A comparison of the antifouling performance of air plasma spray (APS) ceramic and high velocity oxygen fuel (HVOF) coatings for use in marine hydraulic applications.** Biofouling, 34(5), 479-491.

[9] BERGER, J. E., SCHULZ, R., SAVOIE, S., GALLEGO, J., KIMINAMI, C. S., BOLFARINI, C., & BOTTA, W. J. (2017). **Wear and corrosion properties of HVOF coatings from Superduplex alloy modified with addition of boron**. Surface and Coatings Technology, 309, 911-919.

[10] YILBAS, B. S., TOOR, I. H., PATEL, F., & BAIG, M. A. (2013). **Effects of Laser Re-melting on the Corrosion Properties of HVOF Coatings**. Journal of materials engineering and performance, 22(5), 1505-1511.

[11] CHUN, H. G., CHO, T. Y., YOON, J. H., & LEE, G. H. (2015). **Improvement of surface properties of Inconel 718 by HVOF coating with WC-metal powder and by laser heat treatment of the coating.** Advances in Materials Science and Engineering, 2015.

[12] CASTRO, R. D. M., ROCHA, A. D. S., CURI, E. I. M., & PERUCH, F. (2018). **A comparison of microstructural, mechanical and tribological properties of WC-10Co4Cr-HVOF coating and hard chrome to use in hydraulic cylinders**. American Journal of Materials Science. Vol. 8, no. 1 (2018), p. 15-26.

[13] FUJITA, H., NGUYEN, D. C., VU, N. P., BANH, T. L., & PUTA, H. H. (Eds.). (2018). **Advances in Engineering Research and Application: Proceedings of the International Conference**, ICERA 2018 (Vol. 63). Springer.

[14] MANZAT, A., & GADOW, R. (2018). **Friction Reduction with Thermally Sprayed Cylinder Liner Coatings**. In Reibungsminimierung im Antriebsstrang 2015 (pp. 217-232). Springer.

[15] HÄRKISAARI, P. (2015). **Wear and friction effects on energy consumption in the mining industry** (Master's thesis). Tampere University of Technology, Material Sience Engineering, Tampere, 2015.

[16] HOLMBERG, K., ERDEMIR, A. (2017**) Influence of tribology on global energy consumption, costs and emissions**. Friction, 5, 263–84.

[17] CASTRO, R. M., CAVALER, L. C. C., MARQUES, F. M., BRISTOT, V. M., & ROCHA, A. S. (2014). **Comparative of the Tribological Performance of Hydraulic Cylinders Coated by the Process of Thermal Spray HVOF and Hard Chrome Plating**. Tribology in Industry, 36(1).

[18] HAWTHORNE, H. M., ARSENAULT, B., IMMARIGEON, J. P., LEGOUX, J. G., & PARAMESWARAN, V. R. (1999). **Comparison of slurry and dry erosion behaviour of some HVOF thermal sprayed coatings**. Wear, 225, 825-834.

[19] HUANG, Q., QIN, E., LI, W., WANG, B., PAN, C., & WU, S. (2020). **The Cavitation Resistance of WC-CoCr Cermet Coating Deposited by HVOF for Hydraulic Application.** Journal of Thermal Spray and Engineering, 3(1), 68-73.

[20] LEE, S. S. (2020). **Wear behaviors of WC-CoCr and WC-CrC-Ni coatings sprayed by HVOF**. Journal of the Korea Academia-Industrial cooperation Society, 21(6), 204-211.

[21] WU, D., LIU, Y., LI, D., ZHAO, X., & LIU, Y. (2016). **Tribo-corrosion properties of WC-10Co-4Cr coating in natural silt-laden waters when sliding against Si3N4.** International Journal of Refractory Metals and Hard Materials, 58, 143-151.

[22] XIANG, D. I. N. G., CHENG, X. D., XIANG, Y. U., CHAO, L. I., YUAN, C. Q., & DING, Z. X. (2018). **Structure and cavitation erosion behavior of HVOF sprayed multi-dimensional WC–10Co4Cr coating**. Transactions of Nonferrous Metals Society of China, 28(3), 487-494.

[23] DU, P. C., ZHU, X. P., MENG, Y., FENG, H., WANG, Q. F., & LEI, M. K. (2017). **Water-lubricated tribological behavior of WC-Ni coatings deposited by off-angle HVOF spraying.** Surface and Coatings Technology, 309, 663-670.

[24] POIRIER, D., LEGOUX, J. G., & LIMA, R. S. (2013). **Engineering HVOF-sprayed Cr_3C_2-NiCr coatings: the effect of particle morphology and spraying parameters on the microstructure, properties, and high temperature wear performance**. Journal of Thermal Spray Technology, 22(2-3), 280-289.

[25] CIUBOTARIU, C. R., FRUNZĂVERDE, D., MĂRGINEAN, G., ȘERBAN, V. A., & BÎRDEANU, A. V. (2016). **Optimization of the laser remelting process for HVOF-sprayed Stellite 6 wear resistant coatings**. Optics & Laser Technology, 77, 98-103.

[26] MURUGAN, K., RAGUPATHY, A., BALASUBRAMANIAN, V., & SRIDHAR, K. (2014). **Optimizing HVOF spray process parameters to attain minimum porosity and maximum hardness in WC–10Co–4Cr coatings**. Surface and Coatings Technology, 247, 90-102.

[27] CUI, G., HAN, B., ZHAO, J., & YANG, Z. (2017). **Microstructure and tribological performance of sulfurizing layer prepared on the laser cladding Co-based alloy coating.** Surface and Coatings Technology, 331, 27-34.

[28] DOWDEN, J. & SCHULZ, W. (2017). **The Theory of Laser Materials Processing. Heat and Mass Transfer in Modern Technology**, Springer.

[29] DUTTA MAJUMDAR, J., & MANNA, I. (2011). **Laser Material Processing**. International Materials Reviews, 56(5-6), 341-388.

[30] VAITHILINGAM, J., GOODRIDGE, R. D., HAGUE, R. J., CHRISTIE, S. D., & EDMONDSON, S. (2016). **The effect of laser remelting on the surface chemistry of Ti6al4V components fabricated by selective laser melting**. Journal of Materials Processing Technology, 232, 1-8.

[31] PIĄTKOWSKI, J., GRABOWSKI, A., & CZEREPAK, M. (2016). **The Influence of Laser Surface Remelting on the Microstructure of EN AC-48000 Cast Alloy**. Archives of Foundry Engineering, 16(4), 217-221.

[32] CHIKARAKARA, E., AQIDA, S., BRABAZON, D., NAHER, S., PICAS, J. A., PUNSET, M., & FORN, A. (2010). **Surface modification of HVOF thermal sprayed WC–CoCr coatings by laser treatment.** International Journal of Material Forming, 3(1), 801-804.

[33] CHIKARAKARA, E., PUNSET, M., PICAS, J. A., BRABAZON, D., & NAHER, S. (2011, May). **Characterization of Laser Modified WC-CoCr Coatings**. In AIP Conference Proceedings (Vol. 1353, No. 1, pp. 1087-1092). AIP.

[34] MIRANDA, R. M., GANDRA, J. P., VILACA, P., QUINTINO, L., & SANTOS, T. G. (2013). **Surface modification by solid state processing**. Cap. 1: Overview of coating technologies. Woodhead Publishing.

[35] CUI, C., YE, F., & SONG, G. (2012). **Laser surface remelting of Fe-based alloy coatings deposited by HVOF**. Surface and Coatings Technology, 206(8-9), 2388-2395.

[36] DAS, B., NATH, A., & BANDYOPADHYAY, P. P. (2019). **Scratch resistance and damage mechanism of laser remelted thermally sprayed ceramic coating**. Surface and Coatings Technology, 364, 157-169.

[37] CHEN, H., XU, C., ZHOU, Q., HUTCHINGS, I. M., SHIPWAY, P. H., & LIU, J. (2005). **Micro-scale abrasive wear behaviour of HVOF sprayed and laser-remelted conventional and nanostructured WC–Co coatings**. Wear, 258 (1-4), 333-338.

[38] SHOJA-RAZAVI, R. (2016). **Laser surface treatment of Stellite 6 coating deposited by HVOF on 316L alloy.** Journal of Materials Engineering and Performance, 25(7), 2583-2595.

[39] SASAKI, S. (2010) **Environmentally friendly tribology (eco-tribology)**. Journal of Mechanical Science and Technology, 24(1):67–71.

[40] LINSINGEN, I. V. (2013) **Fundamentos de Sistemas Hidráulicos** (3ª ed). Florianópolis: UFSC.

[41] GUO, H. F., TIAN, Z. J., & HUANG, Y. H. (2016). **Laser surface remelting of WC–12Co coating: finite element simulations and experimental analyses**. Materials Science and Technology, 32(8), 813-822.

[42] STEEN, W., M.; MAZUMDER, J. **Laser material processing**. springer science & business media, 2010.

[43] ANGELASTRO, A., CAMPANELLI, S. L., CASALINO, G., & LUDOVICO, A. D. (2013). **Optimization of Ni-based WC/Co/Cr composite coatings produced by multilayer laser cladding**. Advances in Materials Science and Engineering, 2013.

[44] PAGANO, N., ANGELINI, V., CESCHINI, L., & CAMPANA, G. (2016). **Laser remelting for enhancing tribological performances of a ductile iron.** Procedia CIRP, 41, 987-991.

[45] BOLELLI, G., BERGER, L. M., BONETTI, M., & LUSVARGHI, L. (2014) **Comparative study of the dry sliding wear behaviour of HVOF-sprayed WC–(W,Cr)2C–Ni and WC–CoCr hardmetal coatings**, Wear, 309, 96–111.

[46] POPOVA, E., & POPOV, V. L. (2015). **The research works of Coulomb and Amontons and generalized laws of friction**. Friction, 3(2):183–190.

[47] FILDES, J. M, MEYERS, S. J., MULLIGAN, C. P., KILAPARTI, R. (2013). **Evaluation of the wear and abrasion resistance of hard coatings by ball-on-three-disk test methods: a case study**. Wear, 302, 1040–1049.

[48] RYMUZA, Z. (1996). **Energy concept of the coefficient of friction**. Wear, 199(2), 187-196.

[49] KENNEDY, F. E., LU, Y., & BAKER, I. (2015). **Contact temperatures and their influence on wear during pin-on-disk tribotesting.** Tribology International, 82, 534-542.

[50] FEDERICI, M., STRAFFELINI, G., & GIALANELLA, S. (2017). **Pin-on-disc testing of low-metallic friction material sliding against HVOF coated cast iron: Modelling of the contact temperature evolution**. Tribology Letters, 65(4), 1-12.

[51] ASHBY, M. F., ABULAWI, J., Kong, H. S. **Temperature maps for frictional heating in dry sliding.** Tribol Trans 1991; 34:577–87.

[52] STRAFFELINI, G. **Friction and wear: methodologies for design and control**. 2015. Springer.

[53] JOHNSON, K. L., KENDALL, K., & ROBERTS, A. (1971). **Surface energy and the contact of elastic solids**. Proceedings of the royal society of London. A. mathematical and physical sciences, 324(1558), 301-313.

[54] MAKKONEN, L. (2012). **A thermodynamic model of sliding friction**. AIP Advances, 2(1), 012179.

[55] ZHOU, L., LI, J., LI, F., MENG, Q., LI, J., & XU, X. (2016). **Energy consumption model and energy efficiency of machine tools: a comprehensive literature review**. Journal of Cleaner Production, 112, 3721-3734.

[56] WU, W., CHEN, G., FAN, B., & LIU, J. (2016). **Effect of groove surface texture on tribological characteristics and energy consumption under high temperature friction**. PloS one, 11(4), e0152100.

[57] GUO, H. F., TIAN, Z. J., & HUANG, Y. H. (2016). **Laser surface remelting of WC–12Co coating: finite element simulations and experimental analyses**. Materials Science and Technology, 32(8), 813-822.

[58] YILBAS, B. S., & AKHTAR, S. S. (2012). **Laser re-melting of HVOF coating with WC blend: Thermal stress analysis.** Journal of Materials Processing Technology, 212(12), 2569-2577.

[59] ŚLODERBACH, Z., & PAJĄK, J. (2015). **Determination of ranges of components of heat affected zone including changes of structure**. Archives of Metallurgy and Materials, 60(4), 2607-2612.

[60] DAS, B., GOPINATH, M., NATH, A. K., BANDYOPADHYAY, P. P. (2018). **Effect of cooling rate on residual stress and mechanical properties of laser remelted ceramic coating**. Journal of the European Ceramic Society, 38(11), 3932–3944.

[61] PANZIERA, R. C., de OLIVEIRA, A. C. C., PEREIRA, M., & RATSZUNEI, F. (2020). **Study of the effects of the laser remelting process on the microstructure and properties of the WC–10Co–4Cr coating sprayed by HVOF.** Journal of the Brazilian Society of Mechanical Sciences and Engineering, 42(3), 119.

[62] GHERKE, G. A. (2017). **Revestimento de Roscas Helicoidais Agrícolas a Base de CrC Depositado Via HVOF Posteriormente Irradiadas com Laser de Nd: YAG de CO_2**. Universidade Federal do Pampa, Alegrete, RS, Brasil.

[63] CHO, T. Y., YOON, J. H., HUR, S. K., CHUN, H. G., & ZHANG, S. H. (2011). **Surface Modification by HVOF Coating of Micron-sized WC-metal Powder and Laser-heating of the Coating.** In Materials Science Forum, 686, 654-660.

[64] HAILANG, L., BO, W., ZHENGWEI, Q., GUOPEI, Z., & DEZHI, W. (2018). **Surface microstructure and anti-wear of WC-CoCr coatings cladded by electron beam.** Rare Metal Materials and Engineering, 47(11), 3338-3344.

[65] AFZAL, M., KHAN, A. N., MAHMUD, T. B., KHAN, T. I., & AJMAL, M. (2015). **Effect of laser melting on plasma sprayed WC-12 wt.% Co coatings**. Surface and Coatings Technology, 266, 22-30.

[66] MARGINEAN, G., & UTU, D. (2010). **Microstructure refinement and alloying of WC–CoCr coatings by electron beam treatment**. Surface and Coatings Technology, 205(7), 1985-1989.

[67] RIZZO, A., GOEL, S., GRILLI, M. L., IGLESIAS, R., JAWORSKA, L., LAPKOVSKIS, V., NOVAK, P., POSTOLNYI, B. O., & VALERINI, D. (2020). **The critical raw materials in cutting tools for machining applications: A review**. Materials, 13(6), 1377.

[68] LIANG, B. L., AI, Y. L., LIU, C. H., & JIANG, N. (2013). **Mechanical Properties of WC-Co Cemented Carbide Prepared via Vacuum Sintering.** In Applied Mechanics and Materials, 275, 1917-1920.

[69] AFZAL, M., AJMAL, M., KHAN, A. N., HUSSAIN, A., & AKHTER, R. (2014). **Surface modification of air plasma spraying WC–12% Co cermet coating by laser melting technique**. Optics & Laser Technology, 56, 202-206.

[70] AFZAL, M., KHAN, A. N., MAHMUD, T. B., KHAN, T. I., & AJMAL, M. (2015). **Effect of laser melting on plasma sprayed WC-12 wt.% Co coatings**. Surface and Coatings Technology, 266, 22-30.

[71] GHADAMI, F., & AGHDAM, A. S. R. (2019). **Improvement of high velocity oxy-fuel spray coatings by thermal post-treatments: a critical review**. Thin Solid Films, 678, 42-52.

[72] LI, Z. L., SHAN, Q., JIANG, Y. H., ZHOU, R., & SUI, Y. D. (2013). **Effect of Co Addition on the Microstructure of Matrix in Tungsten Carbide Reinforced Surface Composite.** In Applied Mechanics and Materials, 376, 54-59.

[73] ZAKHAROVA, E. S., et al. **Morphology of powders of tungsten carbide used in wear-resistant coatings and deposition on the PDC drill bits.** In: Journal of Physics: Conference Series. IOP Publishing, 2017. p. 012058.

[74] LI, Y., GAO, Y., XIAO, B., MIN, T., FAN, Z., MA, S., & XU, L. (2010). **Theoretical study on the stability, elasticity, hardness and electronic structures of W-C binary compounds.** Journal of Alloys and Compounds, 502(1), 28-37.

[75] SUETIN, D. V, SHEIN, I. R, IVANOVSKII, A. L. (2009). **Structural, electronic properties and stability of tungsten mono- and semi-carbides: A first principles investigation**. Journal of Physics and Chemistry of Solids, 70, 64-71.

[76] PIRSO, J., LETUNOVITŠ, S., & VILJUS, M. (2004). **Friction and wear behaviour of cemented carbides**. Wear, 257(3-4), 257-265. ;

[77] YANG, Q., SENDA, T., & OHMORI, A. (2003). **Effect of carbide grain size on microstructure and sliding wear behavior of HVOF-sprayed WC–12% Co coatings**. Wear, 254(1-2), 23-34.

[78] ÖZKAVAK, H. V., ŞAHIN, Ş., SARAÇ, M. F., & ALKAN, Z. (2019). **Comparison of wear properties of HVOF sprayed WC-Co and WC-CoCr coatings on Al alloys**. Materials Research Express, 6(9), 096554.

[79] LI, C. J., & YANG, G. J. (2013). **Relationships between feedstock structure, particle parameter, coating deposition, microstructure and properties for thermally sprayed conventional and nanostructured WC-Co**. International Journal of Refractory Metals and Hard Materials, 39, 2-17.

[80] CHEN, L., HE, D., HAN, B., GUO, Z., ZHANG, L., LU, L., WANG, X., TAN, Z., ZHOU, Z. (2020). **Effect of Laser Remelting on Wear Behavior of HVOF-Sprayed FeCrCoNiTiAl0.6 High Entropy Alloy Coating**. Applied Sciences, 10(20), 7211.

[81] PARK, C. K., LEE, J. H., KANG, N. H., & CHUN, E. J. (2020). **Correlation between Microstructure and Tribological Properties of Laser Surface Heat-Treated Stellite Coatings**. Coatings, 10(5), 433.

[82] SOUSA, J. M. S., RATUSZNEI, F., PEREIRA, M., CASTRO, R. M., & CURI, E. I. M. (2020). **Abrasion resistance of Ni-Cr-B-Si coating deposited by laser cladding process.** Tribology International, 143, 106002.

[83] ZUM GAHR K-H. **Microstructure and wear of materials**, Tribology Series. New York: Elsevier Science; 1987.

[84] DESCHUYTENEER, D., PETIT, F., GONON, M., CAMBIER, F. (2017). **Influence of large particle size–up to 1.2 mm–and morphology on wear resistance in NiCrBSi/WC laser cladded composite coatings**. Surface and Coatings Technology, 311, 365-73.

[85] FÉRNANDEZ, M. R., GARCÍA, A., CUETOS, J. M., GONZÁLEZ, R., NORIEGA, A.,CADENAS, M. (2015). **Effect of actual WC content on the reciprocating wear of a laser cladding NiCrBSi alloy reinforced with WC**. Wear, 324-325, 80-89.

[86] García, A., Fernandez, M. R., Cuetos, J. M., Gonzalez, R., Ortiz, A., Cadenas. M.

(2016). **Study of the sliding wear and friction behavior of WC + NiCrBSi laser cladding coatings as a function of actual concentration of WC reinforcement particles in ball-on-disk test**. Tribology Letters, 63(3), 1-10.

[87] HARSHA, S., DWIVEDI, D. K., & AGARWAL, A. (2008). **Influence of CrC addition in Ni-Cr-Si-B flame sprayed coatings on microstructure, microhardness and wear behaviour.** The International Journal of Advanced Manufacturing Technology, 38(1-2), 93-101.

[88] KUMAR, D., PANDEY, S. M., MURTAZA, Q., SINGH, P., & WALIA, R. S. (2021). **Tribological Analysis of Increasing Percentage of CrC Content in Composite Coating by Atmospheric Plasma Spray Technique**. In Optimization Methods in Engineering (pp. 99-113). Springer, Singapore.

[89] SHARMA, S. (2014). **Parametric study of abrasive wear of Co–CrC based flame sprayed coatings by response surface methodology**. Tribology International, 75, 39-50.

[90] ZHAO, D., JIANG, X., WANG, Y., DUAN, W., & WANG, L. (2018). **Microstructure evolution, wear and corrosion resistance of CrC nanocomposite coatings in seawater**. Applied Surface Science, 457, 914-924.

[91] QIAO, Y., FISCHER, T. E., & DENT, A. (2003). **The effects of fuel chemistry and feedstock powder structure on the mechanical and tribological properties of HVOF thermal-sprayed WC–Co coatings with very fine structures**. Surface and Coatings Technology, 172(1), 24-41.

[92] LIU, Y., LIU, W., MA, Y., MENG, S., LIU, C., LONG, L., & TANG, S. (2017). **A comparative study on wear and corrosion behaviour of HVOF-and HVAF-sprayed WC–10Co–4Cr coatings**. Surface Engineering, 33(1), 63-71.

[93] WANG, Q., ZHANG, S., CHENG, Y., XIANG, J., ZHAO, X., & YANG, G. (2013). **Wear and corrosion performance of WC-10Co4Cr coatings deposited by different HVOF and HVAF spraying processes**. Surface and Coatings Technology, 218, 127-136.

[94] BHUSHAN, B. (2013). **Principles and applications of tribology**. 2nd. John Wiley & Sons.

[95] KHMYROV, R. S., SHEVCHUKOV, A. P., GUSAROV, A. V., & TARASOVA, T. V. (2017). **Phase composition and microstructure of WC–Co alloys obtained by selective laser melting**. Mechanics & Industry, 18(7), 714.

[96] ZHANG, S. H., YOON, J. H., LI, M. X., CHO, T. Y., JOO, Y. K., & CHO, J. Y. (2010). **Influence of CO_2 laser heat treatment on surface properties, electrochemical and tribological performanmzce of HVOF sprayed WC–24% Cr3C2–6% Ni coating**. Materials Chemistry and Physics, 119(3), 458-464.

[97] WILKE, M. and JORDAN, H. TRELLEBORG. **An Introduction to Counter Surfaces.** TRELLEBORG SEALING SOLUTIONS, 2020.

[98] CASTRO, R. M, CURI, E. I. M., INÁCIO, L. F. F., & ROCHA, A. S. (2020). **Analysis of the tribological performances of biodegradable hydraulic oils HEES and HEPR in the sliding of Cu–Zn/WC–CoCr alloys using the Stribeck curve**. Journal of the Brazilian Society of Mechanical Sciences and Engineering, 42(1), 1-20.

[99] LUZ, E. M., CASTRO, R. M., PEREIRA, M., SILVA, R. G. N., PEREIRA, A. S. P. **Avaliação do Desempenho Tribológico do Revestimento FeCrNiMo Fabricado por Laser Directed Energy Deposition sob Deslizamento com Óleos Biodegradáveis - engB018.** Anais do I Congresso de Engenharia da Rede PDIMat (engBRASIL2020). Natal: UFRN, 2020. v. 1. p. 81-92.

[100] TONELLI, L., MARTINI, C., & CESCHINI, L. (2017). **Improvement of wear resistance of components for hydraulic actuators: dry sliding tests for coating selection and bench tests for final assessment.** Tribology International, 115, 154-164.

[101] ZHENG, C., LIU, Y., QIN, J., CHEN, C., & JI, R. (2017). **Wear behavior of HVOF sprayed WC coating under water-in-oil fracturing fluid condition**. Tribology International, 115, 28-34.

[102] MA, L., & LUO, J. (2016). **Thin film lubrication in the past 20 years**. Friction, 4(4), 280-302.

[103] ALI, F., KŘUPKA, I., & HARTL, M. (2015). **Reducing the friction of lubricated nonconformal point contacts by transverse shallow micro-grooves**. Proceedings of the Institution of Mechanical Engineers, Part J: Journal of Engineering Tribology, 229(4), 420-428.

[104] IBATAN, T., UDDIN, M. S., & CHOWDHURY, M. A. K. (2015). **Recent development on surface texturing in enhancing tribological performance of bearing sliders**. Surface and Coatings Technology, 272, 102-120.

[105] TANG, W., ZHOU, Y., ZHU, H., & YANG, H. (2013). **The effect of surface texturing on reducing the friction and wear of steel under lubricated sliding contact**. Applied Surface Science, 273, 199-204.

[106] KASEM, H., STAV, O., GRÜTZMACHER, P., & GACHOT, C. (2018). **Effect of low depth surface texturing on friction reduction in lubricated sliding contact**. Lubricants, 6(3), 62.

[107] DEJUN, K., & TIANYUAN, S. (2017). **Wear behaviors of HVOF sprayed WC-12Co coatings by laser remelting under lubricated condition**. Optics & Laser Technology, 89, 86-91.

[108] LUO, J., ZHOU, X. (2020). **Superlubricitive engineering—Future industry nearly getting rid of wear and frictional energy consumption**. Friction, 8, 643–665.

[109] RUNG, S., BOKAN, K., KLEINWORT, F., SCHWARZ, S., SIMON, P., KLEIN-WIELE, J. H., ESEN, C., HELLMANN, R. (2019). **Possibilities of dry and lubricated friction modification enabled by different ultrashort laser-based surface structuring methods**. Lubricants, 7(5), 43.

[110] TZANAKIS, I., HADFIELD, M., THOMAS, B., NOYA, S. M., HENSHAW, I., & AUSTEN, S. (2012). **Future perspectives on sustainable tribology**. Renewable and Sustainable Energy Reviews, 16(6), 4126-4140.

[111] JACOBS, T. D. B., CARPICK, R. W. (2013). **Nanoscale Wear as a stressassisted chemical reaction.** Nat Nanotechnol 8(2): 108–112.

[112] YANG, Y., & SHI, Y. (2018). **Single asperity friction in the wear regime**. Friction, 6(3), 316.

[113] YANG, Y. J., HUANG, L. P., SHI, Y. F. (2016). **Adhesion suppresses atomic wear in single-asperity sliding**. Wear, 352–353: 31–41.

[114] AGHABABAEI, R., WARNER, D. H., MOLINARI, J. F. (2017). **On the debris level origins of adhesive wear**. Proceedings of the National Academy of Sciences of the United States of America – USA, 114(30), 7935–7940.

PARTE III

6. CONCLUSÕES

As principias conclusões do trabalho são:

1. A aspersão térmica por HVOF utilizando a liga WC-10Co4Cr, apresentou-se com uma boa alternativa tecnológica para substituir o revestimento eletrodeposidado de cromo. Ao comparar a resistência mecânica dos revestimentos, a liga WC-CoCr apresentou-se com baixa delaminação e menor densidade de trincas. Na comparação das microdurezas, também se destacou a liga aspergida, obtendo-se ~ 1250 HV, contra 900 HV para cromo duro.

2. Os ensaios de deslizamento a seco por pino sobre disco, diferenças significativas entre os coeficientes de atrito (COF) para o WC-CoCr e o cromo duro foram identificadas. O comportamento do COF para WC-CoCr tem valores próximos de deslizamento lubrificado, o qual foi justificado pela presença de partículas de óxidos (WO_3), que possuem propriedades lubrificantes. Os COF's de 0,64 e 0,18 para o cromo e WC-CoCr, respectivamente, mostram o potencial da técnica e o revestimento depositado.

3. O revestimento WC-CoCr/HVOF apresentou elevada resistência ao desgaste abrasivo, apesar dos testes revelarem a remoção da matriz em alguns pontos, com consequência arrancamento das partículas de WC. Mesmo assim, a liga WC-CoCr teve menor perda volumétrica, comparado ao cromo duro. Para as superfícies de cromo duro, os ensaios de desgaste abrasivo revelaram uma aparência de polimento, quantificada pelo parâmetro de rugosidade Rmr. A medição do Rmr mostrou uma ampliação da área de apoio para as superfícies de cromo duro, de 61,68 para 90,01 % e uma redução de 90,57 para 80,29 % com WC-CoCr. Esse resultado mostrou a dificuldade que o cromo duro teria para manter uma área de apoio adequada às superfícies de vedação, o que reduziria a vida útil desses elementos pela falta de lubrificação entre os contatos.

4. A avaliação do desempenho dos lubrificantes em cada regime de lubrificação mostrou um comportamento diferenciado. O número de Hersey foi um importante modelo matemático para conectar algumas propriedades dos óleos e das condições de contato. O óleo biodegradável HEES se comportou com elevado COF na menor e maior pressão de contato. Esse resultado foi devido às diferenças das propriedades físicas e químicas do HEES, principalmente dos valores do coeficiente de pressão-viscosidade. O óleo biodegradável HEPR se comportou de forma mais estável para as diferentes cargas, porém com o COF de 0,029, contra 0,022 para o HEES, obtidos nos intervalos da concavidade da

curva. A menor viscosidade e menor rugosidade da superfície usada no deslizamento com HEPR, obteve-se uma menor espessura do filme, o que contribuiu com uma menor alteração do COF nas diferentes cargas avaliadas. Também, as maiores concentrações de aditivos de extrema pressão, antidesgaste e antifricção, proporcionaram um melhor desempenho aos lubrificantes.

5. Foram perceptíveis os regimes de lubrificação, assim como a influência das diferentes propriedades físicas e as concentrações de aditivos para cada óleo hidráulico. O coeficiente de desgaste para a esfera de Cu-Zn, foi de 6.90E-5 mm^3/Nm com o óleo HEES, para HLP e HEPR, obteve-se, 2,12E-5 e 8,62E-6 mm^3/Nm, respectivamente, destacando-se o HEPR comparadas ao óleo mineral. Ainda, a técnica de ICP e a norma ISO 4406, foram fundamentais para quantificar a contaminação dos óleos hidráulicos, gerados pelos detritos durante os testes de curta duração. Os resultados mostraram que após os testes, a concentração de cobre para o óleo HEES foi 30 vezes maior do que o HEPR.

6. Os testes lubrificados de longa duração foram importantes para avaliar as diferenças no comportamento dos contatos tribológicos, comparados aos testes de curta duração. Mesmo assim, as médias do COF para cada hora analisada foram menores e mais estáveis para os óleos do tipo HLP e HEPR, comparado ao HEES. Estas estabilidades do COF também foi confirmada no desgaste das esferas, obtendo-se um volume total removido de 2,40 mm^3 para HEES, contra 0,30 e 0,15 mm^3 para o HEPR e HLP, respectivamente.

7. Outro resultado que confirma o desempenho de cada lubrificante, foram os mecanismos de desgaste em cada superfície do disco. Nesse estudo, as propriedades físicas e químicas do óleo HEES, conduziram ao mecanismo de adesão da esfera contra o disco, confirmadas posteriormente pelas análises de EDS. Contudo, para as superfícies lubrificadas com os óleos HLP e HEPR, os mecanismos de desgaste abrasivo foram observados e identificados por *microcuttings, microploughings, grooves e chipping*, com pequena concentração do material da esfera aderido ao disco, resultados que justificam as diferenças entre os óleos, e o maior potencial tribológico do HEPR combinado ao revestimento de WC-CoCr.

8. A refusão à laser mostrou alterações significativas no revestimento de HVOF. O procedimento de refusão gerou condições favoráveis e desfavoráveis para o desempenho dos revestimentos. Quando os parâmetros de potência, velocidade de varredura e diâmetro do feixe de laser são otimizados, os tratamentos térmicos superficiais provaram ser uma boa alternativa de melhoria aos revestimentos depositados por HVOF. Nesse estudo, a menor densidade de energia do laser produziu uma adequada homogeneização na microestrutura,

além da formação de novos carbonetos, o que incrementou os valores da microdureza de 1107 para 1313 HV. Para a maior densidade de energia, uma união metalúrgica do revestimento ao substrato foi observada. Contudo, a microestrutura do revestimento foi completamente alterada, causando a descarbonização da liga, identificada pelas formação das fases de W_2C. Como esperado, esse fato contribuiu com o decréscimo da dureza do revestimento, devido a presença do Fe que foi trazido do substrato.

9. Os modelos matemáticos utilizados para quantificar o desgaste, foram fundamentais para obter os volumes removidos dos pinos e discos. Após os testes de desgaste, ficou evidente que no revestimento sem refusão, a adesão foi fortemente presente no disco. Isto não ocorreu com as superfícies refundidas, devido à densificação das camadas do revestimento, ou pela mudança da microestrutura no caso de LM2. A superfície de LM1 apresentou maior resistência ao desgaste, justificada pela fases de reforço (CrC), além de Co_3W_3C, o que dificultou o arrancamento de WC durante os ensaios de desgaste a seco. Os COF's para as superfícies refundidas foram 4 vezes menor, obtendo-se uma queda no valor médio de 0,45 para WLR, contra 0,10 para às tratadas à laser, resultado pode contribuir para o desenvolvimento de componentes hidráulicos de maior eficiência. Também, os resultados da medição de rugosidade Rmr mostraram que as superfícies refundidas tiverem menor variação na área de apoio, a qual foi identificada pelos conceitos de Abbott-Firestone.

10. Os resultados dos testes lubrificados nos revestimentos, sem e com refusão, mostraram que o óleo biodegradável HEPR protegeu levemente as superfícies, porém, a amostra LM2 ainda apresentou o maior desgaste. Entretanto, o atrito entre o par tribológico foi reduzido consideravelmente, comparado aos testes a seco. Para a amostra WLR, a redução foi aproximadamente de 7 vezes. Essa redução foi atribuída as microcavidades presentes nesta superfície. Entretanto, o decréscimo destas cavidades para as LM1 e LM2, causou uma redução máxima do atrito de até 50 %. Isso mostra que as variáveis do processo de refusão devem ser ainda mais controlada para superfícies que atuam na condição lubrificada e com elementos de vedação. Isso evitaria a redução inadequada dos microporos, já que estes contribuem com o gradiente de pressão localizados, que melhoram o desempenho do filme do óleo. A redução do atrito para WLR também foi atribuído a redução dos mecanismos de adesão do material da esfera sobre o disco.

11. O monitoramento do consumo de energia elétrica e da evolução de temperatura, durante os testes de deslizamento, além da modelagem de cálculo do comportamento termodinâmico, permitiu obter as eficiências de cada tipo de superfície. Nessa avaliação, a técnica de laser

provou ser uma excelente alternativa para aumentar o desempenho dos revestimentos, quando as densidades de energia são adequadas a cada condição. Nesse estudo, constatou que o atrito deve ser considerado não apenas como relação de forças, mas sim como energias que estão interagindo. Relacionar as diferentes formas de energia que se manifestam durante um processo de deslizamento, tais como, energia de atrito, desgaste e energia térmica, é extremamente importante para concluir sobre a eficiência energética.

12. Os resultados demonstraram importantes características tribológicas do revestimento da liga WC-CoCr depositado por HVOF, com melhoria no desempenho após o processo de tratamento térmico a laser. Além disso, as análises do comportamento tribológico usando óleos hidráulicos biodegradáveis sobre revestimentos otimizados energeticamente, promoveram a continuidade do desenvolvimento do movimento da *Green Tribology*, bem como a contribuição específica para a área de sistemas hidráulicos, e para a tribologia moderna. Pretende-se ainda disseminar os resultados dessa pesquisa, por meio de seminários, congressos, palestras e projetos em parcerias com indústrias, a fim de contribuir cientificamente com o desenvolvimento da tribologia, sobretudo com ás áreas relacionadas a engenharia da superfície.

7. SUGESTÕES PARA TRABALHOS FUTUROS

- Os diferentes parâmetros ajustados para a deposição no processo de HVOF, como por exemplo, pressão e vazão dos gases e combustível, vazão do pó, entre outros, podem ser otimizados para obter novas microestruturas dos revestimentos. O objetivo é identificar a influência desses parâmetros nas propriedades mecânicas e tribológicas das ligas. Assim mesmo, aplicar e avaliar outras potenciais ligas usadas em superfícies de componentes hidráulicos, considerando os mecanismos de falha por corrosão, abrasão e erosão.

- Avaliar a tenacidade à fratura dos revestimentos por meio de energia absorvida em testes de impacto, observando as regiões de fissuras e lascamento, a fim de obter dados para aplicações que as superfícies são mais exigidas por resistência ao impacto, como é o caso de componentes utilizados nas indústrias de mineração.

- Submeter diferentes superfícies revestidas por HVOF nos ensaios de atrito e desgaste por deslizamento *reciprocating*, com o propósito de comparar o desempenho tribológico e termodinâmico, com os ensaios de deslizamento rotativo.

- Como foi observado neste trabalho, o comportamento tribológico, bem como os regimes de lubrificação para os óleos biodegradáveis são impactados pelos aditivos que diferem para cada lubrificante. O intuito é quem sabe fazer uma avaliação para diferentes fabricantes de óleos hidráulicos, detectando e validando as diferenças para os HEES e HEPR.

- Usar as técnicas de interferometria ótica para identificar a mínima espessura do lubrificante, durante os ensaios de deslizamento, considerando o regime de lubrificação elastrohidrodinâmico (EHL). Com essa técnica se poderia validar os cálculos analíticos e prever a carga e velocidade de deslizamento para cada óleo biodegradável, obtendo-se a máxima performance do sistema tribológico.

- Fazer uma investigação mais específica sobre o efeito da porosidade nos aspectos de lubrificação. Talvez, simular a porosidade geradas pelo próprio processo de HVOF, usando técnicas de texturização de superfície e avaliar a influência destas cavidades com relação aos regimes de lubrificação, bem como o efeito no desgaste.

- Com os resultados do processo de refusão a laser, observou-se a relação da densidade de energia com a qualidade da microestrutura dos revestimentos. Com isso, para otimizar e estimar a qualidade da microestrutura e diluição do revestimento, seria importante instalar termopares ao longo de toda a seção transversal da zona termicamente afetada (ZTA).

- Aplicar os revestimentos em um cilindro hidráulico, combinando-os com óleos hidráulicos biodegradáveis para validar os resultados de laboratório. A validação poderia ser feita em duas etapas: primeiro através de medições da eficiência mecânica do componente durante o ciclo de operação e segundo por análise de microscopia dos mecanismos de desgaste, obtidas após a desmontagem do componente em teste.

- Viabilizar o uso destes processos alternativos de deposição, com desenvolvimento de novas ligas, com uso de minerais que estão constituídos no Brasil, como é o caso do Nióbio. Além disso, promover mudanças tecnologias mais aprimoradas para que no futuro possa ter sistemas hidráulicos mais eficiências e sustentáveis, com uso de óleos biodegradáveis, técnicas de deposição mais eficientes e ligas de alta performance.

8. REFERÊNCIAS COMPLEMENTARES

AL-SAYED ALI, S. R., HUSSEIN, A. H. A., NOFAL, A. A. M. S., HASSEB ELNABY, S. E. I., ELGAZZAR, H. A., & SABOUR, H. A. (2017). **Laser powder cladding of Ti-6Al-4V α/β alloy**. Materials, 10(10), 1-16.

ARORA, A., JHA, S., VINAY, S. (2019). **Aspects of green-sustainable tribology and its impacts on future product development: A Review**. Ecology, Environment and Conservation, 25, 146-157.

BOSCH REXROTH GROUP. **Offshore products & solutions**. Disponível em: < http://www.offshoretechnologyreports.com/rexroth_bosch.html > Acesso, fevereiro 2017.

BURMA, S. A. **Study of Failure in Hydraulic Systems: Case study of Machinery used in Local Gold Mining**. Master's Degree by Research in Mechanical Engineering, Nile Valley University, Atbara, September 2014.

CASTRO, R. M. **Avaliação das Propriedades de Superfície e do Comportamento ao Desgaste Abrasivo de Hastes de Cilindros Hidráulicos Revestidas pelos Processos HVOF e Cromo Duro Eletrodepositado**. Dissertação de Mestrado, Porto Alegre, Universidade Federal do Rio Grande do Sul – UFRGS, Novembro, 2012.

CATERPILLAR HYDRAULICS. **Trendreport Maschinen im Bergbau**. Magazine Fluid. 2016. Disponível em:< https://www.fluid.de/hydraulik/trendreport-maschinen-im-bergbau-325.html > Acesso em fevereiro 2017.

CIULLI, E. (2019). **Tribology and industry: From the origins to 4.0**. Frontiers in Mechanical Engineering, 5, 55.

CONAMA - Conselho Nacional do Meio Ambiente. Resolução 362/2005. **Regulamentação da Coleta, Transporte, Armazenamento e Destinação Adequada dos óleos lubrificantes usados e contaminados**, 2005. Disponível em: <http://www.mma.gov.br/port/conama/res/res05/res36205.xml>. Acessado em 23/03/2019.

CUI, G., HAN, B., ZHAO, J., & YANG, Z. (2017). **Microstructure and tribological performance of sulfurizing layer prepared on the laser cladding Co-based alloy coating**. Surface and Coatings Technology, 331, 27-34.

DAŠIĆ, P., FRANEK, F., ASSENOVA, E, RADOVANOVIC, M. (2003). **International standardization and organizations in the field of tribology**. Industrial Lubrication and Tribology, 55(6), 287-291.

ENEKES, C., & MURRENHOFF, H. (2010). **How environmentally friendly tribological systems influence the efficiency of axial piston machines**. Tribology Online, 5(5), 245-249.

GAULE, G., & MÜLLER-ZERMINI, B. (2016). **Environmental Approach. Environmentally Friendly and Biobased Lubricants**, 113.

GENG, Z., HOU, S., SHI, G.L., DUAN, D. L., LI, S. (2016). **Tribological Behaviour at Various Temperatures of WC-Co Coatings Prepared using Different Thermal Spraying Techniques**. Tribology International, 104, 36-44.

HAILANG, L., BO, W., ZHENGWEI, Q., GUOPEI, Z., & DEZHI, W. (2018). **Surface microstructure and anti-wear of WC-CoCr coatings cladded by electron beam**. Rare Metal Materials and Engineering, 47(11), 3338-3344.

HAMID, S. **Environmentally Friendly Hydraulic Fluids Applications and Benefits**. 51st National Conference on Fluid Power, Proceedings of…USA, NFPA: 2008. Vol. 51: 147-156.

IGARTUA, A., MENDOZA, G., FERNANDEZ, X., ZABALA, B., ALBERDI, A., BAYON, R., & ARANZABE, A. (2020). **Surface Treatments Solutions to Green Tribology**. Coatings, 10(7), 634.

JOHN DEERE. Disponível em: <http://www.deere.com>. Acesso em outubro, 2016.

JOST, H. P, **Lubrication: Tribology; Education and Research; Report on the Present Position and Industry's Needs** (submitted to the Department of Education and Science by the Lubrication Engineering and Research) Working Group. 1966: HM Stationery Office.

JOST, H. P. (2005). **Tribology micro and macroeconomics: A road to economic savings**. In World Tribology Congress III, Washington DC, 18–22.

KALIN, M., MAJDIČ, F., VIŽINTIN, J., PEZDIRNIK, J., & VELKAVRH, I. (2008). **Analyses of the long-term performance and tribological behavior of an axial piston pump using diamondlike-carbon-coated piston shoes and biodegradable oil**. Journal of Tribology, 130(1), 011013.

KHADEM, M., PENKOV, O. V., YANG, H. K., & KIM, D. E. (2017). **Tribology of multilayer coatings for wear reduction: A review**. Friction, 5(3), 248-262.

KOSKINEN, K. T. & RIIPINEN, H. T. (2008). **Sustainable Development with Water Hydraulics – Possibilities and Challenges**. Proceedings of the 7th - JFPS International Symposium on Fluid Power, Toyama, vol. 7, 11-18.

KOWALSKI, K., ZLOTO, T. (2014). **Exploitation and Repair of Hydraulic Cylinders Used in Mobile Machinery**. TEKA. Commission of Motorization and Energetics in Agriculture, 14, 53-58.

KUMAR, S., & BHARJ, R. S. (2020). **Addressing the Green Tribology Advancement, Future Development, and Challenges.** In Intelligent Manufacturing and Energy Sustainability, Proceedings of ICIMES 2020, (pp. 565-573).

LIU, Y. L., CHENG, J., YIN, B., ZHU, S. Y., QIAO, Z. H., YANG, J. (2017). **Study of the Tribological Behaviors and Wear Mechanisms of WC-Co and WC-Fe3Al Hard Materials under Dry Sliding Condition**. Tribology International, 109, 19-25.

LUO, J., & ZHOU, X. (2020). **Superlubricitive engineering—Future industry nearly getting rid of wear and frictional energy consumption**. Friction, 8, 643-665.

MAJDAN, R., TKÁČ, Z., KOSIBA, J., ABRAHÁM, R., JABLONICKÝ, J., HUJO, L., MOJŽIŠ, M., ŠEVČÍK, P., RÁŠO, M. (2013). **Evaluation of Tractor Biodegradable Hydraulic Fluids on the Basis of Hydraulic Pump Wear**. Research in Agricultural Engineering, 59, 75-82.

MAJDIC, F., & PEZDIRNIK, J. (2010). **Oil-and water-based continuous control valve**. Industrial Lubrication and Tribology. 62/3, 136-143.

MAJDIČ, F., VELKAVRH, I., & KALIN, M. (2013). **Improving the performance of a proportional 4/3 water–hydraulic valve by using a diamond-like-carbon coating**. Wear, 297(1-2), 1016-1024.

MENDONZA, Y. E. A. **Sistematização do Projeto de Circuitos Hidráulicos para o Emprego de Fluidos Biodegradáveis**. Tese de doutorado, UFSC - Universidade Federal de Santa Catarina, setembro, 2013: 228p., Florianópolis.

MILLER, M. (2012). **Fundamentals of Biobased and Biodegradable Lubricants: A Real-World Perspective**. Journal of ASTM International, 9(5), 1-6.

MYSHKIN, N. K., & GORYACHEVA, I. G. (2016). **Tribology: trends in the half-century development**. Journal of Friction and Wear, 37(6), 513-516.

NG, F., HARDING, J. A., GLASS, J. (2017). **Improving Hydraulic Excavator Performance through in Line Hydraulic Oil Contamination Monitoring**. Mechanical Systems and Signal Processing, 83, 176 - 193.

OHE, C. B., JOHNSEN, R., ESPALLARGAS, N. (2009). **Hydraulic Cylinders for Offshore Splash Zone Operation - A Review of Piston Rod Failure Cases and Alternative Concepts**, 28th International Conference on Ocean, Offshore and Arctic Engineering, Hawaii, 28, 1-14.

OLSZAK, A., OSOWSKI, K., MUSIAŁEK, I., ROGOŚ, E., KĘSY, A., & KĘSY, Z. (2020). **Application of Plant Oils as Ecologically Friendly Hydraulic Fluids**. Applied Sciences, 10(24), 9086.

RACHIDI, R., EL KIHEL, B., DELAUNOIS, F., VITRY, V. (2017). **Deschuyteneer D. Wear Performance of Thermally Sprayed NiCrBSi and NiCrBSi-WC Coatings Under Two Different Wear Modes**. Journal of Materials and Environmental Sciences, 08, 4550-4559.

SAPAWE, N., SYAHRULLAIL, S., IZHAN, M. I. (2014). **Evaluation on the Tribological Properties of Palm Olein in Different Loads Applied using Pin-on-Disk Tribotester**. Jurnal Tribologi, 3, 11-29.

SARTWELL, B. D., LEGG, K. O. **Replacement of Chromium Electroplating on Landing Gear Components Using HVOF Thermal Spray Coatings**. U.S. DEPARTMENT OF DEFENSE, Environmental Security Technology Certification Program (ESTCP) , Washington, USA, May, 2004. 50p.

SILVA JUNIOR, G., VOORWALD, H. J. C., CIOFFI, M. O. H. (2017). **Evaluation of Hvof Sprayed WC-13Co-4Cr and Hard Chromium Electroplated on Stainless Steel 15-5PH Fatigue Strength**. Proceedings of the 7th International Conference on Mechanics and Materials in Design, 7, 405-416.

STRMČNIK, E., MAJDIČ, F., & KALIN, M. (2019). **Water-lubricated behaviour of AISI 440C stainless steel and a DLC coating for an orbital hydraulic motor application**. Tribology International, 131, 128-136.

TRELLEBORG SEALING SOLUTION. **Hydraulic Seals / Rod Seals**. Catálogo de Produtos, Suécia, 2011. 149p.

TULÍK, J., HUJO, Ľ., KOSIBA, J., JABLONICKÝ, J., JÁNOŠOVÁ, M. (2017). **Evaluation of New Biodegradable Fluid on the Basis of Accelerated Durability Test, FTIR and ICP Spectroscopy**. Research in Agricultural Engineering, 63, 1-9.

VAITHILINGAM, J., GOODRIDGE, R. D., HAGUE, R. J., CHRISTIE, S. D., & EDMONDSON, S. (2016). **The effect of laser remelting on the surface chemistry of Ti6al4V components fabricated by selective laser melting**. Journal of Materials Processing Technology, 232, 1-8.

WANG, Q., LUO, S., WANG, S., WANG, H., & RAMACHANDRAN, C. S. (2019). **Wear, erosion and corrosion resistance of HVOF-sprayed WC and Cr3C2 based coatings for electrolytic hard chrome replacement.** International Journal of Refractory Metals and Hard Materials, 81, 242-252.

APÊNDICES

A.1 Processo de deposição do cromo duro e HVOF

A.1.1 Procedimento utilizado para disposição dos revestimentos das superfícies das amostras: eletrodeposição de cromo duro e aspersão térmica/HVOF.

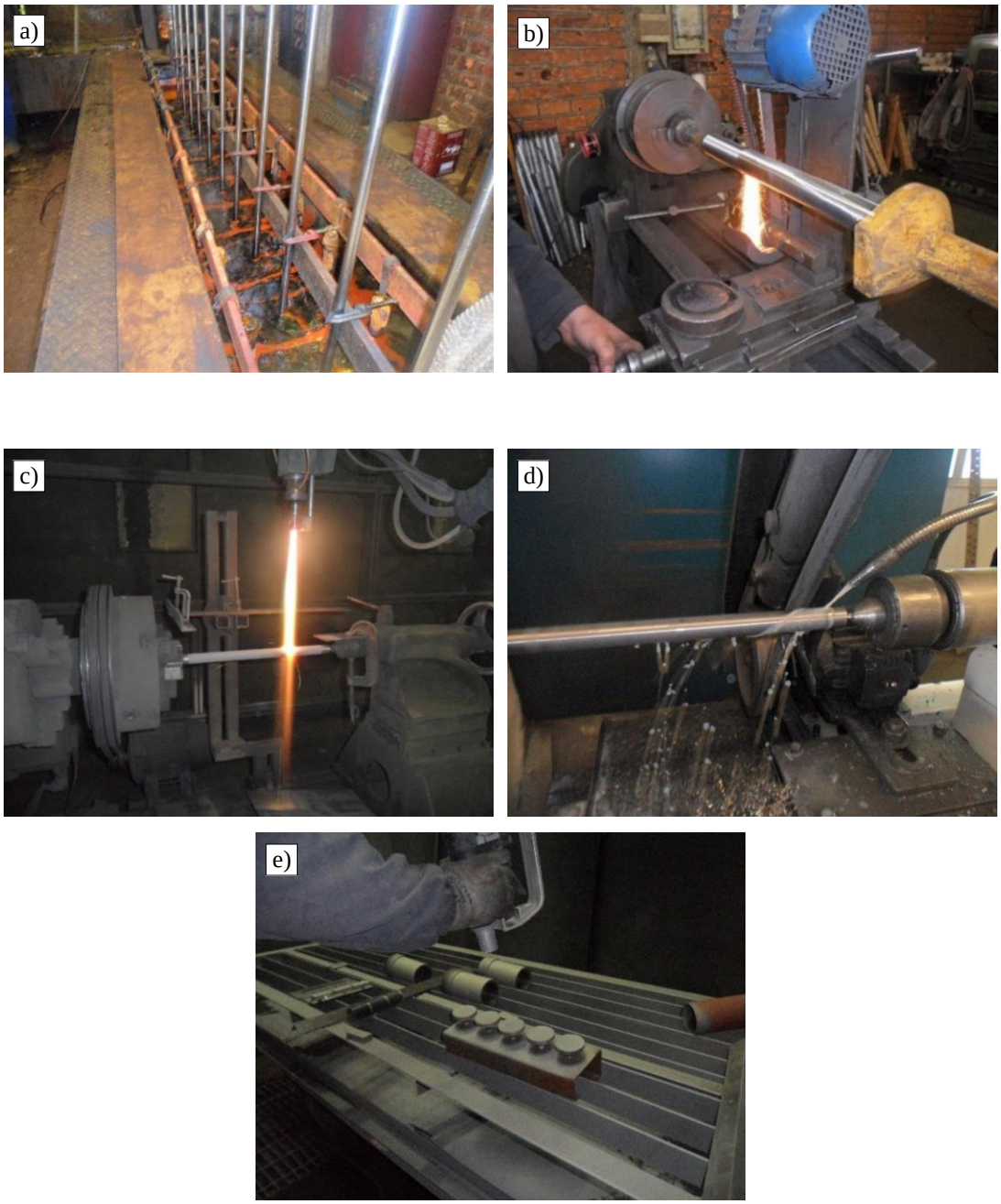

a) Eletrodeposição de cromo duro nas hastes, b) polimento da superfície após processo de cromagem, c) Deposição por aspersão térmica/HVOF nas hastes hidráulicas, d) polimento da superfície após processo de HVOF, e) deposição por HVOF nas amostras para testes de pino sobre disco. Fonte: do Autor

A.2 Análise das propriedades reológicas e contaminação do lubrificante

A.2.1 Comportamento reológico e principais características dos óleos hidráulicos biodegradáveis HEES e HEPR e do óleo mineral do tipo HLP

Durante o deslizamento das superfícies em condição lubrificada, as propriedades reológicas, tais como, tensão de cisalhamento, taxa de cisalhamento e viscosidade, influenciam nos regimes de lubrificação. Dessa forma, o comportamento tribológico das superfícies em deslizamento para cada lubrificante, acabada sendo afetado. As figuras a) e b) mostra os resultados da caracterização dos lubrificantes.

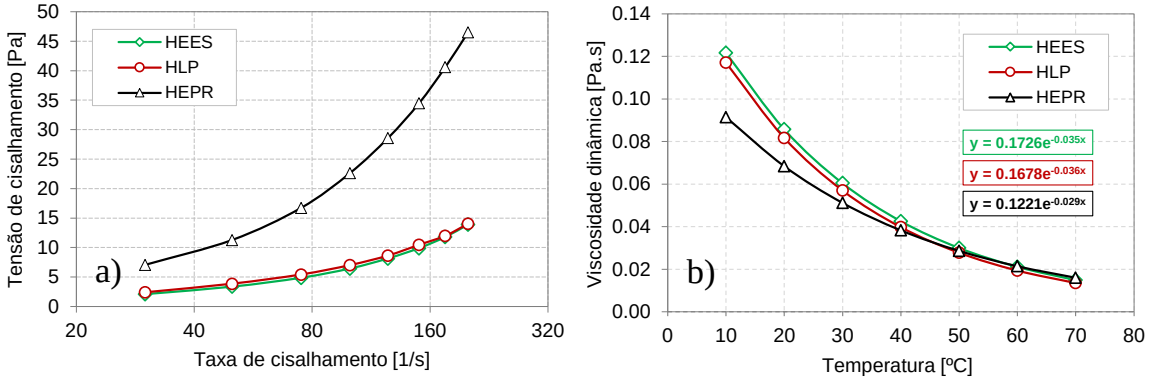

a) Tensão de cisalhamento e da viscosidade dos óleos hidráulicos em relação à taxa de cisalhamento obtida ao qual representa a Lei de Ostwald de Waele. b) Comportamento da viscosidade dinâmica em relação a variação da temperatura, o qual foi obtida a partir da equação de Reynolds. Fonte: do Autor

A.2.2 Principais propriedades e características dos óleos utilizados nos ensaios de deslizamento lubricado.

A tabela a seguir apresenta as principais características e propriedades químicas e físicas dos óleos utilizados nos ensaios de deslizamento lubrificado. Essas propriedades foram identificadas no *datasheet* de cada fabricante.

Nº	Características dos óleos	Parâmetros de teste		
		HEES	HLP	HEPR
1	Densidade a 15ºC, kg/m^3	915	860	880
2	Viscosidade, cSt a 40 ºC	46	41 a 50	44
3	Viscosidade, cSt a 100 ºC	mín 5,8	mín 6,1	mín 6,6
4	Ponto de fulgor, ºC	> 280	> 195	> 240
5	Ponto de fluidez, ºC	- 36	- 36	-45
6	Teste de FZG	> 12	> 11	---
7	Nível de dano ecológico	Baixo	Alto	Baixo

Fonte: do Autor

A.3 Microestruturas e parâmetros do laser usados no processo de refusão

A.3.1 Microestruturas obtidas após os testes preliminares para as diferentes combinações de velocidade de varredura e potência do feixe de laser

Com intuito de obter uma microestrutura e diluição geométrica adequada, diferentes densidades de energia produzidas pelo feixe de laser foram avaliadas . Na figura abaixo apresenta-se os resultados destas combinações, identificadas na apêndice A3.2.

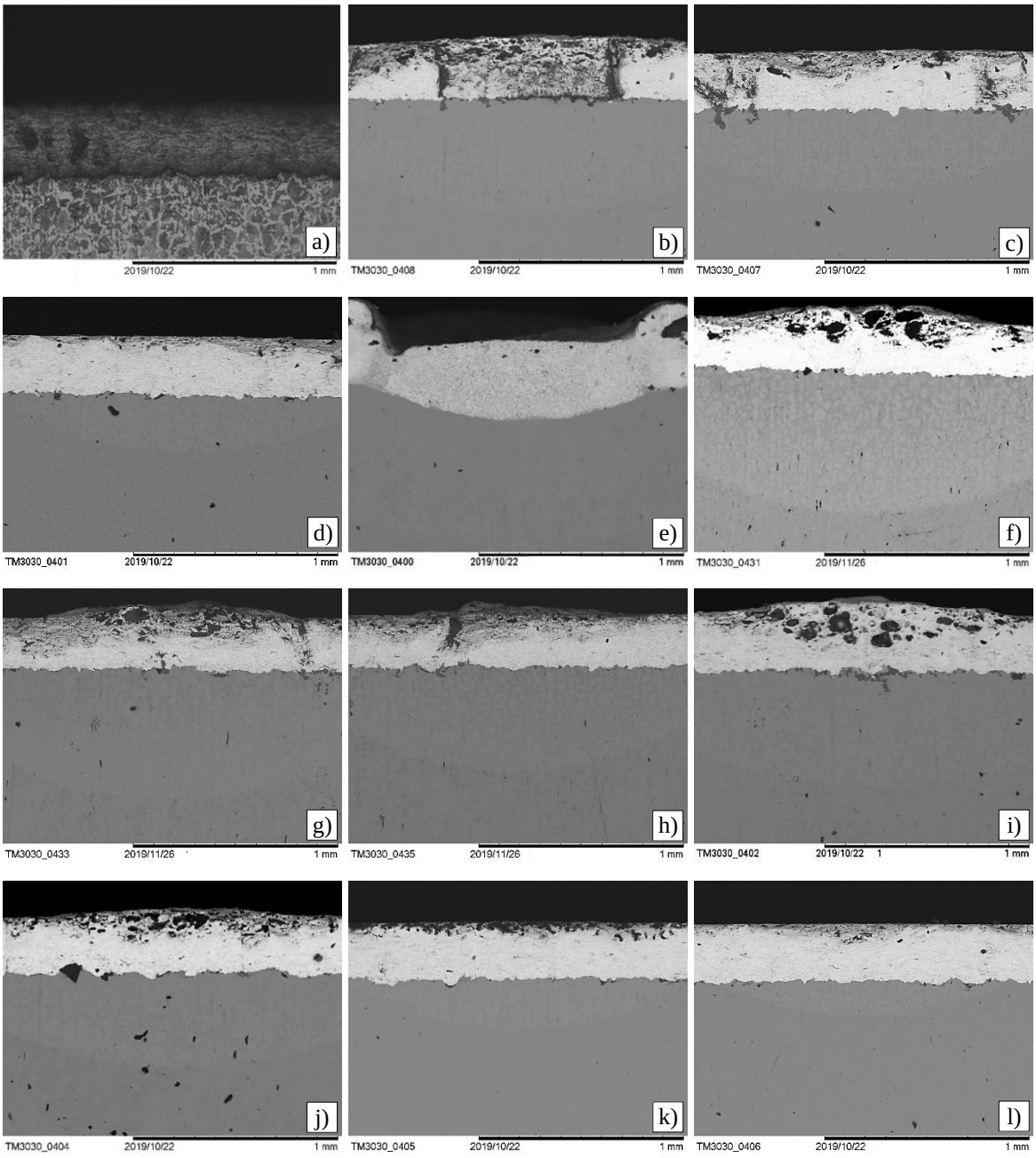

a) sem refusão, b) 100 J/mm^2, c) 50 J/mm^2, 33.3 J/mm^2, 150 J/mm^2, 120 J/mm^2, 100 J/mm^2, 85,7 J/mm^2, 75 J/mm^2, 50 J/mm^2, 25 J/mm^2 e 20 J/mm^2. Fonte: do Autor.

A.3.2 Parâmetros e equipamento usados nos testes preliminares para a obtenção das diferentes densidades de energia do feixe de laser

Nº	Condições	Parâmetros de teste			
		Potência do laser (W)	**Velocidade de varredura (mm/s)**	**Diâmetro de incidência do laser (µm)**	**Densidade de energia (J/mm²)**
1	LMA	400	3.3	1200	100
2	LM0	400	6.7	1200	50
3	LM1	400	10.0	1200	33.3
4	LM2	600	3.3	1200	150
5	LM2.1	600	4.2	1200	120
6	LM2.2	600	5.0	1200	100
7	LM2.3	600	5.8	1200	85.7
8	LM3	600	6.7	1200	75
9	LM4	600	10.0	1200	50
10	LM5	400	13.3	1200	25
11	LM6	400	16.7	1200	20

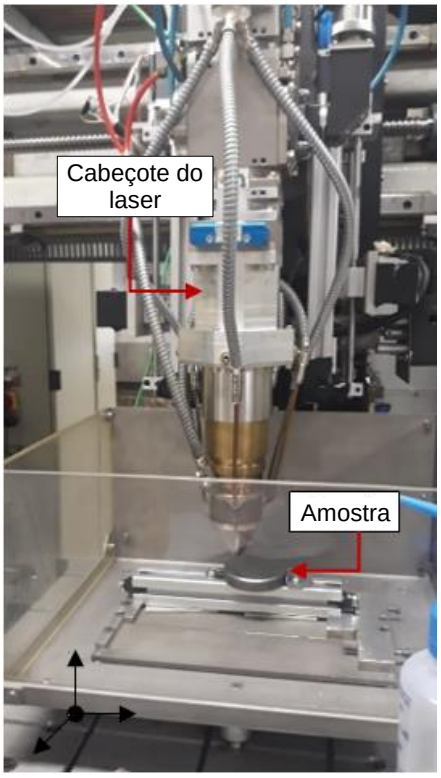

Fonte: do autor

A seleção dos parâmetros de energia do laser foram baseados na experiência da equipe do laboratório de mecânica de precisão – LMP/UFSC, além das propriedades termofísicas dos revestimentos, obtendo-se máxima zona termicamente afetada. O que equipamento é equipamento por um painel de controle, em que os parâmetros de potência, velocidade de varredura, entre outros, são comandados por um controle CNC, o que permite o melhor controle do processo de refusão.